NCAT Report 06-05

PHASE II NCAT TEST TRACK RESULTS

By

David Timm
Randy West
Angela Priest
Buzz Powell
Immanuel Selvaraj
Jingna Zhang
Ray Brown

December 2006

277 Technology Parkway Auburn, AL 36830

PHASE II NCAT TEST TRACK RESULTS

By

David Timm
Gottlieb Assistant Professor
Civil Engineering, Auburn University

Randy C. West
Assistant Director
National Center for Asphalt Technology

Angela Priest
Kimley-Horn & Associates, Inc.

Buzz Powell
Test Track Manager
National Center for Asphalt Technology

Immanuel Selvaraj
Graduate Student
National Center for Asphalt Technology

Jingna Zhang
Research Engineer
Formerly, National Center for Asphalt Technology

Ray Brown
Director
National Center for Asphalt Technology

Sponsored by:
Alabama Department of Transportation
Federal Highway Administration
Florida Department of Transportation
Georgia Department of Transportation
Indiana Department of Transportation
Mississippi Department of Transportation
Missouri Department of Transportation
North Carolina Department of Transportation
Oklahoma Department of Transportation
South Carolina Department of Transportation
Tennessee Department of Transportation

NCAT Report 06-05

December 2006

DISCLAIMER

The contents of this report reflect the views of the authors who are responsible for the facts and accuracy of the data presented herein. The contents do not necessarily reflect the official views or policies of the DOTs from Alabama, FHWA, Florida, Georgia, Indiana, Mississippi, Missouri, North Carolina, Oklahoma, South Carolina, and Tennessee nor the National Center for Asphalt Technology. This report does not constitute a standard, specification, or regulation.

ACKNOWLEDGMENTS

The National Center for Asphalt Technology would like to thank all of the sponsors for their contributions of funding and time during the planning, construction, data collection and analysis, and reporting of the results during Phase II of the Test Track study. Sponsors included the DOTs from Alabama, FHWA, Florida, Georgia, Indiana, Mississippi, Missouri, North Carolina, Oklahoma, South Carolina, and Tennessee.

TABLE OF CONTENTS

CHAPTER 1 INTRODUCTION
- Background
- Overview of 2000 Test Track (Phase I)
- Report Organization
  - Chapter 2 - Overview of 2003 Test Track (Phase II)
  - Chapter 3 - Mixture Performance Studies
  - Chapter 4 - Structural Study
  - Chapter 5 - Items Implemented by DOTs
  - Chapter 6 – Proposed Test Plan for Phase III at the Track
  - Chapter 7 – Observations
  - References
  - Appendix

CHAPTER 2 OVERVIEW OF 2003 TEST TRACK (PHASE II)
- Introduction
- Experimental Design
- Construction
- Traffic

CHAPTER 3 MIXTURE PERFORMANCE STUDIES
- Background
- Overall Performance of Mixture Study Test Sections
- Temperature Measurements at the Test Track
- SMA versus Superpave
- Air Voids versus Rutting
- Relationships between Laboratory Parameters and Rutting
- Laboratory Tests for Predicting Rutting
- Comparison of HMA with Modified and Unmodified Asphalts
- Performance Comparisons of Coarse and Fine-Graded Mixtures

CHAPTER 4 STRUCTURAL STUDY
- Introduction
- Experimental Design
- Structural Design
- Test Section Layout
- Instrumentation
  - Asphalt Strain Gauges
  - Earth Pressure Cells
  - Temperature Profiles
  - Gauge Layout and Installation
- Pavement Response Data Collection
- Mechanistic Pavement Properties
  - FWD Apparatus and Testing Scheme

Backcalculation Cross Section
Pavement Response Under FWD Load
Seasonal Trends in Layer Moduli
Granular Base/Fill Layer Characterization
Subgrade Characterization
HMA Characterization
HMA Modulus – Temperature Characterization
Fatigue Performance and Model Development
Methodology
Dynamic Strain Data
Strain Response Characterization
Fatigue Performance Characterization
Model Development
Subgrade Pressure and Rutting Performance
Introduction
Data Collection
Trends in Base and Subgrade Pressures
Pressure Prediction
Theoretical Pressure Calculation
Base and Subgrade Strain Calculations
Strain Prediction Models
Rutting Progression
Axle Passes and Pavement Strain

CHAPTER 5 ITEMS IMPLEMENTED BY DOTs
Introduction
Grinding to Improve Smoothness
Fine and Coarse-Graded Mixtures
Grade Bumping
Use of SMA
Open-Graded Friction Course
Predicting Rutting Potential
Increasing Asphalt Contents
Comparisons with Other Accelerated Loading Facilities
Aggregate Quality
Smaller Top Size Mixtures
Other Research Issues

CHAPTER 6 OBSERVATIONS

REFERENCES

APPENDIX

PHASE II NCAT TEST TRACK RESULTS

David Timm, Randy West, Angela Priest, Buzz Powell, Immanuel Selvaraj, Jingna Zhang, and Ray Brown

CHAPTER 1: INTRODUCTION

Background

There is a need to be able to quickly test materials and mixtures in-place, under real traffic. There have been many developments during the last few years that need verification prior to adopting. One such development is the new proposed mechanistic pavement design procedure. Another is the development of proposed performance tests that need verification. It will take at least 15 to 20 years to verify these procedures on existing highways. However, accelerated loading facilities such as the National Center for Asphalt Technology (NCAT) Test Track can accomplish these verification studies safely in two to three years. This can be done at reduced cost and without adversely affecting the driving public.

The NCAT test track was built in 2000 and has now been in use for five years. Experimental sections on the 1.7 mile Pavement Test Track are cooperatively funded by a number of state DOTs and the Federal Highway Administration (FHWA), with operation and research managed by NCAT. State DOTs that have sponsored work at the track include: Alabama, Florida, Georgia, Indiana, Missouri, Mississippi, North Carolina, Oklahoma, South Carolina, and Tennessee. In 2000, forty-six different test sections were installed at the facility, each at a length of 200 feet. Materials used locally by the section sponsors were transported to NCAT during construction to maximize the applicability of results to the sponsors. In 2003, many of these sections were rebuilt and traffic again initiated.

Overview of 2000 Test Track (Phase I)

Ten million equivalent single axle loadings (ESALs) were applied over a two-year period with field performance documented weekly. As a consequence of the conservative thickness design (24 inches of HMA used in every section), mixture rutting was the primary study distress on the 2000 track. The report on Phase I (Brown et al, 2002) is available on the NCAT website at www.ncat.us.

Unlike conventional efforts on public roadways, research at the NCAT Test Track is conducted in a closed-loop facility where axle loadings are monitored and environmental effects are identical for every mix. With this approach, pavement performance evaluations can be safely obtained after two years rather than after approximately 15 years of traffic on typical roadways.

In Phase I sponsors typically compared the performance of two or more sections constructed with different local materials and/or methods to obtain information that could be used to build future pavements with improved performance.

Report Organization

This report consists of seven chapters that are briefly described below. The report, generally speaking, is meant to be a summary document of the 2003 Test Track research efforts along with discussion of some of the Phase I work. In many cases throughout this report, other published NCAT reports are referenced which contain much more detail on the particular topic.

Chapter 2 - Overview of 2003 Test Track (Phase II)
This portion of the report includes a general discussion of the experimental design for Phase II at the track. It also includes some discussion of the construction along with the traffic that was applied to the test sections.

Chapter 3 - Mixture Performance Studies
The mixture studies include analysis of the sections that were left in place from Phase I and those mill and overlay sections for Phase II. The main purpose of this part of the study was to look at the effects of materials and mixtures on performance, primarily rutting. Several topics are discussed including: effects of modified and non-modified asphalts, effect of fine-graded vs. coarse-graded mixtures, performance comparison of Superpave and SMA, effect of air voids on rutting, prediction of rutting from performance tests, and effect of materials on skid resistance.

Chapter 4 - Structural Study
As noted above, eight test sections were constructed to examine the structural performance of several different pavement designs. The primary variables were thickness of HMA and modified vs. unmodified asphalts. The structural study section of the report includes information on the design of the structural sections, instrumentation, data collection and processing. The chapter also includes discussions of mechanistic properties including the soil, granular base, and HMA. Information concerning strain at the bottom of the HMA layer and measured stresses on top of the base and subgrade are presented with corresponding cracking and rutting performance.

Chapter 5 - Items Implemented by DOTs
For the track to be effective, information learned at the track must be implemented. The sponsors were polled to determine what they had learned and implemented from the track work. A summary of items that have been implemented is provided.

Chapter 6 – Proposed Test Plan for Phase III at the Track
Plans are being finalized for Phase III of the Test Track. The plan is to build approximately 15 structural sections, approximately 10 mill and inlay and to leave the remaining sections in place. The amount of traffic to be applied will again be 10 million ESALs. Phase III will be completed after three years in 2008.

Chapter 7 - Observations
Observations based on Phase II work are provided in the final chapter.

References

Appendix
A summary table of data from mixes representing the various test sections is provided in the appendix.

CHAPTER 2: OVERVIEW OF 2003 TEST TRACK (PHASE II)

Introduction

Following the completion of the initial three year cycle of the track, sponsors were again given the opportunity to plan research that best fit their needs for the second cycle. Many states elected to leave some or all of their original sections in place for additional traffic and extended performance evaluations. Twenty-three of the original 46 test sections were left for continued evaluations and twenty-two new sections were built in 2003. One section was removed to serve as a transition section for new construction.

Of the 22 new test sections, eight sections were utilized for a structural experiment by removing the existing pavement all the way down to uniform subgrade materials (approximately 30 inches) and rebuilding the pavement structure with varying thicknesses and materials. Fourteen of the new test sections were shallow mill and inlay (i.e., between ¾ and 4 inches deep) rutting study sections. Figure 2.1 illustrates the layout of the 2003 Test Track.

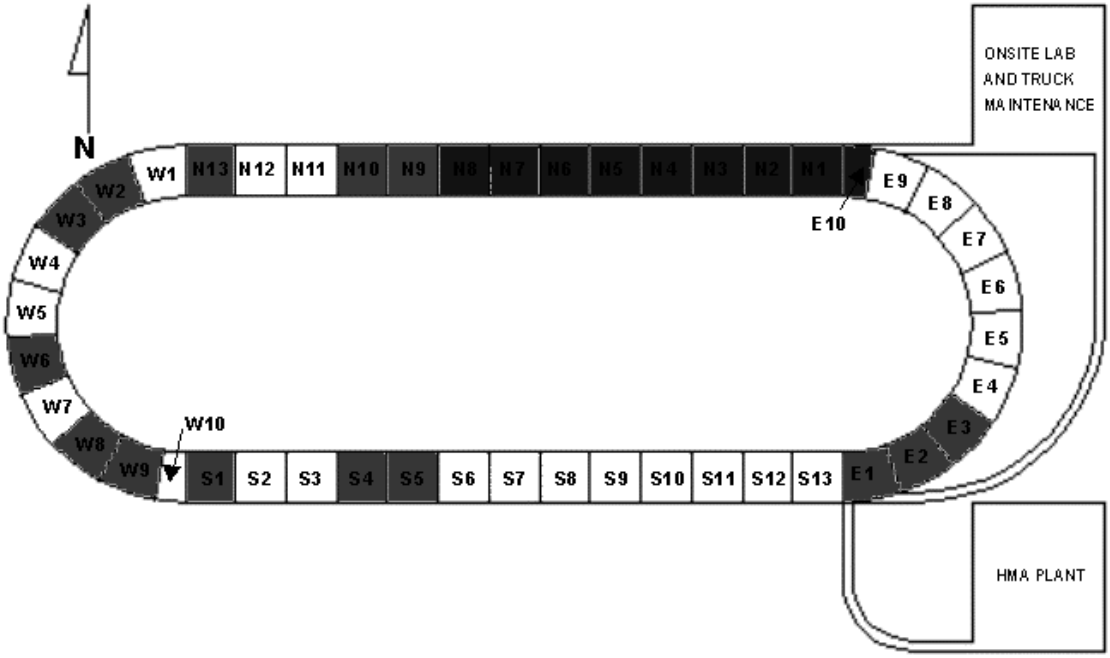

Figure 2.1 2003 Experiment (Black = Structural Sections, Gray = Rutting Studies, White = Left in Place).

The primary objective of the 2003 Test Track was to evaluate field performance of several experimental pavements. Rutting was expected to be minor in sections that were originally built in 2000 and subjected to a second round of traffic. The eight test sections (N1 through N8) in the structural experiment were monitored for structural distresses (primarily fatigue cracking). The goals of the structural experiment were to help validate mechanistic pavement design concepts and to learn more about characterization of pavement materials and evaluation of pavement responses. For the 14 sections that were mill and inlay sections, rutting was the anticipated distress. In addition to evaluation of field performance for individual sections, a goal of the project was to evaluate the potential to predict performance.

Experimental Design

Many sponsors chose not to replace their test sections for the 2003 track so they could extend their rutting comparisons to 20 million ESALs and broaden performance comparisons to include durability. Weekly field performance testing was conducted to characterize how rutting, roughness, texture, density, friction, and surface deflection changed as traffic accumulated beyond the 10 million ESALs originally applied.

Fourteen sections were milled to a depth of ¾ to 4 inches as specified by the research sponsors. While some states wanted to conduct another full depth (4 inch) rutting experiment, other states chose to compare the performance of shallow mill and inlay pavement preservation techniques. In cases where full (4 inch) depth rutting mixes were placed, stone matrix asphalt (SMA) was a mix type that was often used. Several sponsors investigated the effect of loosening aggregate specification requirements on performance of SMA. For example, will mixes designed with aggregates having high Los Angeles (LA) abrasion loss exhibit more production and performance problems than mixes produced using aggregates having lower LA abrasion values?

In cases where pavement preservation studies were planned, shallow mill and inlay methods were required. In these comparisons, sponsors evaluated various thin overlay options to determine which ones were most cost effective.

Only the outside (traffic) lane was replaced. The existing inside lane was used as a haul road and work platform. Milling was extended approximately 1.5 feet beyond the existing centerline and edgeline. Specifications to control milling and pavement inlay thicknesses had acceptance requirements to ensure the final pavement section was constructed to meet the intended objective.

Eight test sections were sponsored for construction of a structural experiment on the 2003 track. The two primary experimental factors were HMA thickness and modified versus unmodified asphalt. The structural sections were instrumented with various gauges to measure temperature at various depths in the HMA, longitudinal and transverse strain at the bottom of the HMA, and pressure applied to the top of the aggregate base and subgrade. The pavement was also instrumented to measure truck wheel wander as the trucks were driven over the eight structural sections.

Construction

The project was developed, let and administered by ALDOT under the guidance of the sponsor oversight committee. East Alabama Paving Company was the low bidder on the track reconstruction project. Contract specifications allowed the contractor to bid the job using an offsite plant within a 30-minute haul distance from the track. East Alabama Paving chose to use the track's prepared plant site as a staging area for out-of-state aggregate stockpiles and to produce mix at their plant located approximately 10 minutes away.

Trial mixes were run through the contractor's HMA plant before any final mixes were placed to verify that produced mix properties met each sponsor's expectations. Sponsors had an opportunity to evaluate these results and make necessary changes before final mixes were produced for on-track placement.

When mix was produced for placement on the surface of the track (Figure 2.2), a number of samples were fabricated in the laboratory using a Superpave gyratory compactor (SGC). These samples were compacted to the sponsor-designated design gyration level for laboratory performance testing of various types. Additionally, a large amount of loose material was stored in metal buckets so that more samples could be tested at a later time.

Figure 2.2 Construction of Test Sections.

Live bottom trucks were used to place most curve sections and conventional dump trucks used for tangent sections. Paving began only when all necessary trucks were lined up and ready to discharge into the material transfer device (MTD).

Typically, compaction of the test sections included three coverages with the vibratory steel-wheeled roller. As requested by the sponsors, many sections were also compacted with a rubber tire roller.

The structural experiment (shown in Figure 2.3), cosponsored by the Alabama DOT, Indiana DOT, and the Federal Highway Administration, necessitated the deep removal of approximately 1700 feet of the North tangent. This was accomplished by ramping down from either end and milling back and forth until the original subgrade was exposed. An automated tarping system utilized to protect the subgrade from rain as needed prior to new material being placed proved invaluable in the unusually wet season. Details about instrumentation for the structural sections are provided in Chapter 4.

FIGURE 2.3 STRUCTURAL SECTION EXPERIMENT (8 TEST SECTIONS).

Traffic

In order to generate accelerated results, it was necessary to operate a fleet of triple-trailer trucks (20,000 pounds per loaded axle) to apply a design lifetime of heavy axle loadings in two years (Figure 2.4). Over the course of Phases I and II, the total travel distance of the five-truck fleet exceeded three million miles.

Drivers were utilized to operate the trucks to best simulate real traffic. At the beginning of the second cycle, a single truck was operated on the track for approximately one month, and full operations (four trucks) began in December 2003. One reason for beginning traffic with one truck was to provide some seating and aging of the HMA before accelerated loading was initiated. Eight-axle triple trailer trains were used to apply 10 million ESALs within the two-year loading cycle. Trucking operations for Phase II testing will be completed by the middle of December 2005.

Figure 2.4 Triple Trailer Trains Used to Apply Accelerated Loading.

CHAPTER 3: MIXTURE PERFORMANCE STUDIES

Background

A principle mission of the NCAT Test Track is to provide realistic field performance evaluations of asphalt mixtures and comparisons of many mix factors such as comparing modified versus unmodified asphalt binders, fine versus coarse-graded mixtures, SMA versus Superpave, effect of aggregate properties, etc. This chapter deals with many of these types of evaluations and comparisons.

In the comparison of performance of the 45 test sections in Phase III at the track it is important to recognize certain limitations. First, caution must be used when comparing the performance of sections built in the original cycle to new sections built in 2003. It is certainly reasonable to draw conclusions from comparisons within one cycle and verify the conclusions with observations from the second cycle.

Another limitation in the comparison of test sections is the difference between the paths of the trailers in the tangent sections compared to the curve sections. A detailed discussion of wheelpath wander measurements on the North tangent at the Test Track can be found in the report by Timm and Priest (2005). That report concluded that the distribution of wheel loads by the trucks at the track is consistent with wheelpath measurements on typical highways. Although wheelpath measurements have not been made in the curves of the Test Track, it is known that as any vehicle tracks around a curve, its trailing wheels follow in a smaller radius then the leading wheels. Therefore, it is important to group sections by tangents and curves when making correlations, and direct comparisons between specific tangent sections and curve sections should be avoided.

Overall Performance of Mixture Study Test Sections

At the time of this report, the 23 original test sections had been subjected to about 19 million ESALs, and the 22 new sections built in 2003 had carried about 9 million ESALs. Rut depths for the test sections at this point in time are illustrated in Figures 3.1 and 3.2 for the remaining original and new test sections, respectively. These are the average rut depths for the right wheelpath calculated from transverse dipstick profiles (Figure 3.3) taken at three random locations in the sections (A dipstick is a device that can be used to measure the transverse surface profile across a pavement surface. The device begins at a reference point on the edge of the pavement and can provide the change in profile as the device is “walked” across the pavement surface). As can be seen, the rutting performance for all of the original and new test sections is excellent. Most of the sections have less than seven millimeters of rutting (approximately ¼ inch).

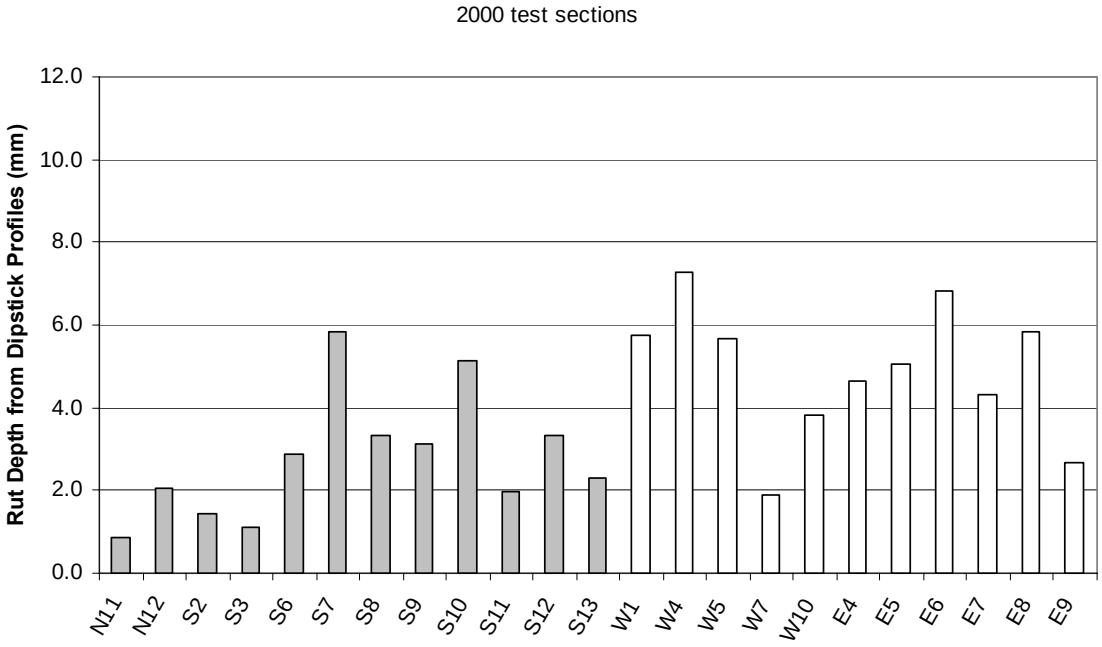

Figure 3.1 Rut Depths After 19 million ESALs for the Remaining Original Test Sections (Gray-Tangent Sections and White-Curve Sections).

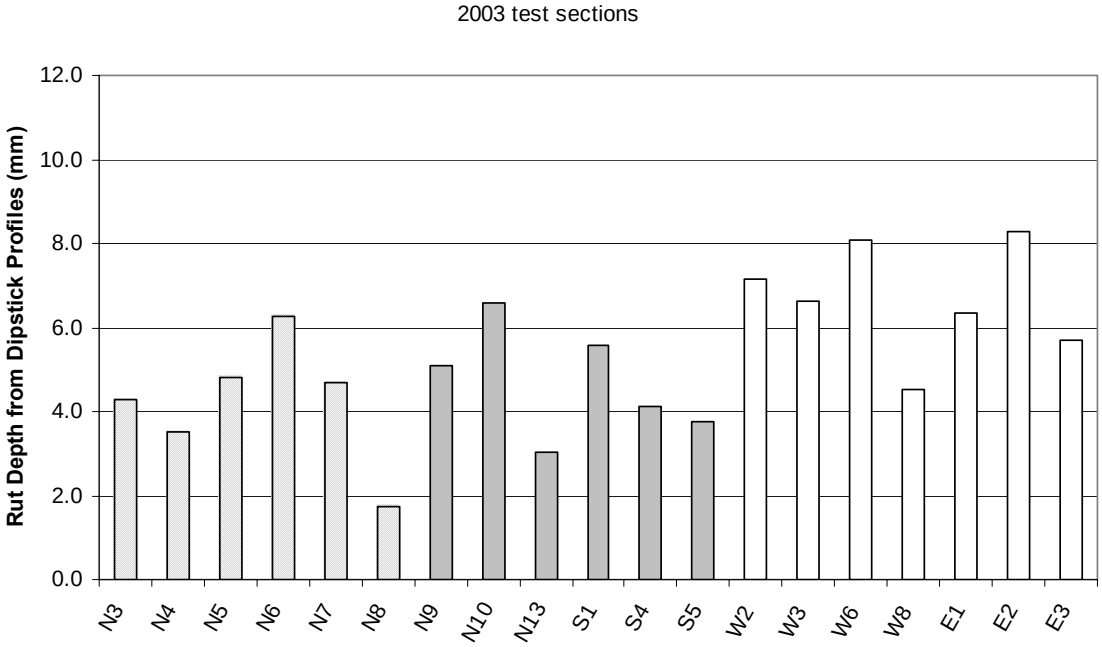

Figure 3.2 Rut Depths After 9 million ESALs for the New Test Sections (Cross Hatched-Structural Sections, Gray-Tangent Sections, and White-Curve Sections).

Figure 3.3 Rutting Measurements with Dipstick.

Changes in the surface texture of the original sections that remained in place for the second cycle are shown in Figure 3.4. Texture measurements were made weekly with an ARAN van using a 500 Hz laser on the right wheelpath. Laser measurements are processed through a 0.5 to 50 mm wavelength filter to generate mean texture depth data in millimeters. Texture measurements are made weekly with a laser on the ARAN van. These results indicate that most sections show a progressive increase in texture over time and traffic. The exceptions are SMA sections, N12 and W1, and OGFC sections, W4, W5, and W7, which show a decrease in texture during the first cycle and then little change for the second cycle. The increase in texture for the dense graded sections can be attributed to minor loss of aggregate particles from the surfaces.

Cracking was only observed in four test sections outside of the structural experiment. These sections were among the older sections that remained in place from the first cycle of the track. The cracked sections are S2, S12, E7, and W10. Cores taken on the cracks have shown that they were top-down cracking and they only extend through the upper two to four inches of the pavement structure. The extent of cracking, locations relative to wheelpaths, and directions (longitudinal or transverse) of the cracks was different for these sections. Further testing and analysis of cores from cracked and uncracked sections is underway to determine properties of the mixtures that may help explain why these sections have cracked and others have not.

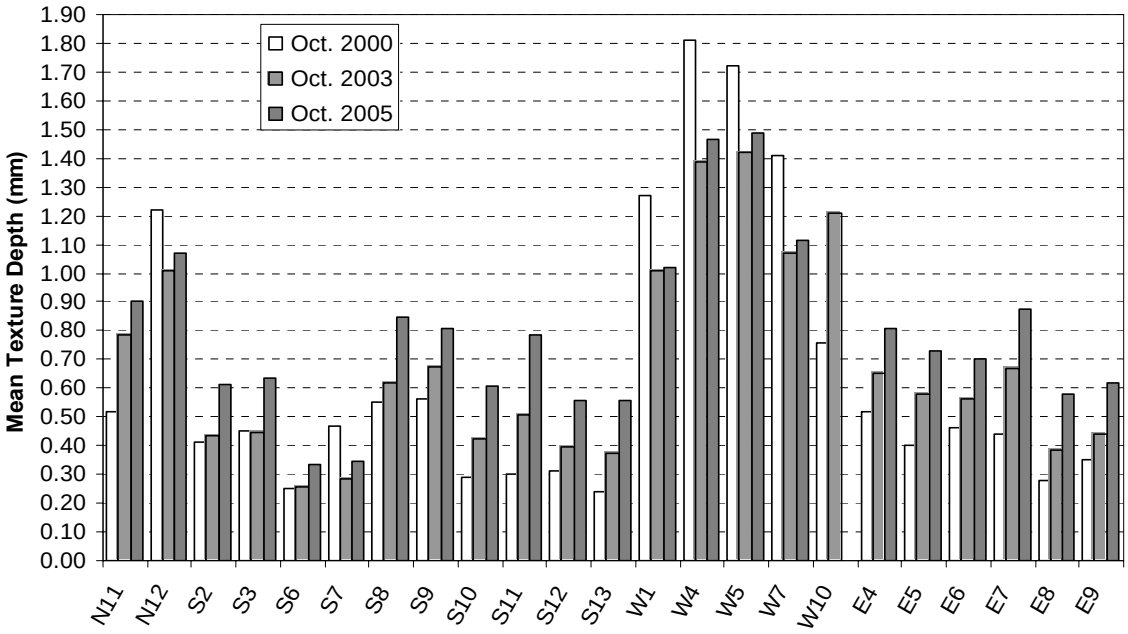

Figure 3.4 Changes in Surface Texture (Mean Texture Depth) of Original Sections.

Temperature Measurements at the Test Track

During construction of the Test Track, temperature probes were installed at pavement layer interfaces within the pavement structure for each test section. Twenty-three dataloggers positioned around the track collected temperature data every minute and recorded the minimum, maximum, and average pavement temperature every hour. Each datalogger receives more than 11,500 temperature inputs per day.

Of the 184 probes installed in 2000, problems were experienced in recording erroneous data from 32 gauges. Therefore, about 17 percent of the gauges were deficient in recording data. New temperature probes were installed in 2003 when the Test Track was reconstructed. Temperature probes had a much lower survivability in the 2003 Test Track than they did in the first cycle. However, the large number of working gauges did provide good pavement temperature data.

Figure 3.5 shows a summary of pavement temperature data for the first and second cycle of the track. This plot is based on temperature measurements of the pavement surface. The maximum temperature recorded each day was averaged for the week. The weekly average maximum pavement surface temperature for each section was averaged to generate this graph. From this plot, it appears that the pavement temperatures during the second cycle were generally slightly lower than during the first cycle.

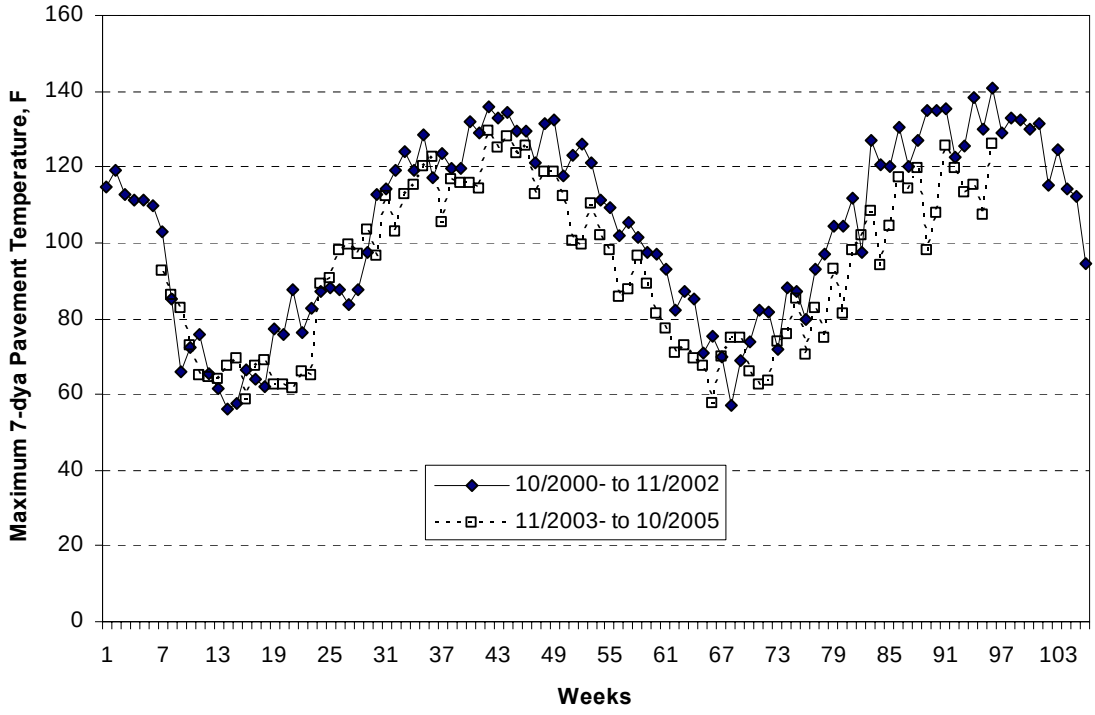

Figure 3.5 Weekly Average Maximum Pavement Surface Temperature for the First and Second Cycle.

SMA versus Superpave

Five SMA test sections were placed in the first cycle of the track. As can be seen in Table 3.1, these SMA mixtures utilized a variety of aggregate types. All of these SMA mixtures were designed with a 50 blow Marshall compactive effort. Section N13 was an all gravel SMA mixture. Although the all gravel mixture had slightly more rutting compared to the adjacent granite SMA section, its performance can still be considered excellent. In fact all of the SMA test sections performed very well.

Table 3.1 SMA Test Sections Built in First Test Track Cycle and String-line Rut Depth Results.

Section	Description	Rut Depth (mm) at 10 Million ESALs
N12	12.5 mm NMAS, Granite, SBS	2.7
N13	12.5 mm NMAS, Gravel, SBS	4.2
W1	12.5 mm NMAS, Granite, SBR	3.2
W2	12.5 mm NMAS, Limestone & Slag, SBR	4.3
W8	12.5 mm NMAS, Sandstone, Limestone & Slag, SBR	4.8

For comparison to Superpave mixtures, the list of Test Track sections was searched for mixtures with the same or very similar aggregates and the same PG binder grade. Also, since the SMA sections in Table 3.1 include sections from tangents and curves, a similar representation of Superpave sections was sought. Comparison Superpave sections are shown in Table 3.2.

Section S5 was designed with 125 gyrations in the SGC; the other mixtures listed here were designed with 100 gyrations. As can be seen, the rutting results for these Superpave sections were very good. Overall, it appears that these Superpave sections had less rutting than the SMA sections. However, for all SMA and Superpave mixtures listed here, the rutting measured is probably primarily due to traffic densification and reorientation of aggregate particles.

Table 3.2 Comparable Superpave Sections and String-line Rut Depth Results for the First Cycle.

Section	Description	Rut Depth (mm) at 10 Million ESALs
S1	12.5 mm NMAS, Granite, SBS	2.4
S5	12.5 mm NMAS, Gravel, SBS	1.2
E10	12.5 mm NMAS Granite, SBR	3.0
N7	12.5 mm NMAS Limestone & Slag, SBR	1.6
W10	12.5 mm NMAS, Gravel, SBR	2.6

No cracking was observed for any of the SMA sections (Table 3.1) or the Superpave Sections (Table 3.2). Minor raveling of coarse aggregate particles was noted for section W10 at the end of the first cycle as shown in Figure 3.6.

Figure 3.6 Photograph Showing Slight loss of Coarse Aggregate Particles in Section W10.

SMA sections N12 and W1 from the first cycle remained in place for the second cycle. These sections continued to perform very well with very minor additional densification and no cracking observed after five years and 19 millions ESALs.

Seven new SMA sections were placed for the second cycle of the Test Track. These sections are listed in Table 3.3. As with the SMA mixtures placed in the first cycle, these sections also had a wide range of aggregate types. All of the 2003 SMA mixtures contained an SBS modified binder meeting the requirements of PG 76-22.

Table 3.3 New SMA Sections Placed in 2003 and Preliminary Rut Depth Results.

Section	Description	Mix Design Compaction	Rut Depth (mm)[1] at 9 Million ESALs
N7	9.5 mm NMAS, Granite	Marshall 50	4.7
N9	9.5 mm NMAS, Limestone	SGC 75	5.1
N10	9.5 mm NMAS, Limestone & Chert	SGC 75	6.6
N13	12.5 mm NMAS, Granite	SGC 50	3.0
S1	12.5 mm NMAS, Granite	SGC 50	5.6
E1	12.5 mm NMAS, Limestone	SGC 50	6.3
W2	12.5 mm NMAS, Porphyry and Limestone	SGC 75	6.6

[1] Rut Depths calculated from Dipstick Profiles

No cracking or other surface problems had been observed in any of the 2003 SMA test sections after 9 million ESALs.

Another piece of valuable information gained from the 2003 SMA test sections deals with the mix design compactive effort. As noted above for the SMA sections placed in the first cycle, all of the mix designs utilized a 50 blow Marshall compactive effort. This has historically been the method used to design SMA mixtures in the U.S. and around the world. The Maryland State Highway Agency has successfully used 100 gyrations in a Superpave Gyratory Compactor (SGC) for their SMA mix design for several years. However, many contractors and other agencies have found that 100 gyrations overcompacts SMA and tends to excessively break aggregate. Several recent research studies have investigated the use of lower gyrations for designing SMA mixtures. These studies indicate that 50 to 75 gyrations provide the same density as achieved with the Marshall hammer and should be used for SMA mix design. Six of the seven SMA sections placed in the second cycle were designed using an SGC. As shown in Table 3.3, three of these mixes used 75 design gyrations and three used 50 design gyrations. The excellent performance of the SMA test sections designed with 75 and 50 gyrations provides confirmation that this range of compactive effort will provide good SMA mix designs.

Air Voids versus Rutting

The air voids in laboratory compacted samples is a key factor in mix design and QC/QA testing of hot mix asphalt. Most agencies utilize air voids as a pay factor item in acceptance decisions.

During construction of the Test Track, samples of the mixtures from each test section were obtained and compacted immediately in the track laboratory to the design number of gyrations. Mix samples for each section were also tested to determine the maximum theoretical specific gravity. Air voids of the test section mixes were then calculated.

The average laboratory air void results for the different test sections ranged from 2.0% to 4.8% for the first cycle. Figure 3.7 shows the correlation of the air voids for the specimens to the rut depths from the respective test sections after 10 million ESALs for the first cycle tangent sections. The data were grouped by the PG grade of the binders used in the test sections. As will be discussed in more detail later, grouping by PG grade was necessary to make any logical observations with the test track data. Several observations can be made from this plot. First, it is clearly evident that most sections with PG 76-22 binder had less rutting on the track compared to the sections with PG 67-22 binder. It is also evident that the correlations between rutting and laboratory air voids are weak for both groups. Although the trends for both groups of data show that lower air voids correspond to increased rutting, the mixes with PG 67-22 appear to be more sensitive to lower void levels.

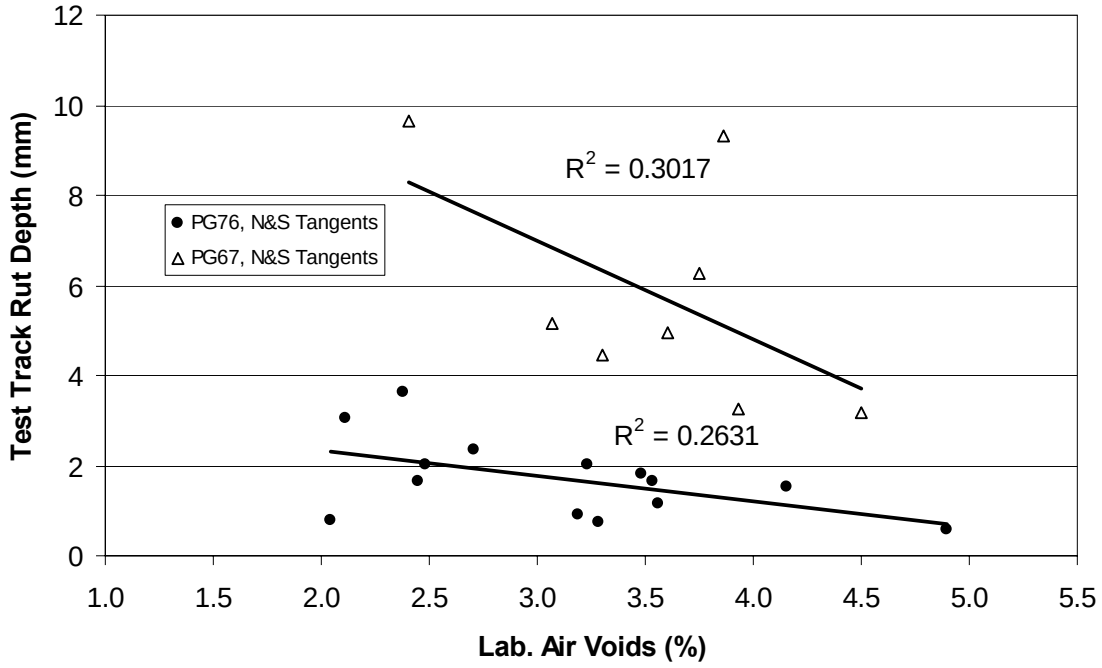

Figure 3.7 Correlation of Lab Compacted Air Voids to Test Track Rutting at 10 Million ESALs for First Cycle Tangent Sections.

The same analysis was conducted for the second cycle. However, fewer new test sections were available for examination. In fact, outside of the structural experiment, no sections were placed with an unmodified asphalt binder on tangent sections. The available data is plotted in Figure 3.8. The data indicates that the amount of observed rutting is not a function of air voids, over the range of air voids investigated, when the PG grade used is bumped to PG 76-22.

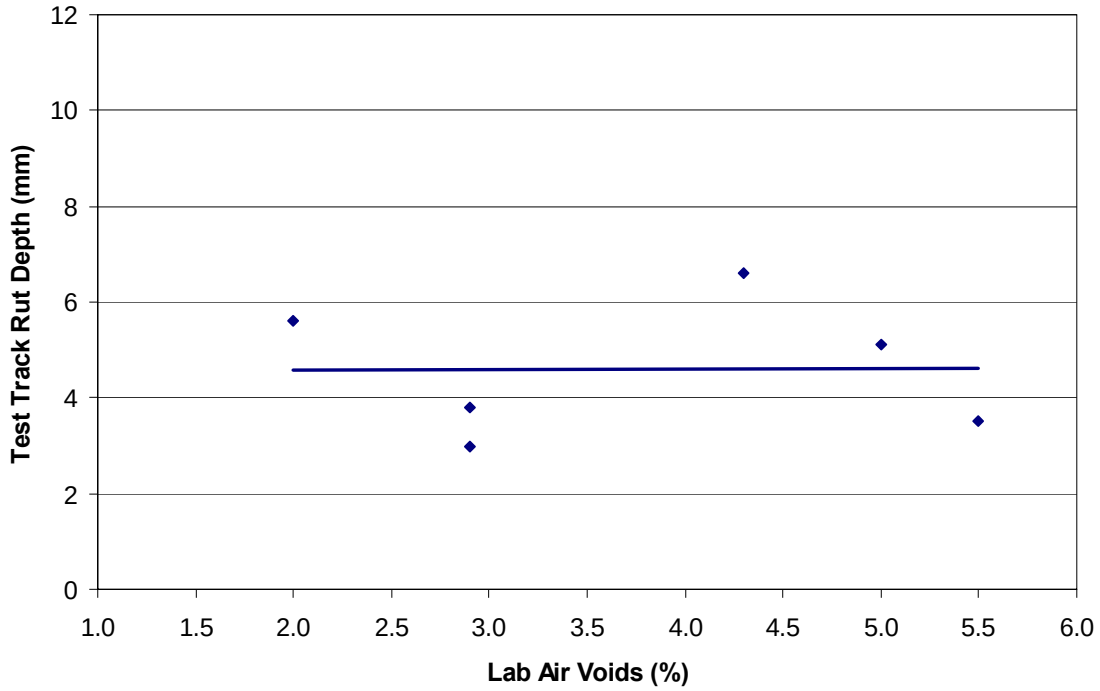

Figure 3.8 Correlation of Lab Compacted Air Voids to Test Track Rutting at Nine Million ESALs for Second Cycle Tangent Sections, PG 76-22 Sections.

Based on the poor correlations shown in this analysis, laboratory air voids alone do not appear to be a good indicator of rutting performance. This clearly shows the need for some type of performance test to provide an estimate of rutting potential.

Relationships Between Laboratory Parameters And Rutting

An analysis was conducted to evaluate basic aggregate and asphalt binder characteristics and mixture compaction characteristics and their possible relationships to rutting. The laboratory characteristics included in the analysis were:

1. Compaction slope determined from compaction in the Superpave Gyratory Compactor (SGC).
2. Number of gyrations to achieve 92% of the maximum theoretical specific gravity (N@92%Gmm).
3. The Compaction Energy Index determined from the SGC compaction process as recommended by Faheem, 2004.
4. The percentage of maximum theoretical specific gravity at N_{ini} ($\%G_{mm}$ @ N_{ini}).
5. The number of gyrations with the SGC to reach the Locking Point of the mixture.
6. The Coarse and Fine Aggregate Ratios as determined using the Bailey Method recommended by Pine (2004) and Vavrik (2002).
7. Mix parameters such as gradation, aggregate shapes, binder grade, and mix volumetric properties.
8. The Primary Control Sieve Index (PCSI), which is difference in % passing from the gradation to point on the maximum density line for the primary control sieve. It represents the relative coarseness or fineness of the gradation. A negative PCSI generally indicates a fine gradation and positive PCSI indicates a coarse gradation.

The mixtures used in this analysis were the tangent surface mixtures (N and S sections) placed in the first cycle. Each of the parameters listed in Table 3.4 was calculated from the quality control samples taken during construction. Regressions between these parameters and the field rut depth after 10 million ESALs were analyzed, and those parameters which yielded the best correlations were analyzed further by performing multiple stepwise regressions.

Relationships between the individual parameters listed in Table 3.4 and measured rut depths for the tangent sections were analyzed by determining the least-squares regression equations. Table 3.4 shows the correlation coefficient, *R*, for each correlation. The coefficient of correlation was used here rather than the more familiar coefficient of determination, R^2, because the sign of *R* is indicative of whether the parameters are positively correlated or inversely correlated. Columns 2 and 3 of the table show the correlations when modified and unmodified sections were included. In this case, the best correlation is with the actual PG grade and the expected trend is observed; as the PG grade of the binder increases, the rut depth decreases ($R = -0.78$). On the other hand, the higher the asphalt content, the higher the rut depth ($R = 0.41$). Many of the parameters have very poor correlations with rutting or do not follow the expected trend.

Table 3.4 Correlation and Expected Trend Between Rutting And Each Parameter.

	All Tangent Sections		**Sections with PG76**		**Sections with PG67**	
Parameter	***R***	**Expected trend**	***R***	**Expected trend**	***R***	**Expected trend**
Lab Air Voids	-0.039	inconclusive	-0.513	correct	-0.549	correct
PCSI	-0.230	inconclusive	-0.254	inconclusive	0.111	inconclusive
%Gmm@Nini	-0.141	inconclusive	0.265	correct	-0.281	incorrect
N@92%Gmm	0.123	inconclusive	-0.427	inconclusive	0.181	inconclusive
CEI	0.136	inconclusive	-0.398	inconclusive	0.230	inconclusive
Slope	0.176	inconclusive	0.004	inconclusive	0.449	correct
LockPt1	0.265	correct	-0.070	inconclusive	0.603	correct
CA Ratio	-0.020	inconclusive	-0.297	inconclusive	-0.356	inconclusive
FAc Ratio	-0.251	inconclusive	-0.241	inconclusive	-0.754	inconclusive
FAf Ratio	-0.010	inconclusive	0.069	inconclusive	0.398	inconclusive
VMA	-0.075	inconclusive	-0.228	incorrect	-0.458	incorrect
VFA	-0.011	inconclusive	0.488	correct	0.280	correct
CAA	0.106	inconclusive	0.538	incorrect	0.491	incorrect
F&E 3:1	-0.210	incorrect	0.110	inconclusive	-0.336	incorrect
FAA	0.082	inconclusive	0.504	incorrect	-0.279	correct
AC%	0.409	correct	0.243	correct	0.694	correct
Actual PG Grade	-0.780	correct	x	x	x	x

Since most of the correlations between individual parameters and measured rutting were not fruitful (other than the PG grade which was clearly significant), a multiple regression analysis was performed in order to identify if the interaction of different parameters explain more than a single parameter.

For the multiple regression analysis, the following parameters were used as predictor variables: Uncompacted voids in coarse aggregate, uncompacted voids in fine aggregate, asphalt content, laboratory air voids, voids in mineral aggregate (VMA), voids filled with asphalt (VFA), actual

PG grade, compaction slope, Compaction Energy Index (CEI), $\%G_{mm}$ @ N_{ini} , N@92%Gmm, N@lockpoint, Coarse and Fine Aggregate Ratios, and PCSI.

The stepwise analysis performs multiple linear regressions for the response variables versus the predictors. Stepwise regression removes and adds variables to the regression model with the purpose of identifying a useful subset of the predictors. Minitab reports the R^2, adjusted R^2, C_p statistic and the standard error of the regression model. The C_p statistic is calculated as follows:

$$C_p = \frac{SSE_p}{MSE_m} - (n - 2p) \qquad (3.1)$$

where

SSE_p = the sum of squares of error for the best model with p predictors;
MSE_m = the mean square error for the model with all m predictors;
n = the number of data points and;
p = the number of predictor variables in the best model Minitab (1994).

The best model is selected by choosing the model with the least number of predictor variables, the highest R^2, C_p less than the number of predictor variables and minimum standard error of the regression. Once the best predictors are determined, a multiple linear regression is performed to determine the coefficients for each predictor.

Based on this analysis, the best model for rutting including up to two factors is PG grade and FAc (the coarse aggregate to fine aggregate ratio as determined by the Bailey Method).The regression equation is:

Rut Depth = 41.46 – 0.413 Actual PG grade– 14.86 FAc (3.2)

R^2 = 0.73
Adjusted R^2 = 0.71
MSE = 1.93
Cp = 3.0
N = 22

This analysis showed that the most influential factor in the HMA resistance to rutting is clearly the grade of the binder. (The effect of aggregate quality could not be determined since there were no poor aggregates used in the study.) The correlation between the rut depth and the actual PG grade was r = -0.78, which is the expected trend for this relationship.

The best fit equation for two independent variables is provided in equation 3-2 and indicates that the coarse aggregate to fine aggregate ratio from the Bailey method along with the grade of AC binder is important. This equation has an R^2 of 0.71 but this is not greatly better than that for PG grade alone which has an R^2 of 0.61. The addition of other variables was not evaluated since models with more than a couple of independent variables generally have little practical significance.

Laboratory Tests for Predicting Rutting

One of the greatest needs in the pavement engineering field is a simple and reliable test that will indicate whether or not an asphalt mixture will perform satisfactorily under traffic.

Figure 3.9 shows the correlation of results from APA testing to rutting measured at the end of the first cycle of traffic. This figure only includes sections from the North and South tangents to eliminate potential of bias due to trailer wander in the curve sections. This figure shows results from APA testing of SGC specimens and cores taken from the ends of the sections. SGC specimens were compacted to N_{design} gyrations for each respective mix. Although the trend is correct for this data, the correlation for the SGC specimens is poor. The APA tests on the cores were conducted at the University of Tennessee. This data set included only 15 of the 26 tangent sections. However, the correlation is much better.

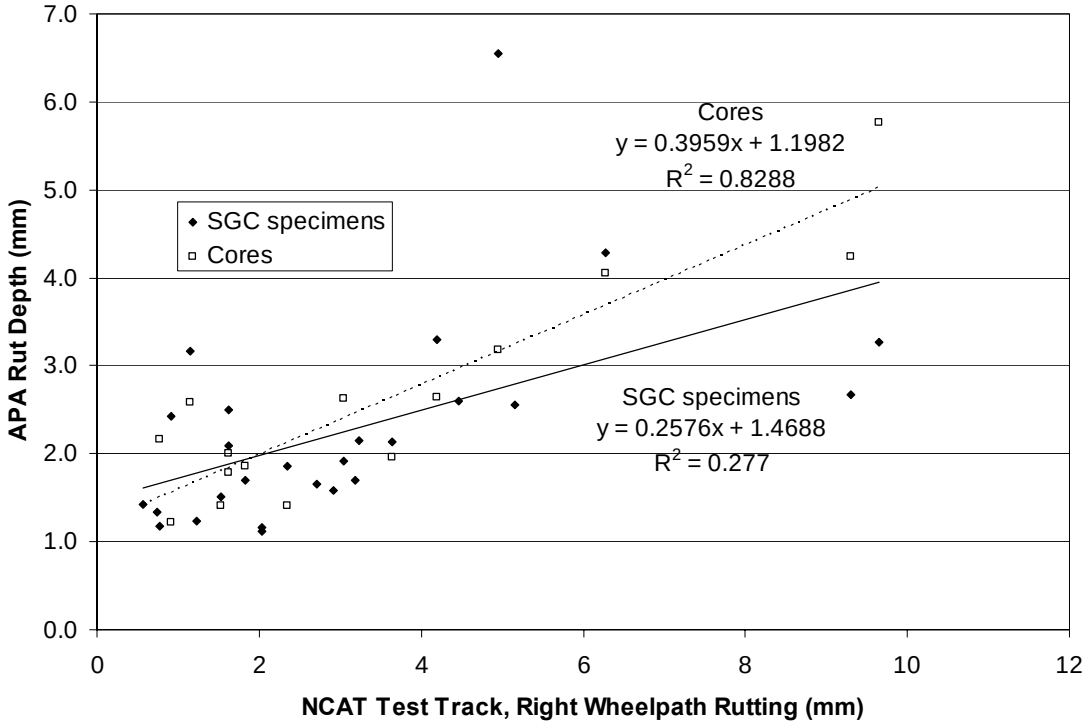

Figure 3.9 Correlation of APA Rut Test Results to Test Track Rutting.

Comparison of HMA with Modified and Unmodified Asphalts

One issue that continues to concern DOTs is the practice of grade bumping or modified vs. unmodified asphalts. Recall that in the first cycle of testing Brown, et al (2002) the modified asphalts (PG 76-22) reduced the rutting by more than 60% over the unmodified sections (PG 67-22). This work was continued in Phase II of the track to determine if the reductions in Phase I could be verified in Phase II.

Rutting measurements were taken weekly using a dipstick throughout the life of the project. After 9 million ESALs on Phase II, the rutting shown in Figure 3.10 was measured on sections where side by side comparisons could be made between modified sections and unmodified sections. This resulted in an average rut depth for the unmodified asphalt mixture of 6mm in the eight sections. The modified sections had an average rutting of 2.7mm. So the results of this

series of tests resulted in a reduction of 55% when using a modified asphalt, compared to 60% on the Phase I tests. Even so, there was no significant rutting in any of the modified or unmodified sections that were used for the mixture study.

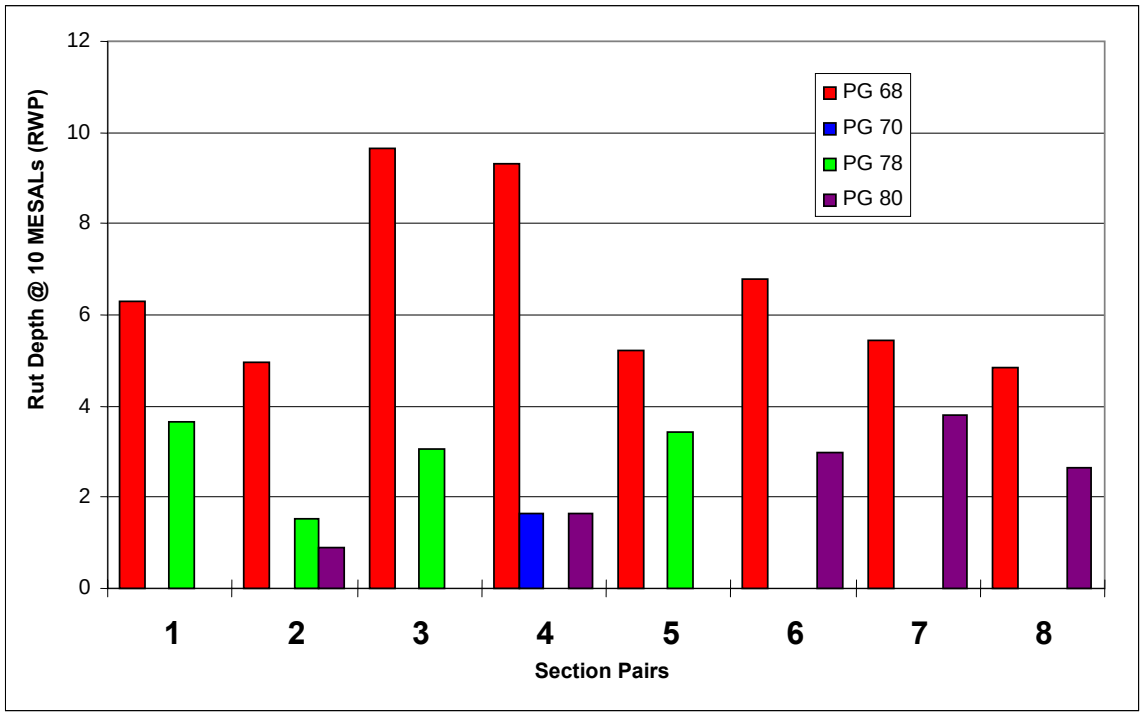

Figure 3.10 Comparison of Rutting Between Modified and Unmodified Sections.

Only one of the sections used in the comparison between modified and unmodified asphalts had any cracking. The section with 74 linear feet of cracking was a modified asphalt that was classified as a PG 80-22.

Performance Comparisons of Coarse and Fine-Graded Mixtures

At the beginning of Superpave implementation, there was a general shift toward the use of coarser gradations for HMA mixtures. It was initially believed that coarse-graded mixtures would provide improved rutting resistance due to better interlock of coarse aggregate particles. However, the performance results at Westrack appeared to contradict that hypothesis. Some pavement engineers began to question the assumption that coarse graded mixtures were more rut resistant. Other pavement issues, such as permeability of coarse-graded mixtures, difficulty with field compaction, tender mixes, and segregation also fueled the debate about whether coarse-graded mixtures were really superior to fine-graded mixtures.

The Test Track provided an excellent opportunity to make comparisons between coarse and fine-graded HMA. An initial review of the performance of the test sections at the completion of the first cycle indicated that both gradations provided very good rutting resistance. However, further analysis was needed with regard to many other measures of performance. Also, a few sections were left in place during the second cycle which allowed for extended comparisons.

Although all of the test sections at the Test Track could be categorized according to their gradation for broad analysis, the many other factors which make test sections unique would

make direct comparisons difficult. Therefore, this analysis deals with a small group of test sections where more direct comparisons could be made. Nine sets of test sections from the first cycle are shown in Table 3.5. Within each set, aggregate sources, nominal aggregate size, binder grade, and the design procedure were the same; the only difference between sections within the set was the gradation and consequently, the optimum asphalt content. All of the test sections in these comparisons are 12.5 mm nominal maximum aggregate size mixtures. Six of the sets had at least one of the sections replaced in 2003. Comparisons of these sets include analyses of differences in design asphalt content, field compactability, rutting performance, friction, permeability, smoothness, and noise. As can be seen from the table, three of the sets have a section with an intermediate gradation. Three sets also remained in place for the second traffic cycle. These were sets 1, 2, and 4 (as indicated by +2 after the section number). These sections provide a better indication of the effect of gradation on long term durability.

Table 3.5 Gradation Comparison Section Sets.

Set	Description: Agg type, Actual PG grade, Modifier Type, Added Aspahlt	Coarse Gradation Section	Intermediate Gradation Section	Fine Gradation Section
1	Granite, PG 68	S9-1+2		S10-1+2
2	Limestone & RAP, PG 68	S7-1+2		S6-1+2
3	Granite, PG 68	E2-1	E6-1+2	E8-1+2
4	Granite, PG 78, SBS	E4-1+2	E5-1+2	E9-1+2
5	Granite, PG 80, SBR	E3-1	E7-1+2	E10-1
6	Limestone & Slag, PG 78, SBS	N9-1		N1-1
7	Limestone & Slag, PG 68	N6-1		N4-1
8	Limestone & Slag, PG 68, Opt.+	N5-1		N3-1
9	Lms & Slag, PG 78, SBS, Opt.+	N10-1		N2-1

Comparisons of the following data are analyzed for each set: asphalt content, compactability, rut depths, cracking, skid resistance, tire-pavement noise, and texture change. Although statistical analyses are used to discern differences in test track measurements in many comparisons, the practical differences in performance between sections are also discussed.

Asphalt Content - An inherent difference between coarse and fine-graded mixtures is the optimum asphalt content. Some pavement engineers have noted that Superpave mixtures have lower asphalt contents compared to the mix designs used prior to Superpave. Some of the difference can be attributed to shifts in gradation during this time. Optimum asphalt content is also affected by compactive effort. For each set in this analysis, the mixtures have the same compactive effort. Table 3.6 shows the asphalt contents from production testing for each mixture. As expected, for most sets, the asphalt content for the fine gradations was highest, the coarse graded mixtures were lowest, and the intermediate gradations were in between. On average, the fine graded mix of each set had about 0.6% higher asphalt content than the corresponding coarse mix. This difference is believed to be significant in its effect on mixture durability; the mixtures with higher asphalt content should have better durability.

Table 3.6 Production Asphalt Contents (%) for Gradation Sets.

Set	Sections (Cse./Int./Fine)	Description	Coarse Section	Int. Section	Fine Section
1	S9/ /S10	Granite, PG 68	4.7		5.2
2	S7/ /S6	Lms & RAP, PG 68	6.6		6.2
3	E2/E6/E8	Granite, PG 68	4.7	5.0	5.6
4	E4/E5/E9	Granite, PG 78, SBS	4.7	5.1	5.4
5	E3/E7/E10	Granite, PG 80, SBR	4.8	4.8	5.8
6	N9/ /N1	Lms & Slag, PG 78, SBS	6.7		7.4
7	N6/ /N4	Lms & Slag, PG 68	6.8		6.8
8	N5/ /N3	Lms & Slag, PG 68, Opt.+	6.9		7.6
9	N10/ /N2	Lms & Slag, PG 78, SBS, Opt.+	6.8		7.8

Compactability - Gradation type is also generally believed to influence compactability during pavement construction. Test track construction records were examined for the gradation comparison sets to determine if more compactive effort was necessary for one gradation compared to the other or if a higher density was achieved for the same compactive effort. The available data is shown in Table 3.7. No compaction data was available for the three pairs in the East curve. For set 1, the coarse section received more passes with the vibratory and static steel wheel roller, but the fine section received many more passes with the rubber tired roller. The temperatures at the start of rolling were almost the same and the final densities were similar. For set 2, the fine section was rolled much more, but the temperature at the start of compaction was about thirty degrees lower. Therefore there is insufficient information for the first two pairs to draw a conclusion regarding compactability. For sets 6, 7, and 9, the data clearly shows that the fine sections required less compactive effort than the corresponding coarse sections. For set 8, the compactive effort was similar for both gradations, but the mat temperature was 24ºF lower at the beginning of compaction operations for the fine mix. This data does not give a clear indication of which gradation type is easy to compact but the trend appears to be that the fine-graded mixes are easier to compact. This appears also to match the experience of many state DOTs.

Table 3.7 Roller Patterns, Compaction Temperature, and Final Construction Density for Test Sections.

Set	Section	Gradation Type	Vibratory Roller Passes	Static Roller Passes	Rubber Tire Roller Passes	Temperature at Start of Compaction (ºF)	Density (% of Gmm)
1	S7	coarse	4	1		283	93.2
	S6	fine	2		8	281	92.9
2	S9	coarse	2	1		274	93.4
	S10	fine	4	2		243	93.6
6	N9	coarse	6			222	94.5
	N1	fine	2	1		240	95.1
7	N6	coarse	6	1		249	94.4
	N4	fine	2			225	93.4
8	N5	coarse	3	2		253	93.8
	N3	fine	2	3		229	94.1
9	N10	coarse	6			234	94.7
	N2	fine	2	1		237	94.7

Rutting Data - Rutting of the NCAT test track sections was measured using two techniques. Each week, measurements were made with a FACE technologies dipstick along three transverse lines across the test sections. The three locations were randomly determined prior to trafficking. From the dipstick measurements, transverse profiles were constructed and rut depths were calculated for each wheelpath. Rutting data from the dipstick profiles were used with traffic data to monitor changes in the rut depths over time and traffic.

The second method for measuring rutting at the test track involved pulling a string-line across the sections at the three locations used for the dipstick profiles. For each of the three transverse locations per section, rut depths were measured from the string-line to the deepest part of the depression in each wheelpath. String-line measurements were felt to best represent the true rutting. However, string-line measurements were only made at the conclusion of trafficking for the cycles. Since this report was prepared prior to the conclusion of the second cycle, the rutting data used for sections subjected to both cycles is based on dipstick profiles.

Table 3.8 shows the rut depths measured by the string-line technique at the conclusion of the first cycle for each of the gradation comparison sets. It can be seen for sets 4 and 8 that the average rut depths at ten million ESALs were very similar (less than 1 mm difference). Three of the remaining seven pairs had greater rut depths for the fine-graded mixtures, and the other four had more rutting for the coarse-graded mixtures.

Table 3.8 Average Right Wheelpath Rut Depths (mm) at 10 Million ESALs.

Set	Sections (Cse./Int./Fine)	Description	Coarse Section	Int. Section	Fine Section
1	S9/ /S10	Granite, PG 68	3.2		5.2
2	S7/ /S6	Lms & RAP, PG 68	4.8		3.2
3	E2/E6/E8	Granite, PG 68	6.5	5.4	5.2
4	E4/E5/E9	Granite, PG 78, SBS	3.9	5.0	3.4
5	E3/E7/E10	Granite, PG 80, SBR	5.9	3.8	3.0
6	N9/N1	Lms & Slag, PG 78, SBS	0.9		3.6
7	N6/N4	Lms & Slag, PG 68	5.0		6.3
8	N5/N3	Lms & Slag, PG 68, Opt.+	9.3		9.7
9	N10/N2	Lms & Slag, PG 78, SBS, Opt.+	1.6		3.0

An analysis of variance was conducted using rut depth as the response variable and "Set" and "Gradation" as fixed-effect factors. The comparisons here are only between Coarse and Fine gradations. The output of this analysis indicated that Gradation was not a significant factor affecting rut depth ($P = 0.228$).

Three of the nine original section sets for gradation analysis remained in place for the second cycle and therefore were subjected to traffic over a five year period. The average rut depths in the right wheelpaths for these sections are shown in Table 3.9. This data is based on rut depths calculated from dipstick profiles taken after an accumulated nineteen million ESALs. This data also shows that both coarse and fine-graded sections continue to perform very well. As before, neither coarse nor fine gradation type appears to be consistently better than the other in regard to resistance to deformation.

Table 3.9 Right Wheelpath Rut Depths (mm) for Coarse/Fine Pairs at 19 Million ESALs.

Set	Sections (Cse./Int./Fine)	Description	Coarse Section	Int. Section	Fine Section
1	S9/ /S10	12.5 Granite, PG 68	3.1		4.1
2	S7/ /S6	12.5 Limestone/RAP, PG 68	5.7		4.3
4	E4/E5/E9	12.5 Granite, PG 78, SBS	4.8	5.0	2.3

Cracking - Very few sections were observed to have any form of cracking at the conclusion of trafficking for the first cycle. This cracking was limited to a few minor edge cracks and cracks along longitudinal joints. Of the sections that remained in place for the second cycle, three sections had identifiable cracking: S2, S13, and E7. Only E7 is of significance in this analysis of effect of gradation on cracking. Since S2 is coarse-graded, S13 is fine-graded, and E7 is an intermediate grade, there is no clear trend between gradation and cracking.

Skid Resistance - Skid resistance of a pavement surface is a very important performance consideration. The most common measure of skid resistance for highways is ASTD E 274,

Standard Method for Skid Resistance of Paved Surfaces Using a Full-Scale Tire. Skid tests using this standard were conducted monthly on all track sections by the Alabama Department of Transportation (Figure 3.11). Plots of skid resistance versus time were made for each coarse-fine pair. An example of this graphical analysis is shown in Figure 3.12. From these graphs, it was apparent that for most pairs there was no practical difference between the coarse-graded and fine graded sections. For a few pairs, there was some apparent difference in skid resistance. To better quantify the possible differences in skid resistance, the data for each pair were analyzed using paired t-test. The results of this statistical analysis are shown in Table 3.10. Overall there does not appear to be a significant difference in friction between fine-graded and coarse-graded mixtures. Of course this probably will not be true for all aggregates such as those that tend to polish.

Figure 3.11 Measuring Friction with Skid Trailer.

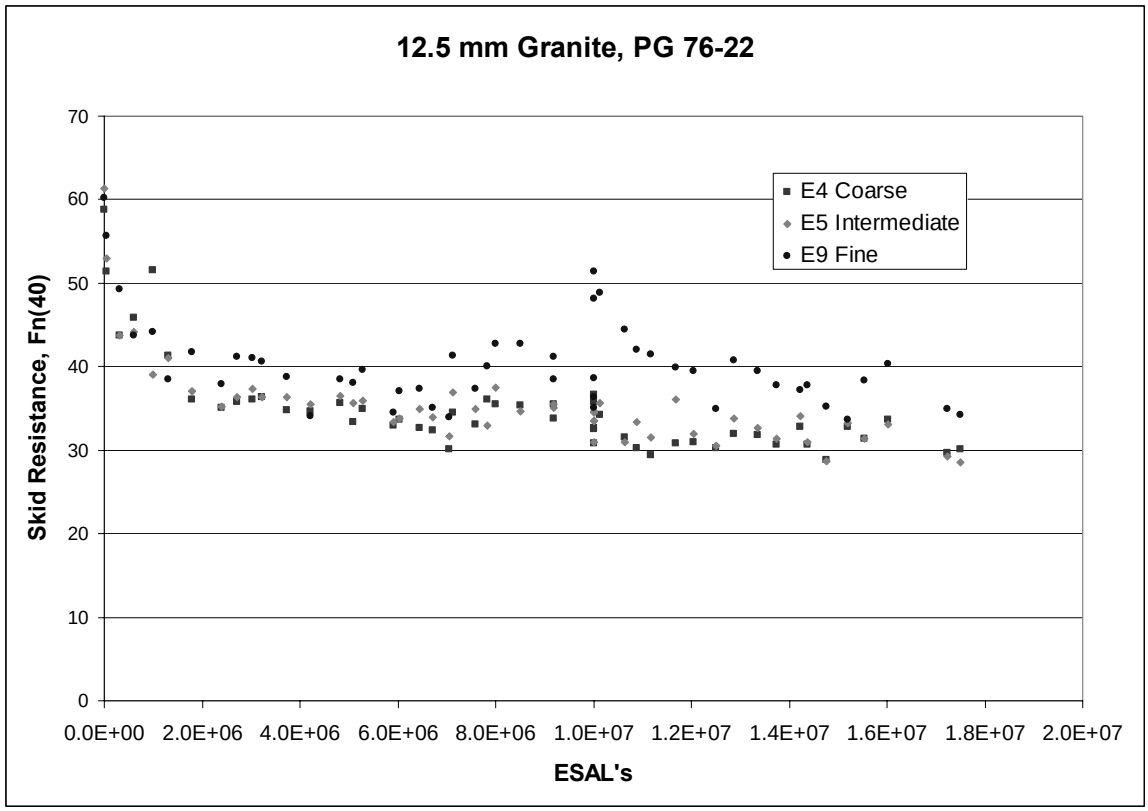

Figure 3.12 Comparison of Skid Resistance for Coarse-Fine Analysis Pair 6.

Table 3.10 Summary of Paired t-tests for Skid Resistance of Coarse and Fine Graded Superpave Sections.

Pair	Sections (Coarse/Fine)	95% Confidence Interval for Difference of Skid Data	P value	Best
1	S9/S10	-0.0018 to 1.7818	0.050	Coarse
2	S7/S6	-1.6508 to 1.6008	0.975	Same
3	E2/E8	0.9894 to 3.2406	0.001	Coarse
4	E4/E9	-4.0708 to -0.9292	0.004	Fine
5	E3/E10	-5.7353 to -3.8047	0.000	Fine
6	N9/N1	-0.8320 to 1.2220	0.695	Same
7	N6/N4	1.6389 to 5.2411	0.001	Coarse
8	N5/N3	-0.0040 to 1.2341	0.051	Same
9	N10/N2	-0.1540 to 1.1840	0.124	Same

Tire-Pavement Noise - In recent years, tire-pavement noise has received a lot of attention. Studies have shown that pavement surface type (gradation or macrotexture) can be a significant factor in tire-pavement noise. NCAT conducted tire-pavement noise measurements using the close-proximity method (CPX) in accordance with ISO Standard 11819-2 on the track test sections.

CPX measurements were made on the track sections in September 2001, which was about one year after the construction of the original test sections was completed. Sound intensity measurements using an Aquatread tire were made for three laps of the track for statistical analysis of variance. Average decibels for the sections in the nine pairs are shown in Table 3.11.

Table 3.11 Average Sound Intensity Measurements ((dB(A)) for Coarse and Fine-graded Section Sets.

Set	Sections (Coarse/Fine)	Description	Coarse Section	Fine Section
1	S9/S10	Granite, PG 68	95.08	94.21
2	S7/S6	Limestone/RAP, PG 68	94.79	94.97
3	E2/E8	Granite, PG 68	95.03	94.89
4	E4/E9	Granite, PG 78, SBS	95.72	94.39
5	E3/E10	Granite, PG 80, SBR	94.94	93.05
6	N9/N1	Limestone/slag, PG 78, SBS	94.83	94.15
7	N6/N4	Limestone/slag, PG 68	95.11	94.70
8	N5/N3	Limestone/slag, PG 68, Opt.+	94.45	94.17
9	N10/N2	Limestone/slag, PG 78, SBS, Opt.+	94.73	94.48

Although the differences between the tire-pavement noise measurements within each pair seems small, differences between coarse and fine sections analyzed using a paired t test statistic indicate that the tire-pavement noise for the coarse sections was greater than the fine sections. Since replicate measurements were made, the experiment was also analyzed as a randomized complete block design where the blocks are the pairs. This analysis confirmed that gradation was statistically significant ($P = 0.003$) on tire-pavement noise measurements.

Permeability - Permeability of some Superpave mixtures has been reported to be a problem. In general, it has been noted that coarse-graded mixtures are more permeable than fine-graded mixtures at the same air void contents typical of new construction. Permeability of HMA pavements has been measured with several different procedures. In the past several years, the two most common methods used to measure permeability have been the former ASTM provisional standard based on the Carol-Warner laboratory permeameter device and the simple falling-head field permeameter developed by NCAT. Some sections of the test track were tested for permeability using the NCAT field permeameter. One of those occasions was during a study to evaluate the repeatability of the field permeability procedure. During these experiments, only one of the coarse versus fine-graded comparison pairs was used in the field tests. Based on 70 measurements, the average field permeability of section S9, a coarse graded mixture was 79×10^{-5} cm/sec, and its companion fine graded section, S10, was 5×10^{-5} cm/sec. Although the coarse section was more permeable, its average result was still considered to be well below the general

critical range of $100x10^{-5}$ cm/sec. Later measurements of permeability at the track resulted in even lower permeability results for these and all test sections except those with OGFC as the surface layer. The low permeability results for the NCAT test sections can be attributed to the high level of density achieved during construction. There is really not enough data from the track to clearly show the differences in permeability between fine and coarse-graded mixtures. However, there have been sufficient studies to show that coarse-graded mixes become permeable if the amount of compaction is slightly less than desirable. This is a bigger problem with coarse-graded mixes than with fine-graded mixes.

CHAPTER 4: STRUCTURAL STUDY

Introduction

The structural study as part of the 2003 Test Track experiment was conducted to meet the needs of mechanistic-empirical (M-E) pavement design. Specifically, pavement sections were constructed to various thicknesses and with various material composition, with embedded instrumentation, to study the interaction between pavement response and performance. This chapter details the pavement sections, instrumentation systems, mechanistic pavement properties, fatigue performance and rutting performance.

Experimental Design[1]

With only eight sections devoted to the structural experiment, and many factors that could be investigated, it was impossible to execute a full factorial examining all possible combinations. Therefore, it was decided to focus primarily upon the effects of HMA thickness and binder modification as they relate to structural performance. In future testing cycles, as more sections may be devoted to a structural experiment, additional factors may be evaluated. In fact, the results of this experiment will help guide future experimental designs.

Generally speaking, the eight sections were designed for varying traffic levels arriving at a thin, medium and thick design for three sections using an unmodified binder (PG 67-22). These three sections were repeated with another three, but with an SBS polymer modified binder (PG 76-22) used throughout the depth of the HMA. The final two sections were designed for the medium traffic level with a stone-matrix asphalt (SMA) surface course of one inch. The last section, in addition to the SMA surface course, had a rich bottom with an additional 0.5% binder. For all sections, the layers beneath the HMA consisted of a six inch dense graded aggregate base used previously in the 2000 Test Track research cycle. Beneath the base was a fill layer to bring all of the test sections to the same elevation. The fill was the same material as previously used at the Test Track.

It was hypothesized that these eight sections would exhibit differing performance and types of distress over the two-year trafficking cycle. The varying thicknesses were selected to ensure that some meaningful distresses (i.e., fatigue cracking, structural rutting) were observed; some earlier than others. Also, the modified binders, rich bottom and modified surface sections were selected to allow meaningful comparisons between conventional and modified mixes.

The layout of the test sections was such that construction and rehabilitation efforts were made as efficient as possible. For example, it was more efficient to place the thick sections together to more easily maintain a uniform cross slope.

Structural Design[1]

The structural design of the eight sections was done according to the 1993 AASHTO Design Guide methodology. The input parameters are defined in Table 4.1. The level of reliability and variability were chosen to be consistent with current AASHTO recommendations (Huang, 1993). The axle weights were the current weights on the triple trailers in use at the track. The structural coefficients (a_i) were the same as used previously in designing the existing test sections. Since similar materials were again utilized, they were considered still appropriate. Additionally, the

[1] Excerpt from Timm et al, 2004

drainage coefficients (m_i) for the unbound material were assumed to have a value of 1.0. The stiffnesses of the aggregate base and improved soil were correlated using the structural coefficients and figures in the 1993 AASHTO Guide.

Table 4.1 Structural Design Inputs (Timm et al, 2004).

Input Parameter	Value
Reliability	95%
Variability	0.45
ΔPSI	1.2
Axle Weights per Truck	Steer Axle = 12 kip Tandem Axle = 40 kip 5 Single Axles = 20 kip / axle
HMA Structural Coefficient (a_1)	0.44
Dense Graded Aggregate Base Coefficient (a_2)	0.14
Dense Graded Aggregate Base Stiffness	30,000 psi
Improved Subgrade Soil Structural Coefficient (a_3)	0.05
Improved Subgrade Soil Stiffness	8,000 psi
Subgrade Soil Stiffness	5,500 psi

Since the structural sections were meant to be integrated with the existing test sections, shown in Figure 4.1, the total thickness of the new designs had to equal 30 inches (42 inches including the existing improved subgrade). Also, it was decided to use a six inch granular base, so the remaining 24 inches were comprised of HMA on the top and improved soil on the bottom. The structural design determined these two values for each of the three traffic levels.

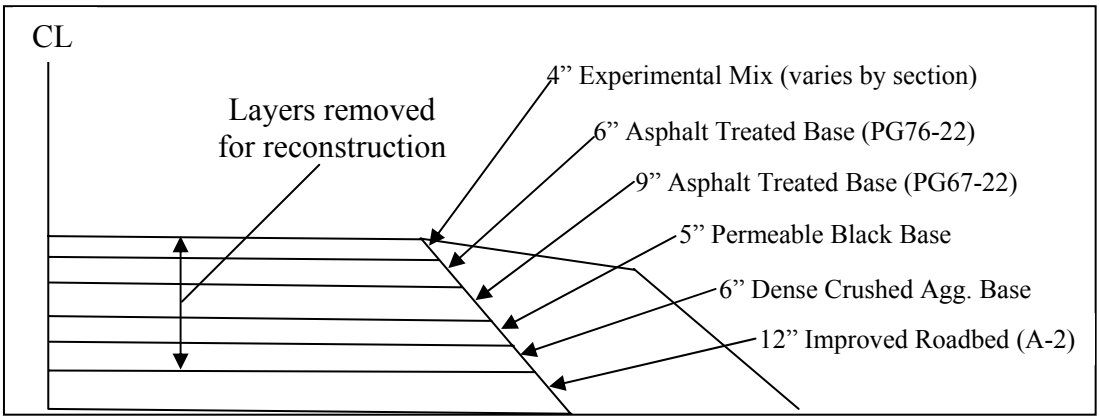

Figure 4.1 Test Track Cross Section Prior to Reconstruction in 2003 (after Jess, 2004).

The number of design ESALs was calculated according to the AASHTO methodology for the axle weights given above (Table 4.1) with the 12 kip steer axle treated as a single axle. It was expected that approximately 965,000 laps of the design vehicle would be applied to the sections, and ESALs would be computed accordingly. It should be noted that an iterative procedure was used to ensure convergence between the structural number (SN) to determine equivalency factors and the required SN obtained from the AASHTO design equation.

As stated above, the objective of the pavement design was to determine the HMA thickness and amount of additional fill. To that end, the following equations were derived and used to find the appropriate thicknesses of each layer.

$$SN = a_1D_1 + a_2D_2 + a_3(D_3 + D_4) \quad (4.1)$$

where: a_1, a_2, a_3 are given above
D_2 = 6 in.
D_4 = 12 in. (existing)
D_1 = unknown HMA thickness, in.
D_3 = unknown additional fill thickness, in.

$$D = D_1 + D_2 + D_3 + D_4 \quad (4.2)$$

where: D = 42 in.

Once the appropriate SN values were determined for each traffic level, the two above equations were solved for the two unknowns, D_1 and D_3. Table 4.2 lists the resulting design thicknesses for each of the three traffic levels. Additionally, since all the traffic would be applied to each of the sections, it was instructive to determine the reliability level at one traffic level. For the purposes of this study, reliability at the previous level of ESALs (10 million) is listed in Table 4.2.

While these thicknesses were derived directly from the AASHTO Guide, it was thought to be beneficial to expand the range of thicknesses, for experimentation sake, to include more diversity in the cross sections. Therefore, it was recommended to change the thicknesses as shown in Table 4.3 which should aid in distinguishing the sections in terms of structural performance.

Table 4.2 2003 Test Track Structural Sections – Preliminary Design (Timm et al, 2003).

Traffic	ESALs, 10^6	HMA, in. (D_1)	GB, in. (D_2)	Additional Fill, in. (D_3)	SN	Reliability at $10*10^6$ ESAL
Full	9.6	9.6	6	14.4	6.4	94.8%
2 / 3	6.3	8.7	6	15.3	6.0	87.9%
1 / 3	3.1	7.2	6	16.8	5.4	67.7%

Table 4.3 2003 Test Track Structural Sections – Final Design (Timm et al, 2003).

Traffic	HMA, in. (D_1)	GB, in. (D_2)	Additional Fill, in. (D_3)	SN	Reliability at $10*10^6$ ESAL
Full	9	6	15	6.2	92%
2 / 3	7	6	17	5.4	68%
1 / 3	5	6	19	4.6	30%

Test Section Layout[2]

As stated previously, the test sections were laid out to minimize construction and rehabilitation efforts. Figure 4.2 summarizes the experimental sections, in addition to the final section assignments (i.e., N1 – N8).

[2] Excerpt from Timm et al, 2004

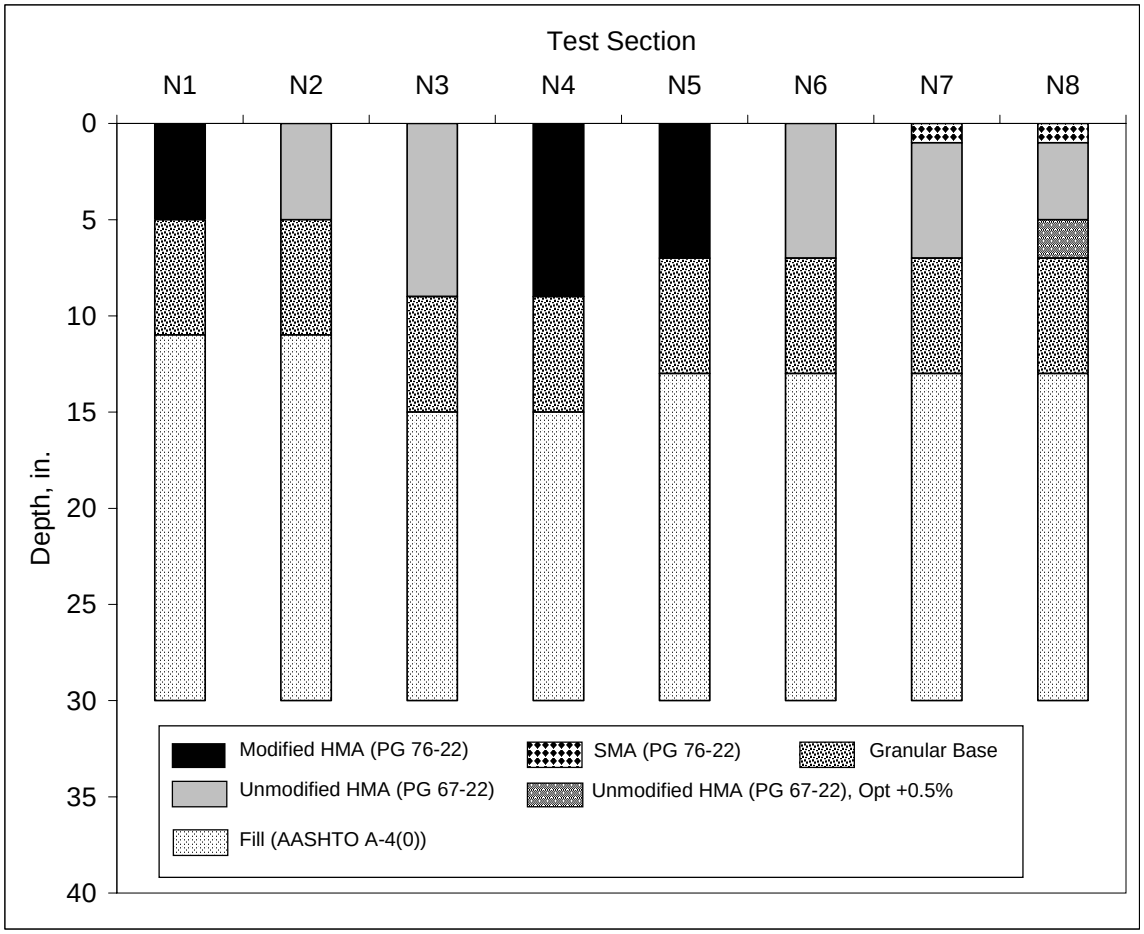

Figure 4.2 Final Design and Section Layout (after Timm et al, 2005).

Instrumentation[2]

For a mechanistic pavement design experiment, it is well known that there are two primary critical locations to monitor pavement responses under load. These are at the bottom of the asphalt concrete layer and at the top of the unbound granular layers, respectively. Responses in these two locations have been correlated to fatigue cracking and structural rutting, respectively (e.g., Timm and Newcomb, 2003). Therefore, when selecting instrumentation, it was desired to have gauges that would measure responses in these locations. Prior to evaluating instrumentation vendors, experiences from two previous, yet ongoing, instrumented pavement studies were reviewed. The Minnesota Road Research Project (Baker et al, 1994) and the Virginia SmartRoad (Smart Road, 2003) both had extensive literature and web-site information regarding their experiences in instrumenting their respective pavement sections. Based on these findings, asphalt strain gauges, pressure plates and thermistors were selected and are described below.

Asphalt Strain Gauges

Gauges manufactured by Construction Technologies Laboratories (CTL) appeared reasonably priced with a short delivery time and had been widely used to instrument flexible pavements. A strain gauge, with dimensions in inches, is shown in Figure 4.3. The sensor itself is a 350Ω Wheatstone Bridge mounted on a nylon 6/6 bar. There are four active gauges; two aligned with the maximum longitudinal strain and the other two with the transverse strain. The approximate stiffness of the nylon is 340,000 psi. Individual calibration sheets were provided with each

gauge. The CTL gauges were designed and constructed to be applicable to most pavement cross-sections. The maximum range on the gauges was ±1,500 με which is well within expected strain ranges for most flexible pavements.

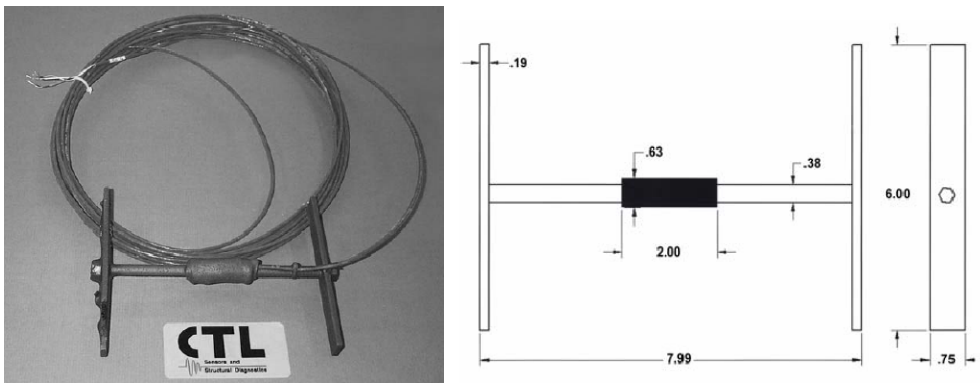

Figure 4.3 CTL Asphalt Strain Gauge (Timm et al, 2004).

Earth Pressure Cells

The role of the earth pressure cell is to measure the dynamic vertical pressures generated under moving loads. As will be explained later in this chapter, these gauges were placed at the top of the granular base course and at the top of the subgrade. While it would be advantageous to also measure vertical strain, these types of gauges were not used because of prohibitively high cost.

The gauge used in this experiment was the Geokon 3500 earth pressure cell. Pictured in Figure 4.5, this device consisted of two circular stainless steel plates welded together around their periphery and spaced apart by a narrow cavity filled with de-aired oil. Changing earth pressure squeezes the two plates together causing a corresponding increase of fluid pressure inside the cell. The semi-conductor transducer converts this pressure into an electrical signal which is transmitted as a voltage change via cable to the readout location. Figure 4.5 shows one test cell just after receipt at the Test Track in addition to the profile of the plate.

Figure 4.4 Geokon Earth Pressure Cell (Timm et al, 2004).

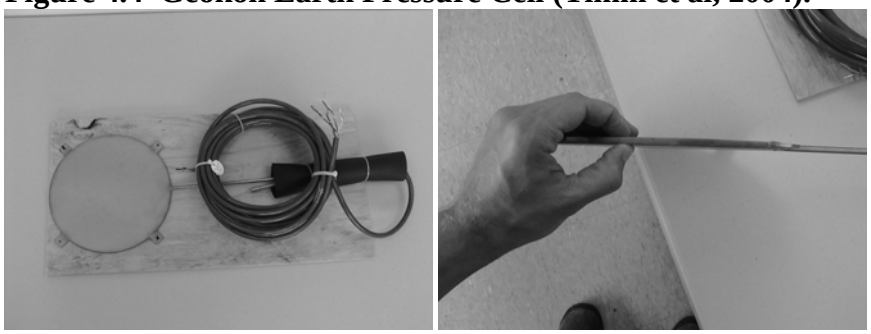

Figure 4.5 Geokon Earth Pressure Cell at the Test Track (Timm et al, 2004).

For the structural experiment, two different full scale gauges were selected corresponding to the two different expected pressure ranges. Since one set of gauges was installed deeper in the structure (top of subgrade) and the other set was closer to the surface (top of base), 14.5 psi (100 kPa) and 36.3 psi (250 kPa) gauges were selected, respectively. These full scale values were arrived at through a preliminary mechanistic analysis using WESLEA for Windows, a layered elastic pavement analysis computer program (Van Cauwelaert et al, 1989; Timm et al, 1999). Estimates were made regarding material properties and wheel loadings, stresses were calculated at the top of the base and subgrade and it was found that the 14.5 psi and 36.3 psi gauges would work well for the subgrade and base, respectively.

Temperature Profiles

For each test section, four thermistors were bundled together to provide temperature information near the surface, at 2 in., 4 in. and 10 in. depth. A thermistor bundle is pictured in Figure 4.6, while a full description of these gauges was provided by Freeman, et al (2001).

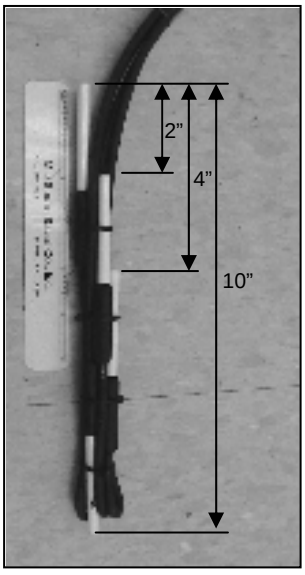

Figure 4.6 Thermistor Bundle for In Situ Temperature (Timm et al, 2004).

Gauge Layout and Installation

The gauges were arranged as depicted in Figure 4.7. The gauge array was centered in the outside wheelpath, with asphalt strain gauges also offset from the center of the wheelpath by two feet. The asphalt strain gauges were oriented to obtain both transverse and longitudinal strain. Figure 4.8 illustrates the location of the gauges in the depth of the pavement.

At the end of construction, all the pressure and temperature probes were operational. The strain gauges had a lower success rate with 75% of the gauges functioning after construction. Full details regarding the calibration and installation of the gauges has been documented elsewhere (Timm et al, 2004).

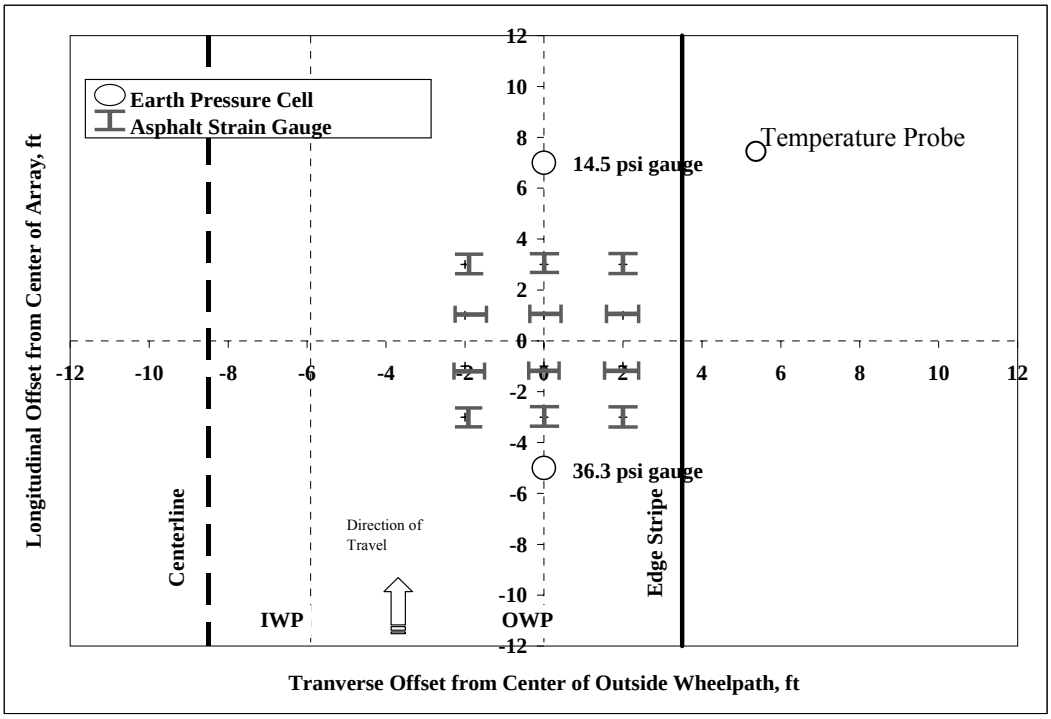

Figure 4.7 Gauge Array.

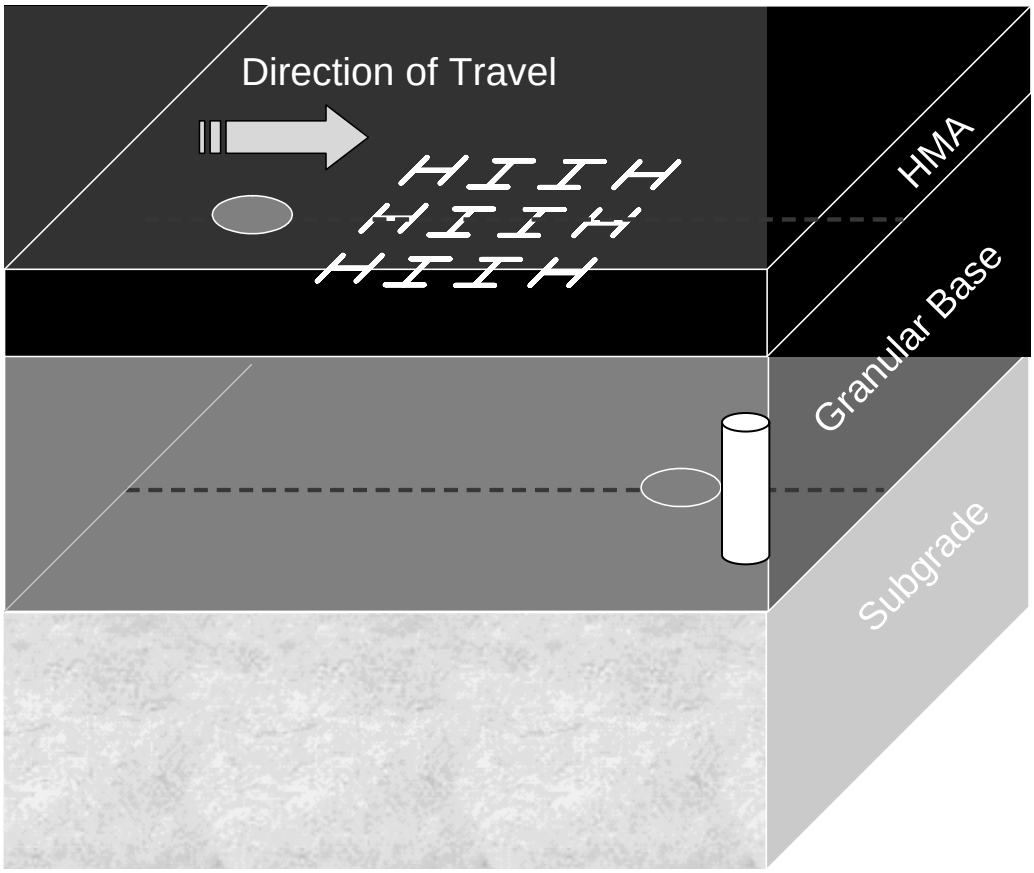

Figure 4.8 3D Schematic of Gauge Arrangement (Timm et al, 2004).

Pavement Response Data Collection

At the start of the 2003 Structural Study, data were collected from the strain and pressure gauges on a monthly basis. Once cracking appeared in Section N1, data were collected every week to track pavement integrity as the sections began to crack. Data collection consisted of recording three passes of each truck on each test section. Figure 4.9 shows the strain response for one pass of a triple trailer vehicle.

For each pass of a vehicle, the average strain and pressure responses were determined for the entire vehicle. This accounted for variation due to wheel wander relative to the gauges and enabled an efficient and repeatable data processing scheme. Further details regarding data processing and analysis are documented elsewhere (Priest, 2005; Timm and Priest, 2004).

While the data from the strain and pressure gauges were collected at most once per week, the temperature probes were monitored continuously. Throughout the experiment, temperature readings were obtained every minute and hourly averages were recorded. These data were critical, as will be shown in later sections, to the development of relationships between environmental conditions, material properties and pavement responses.

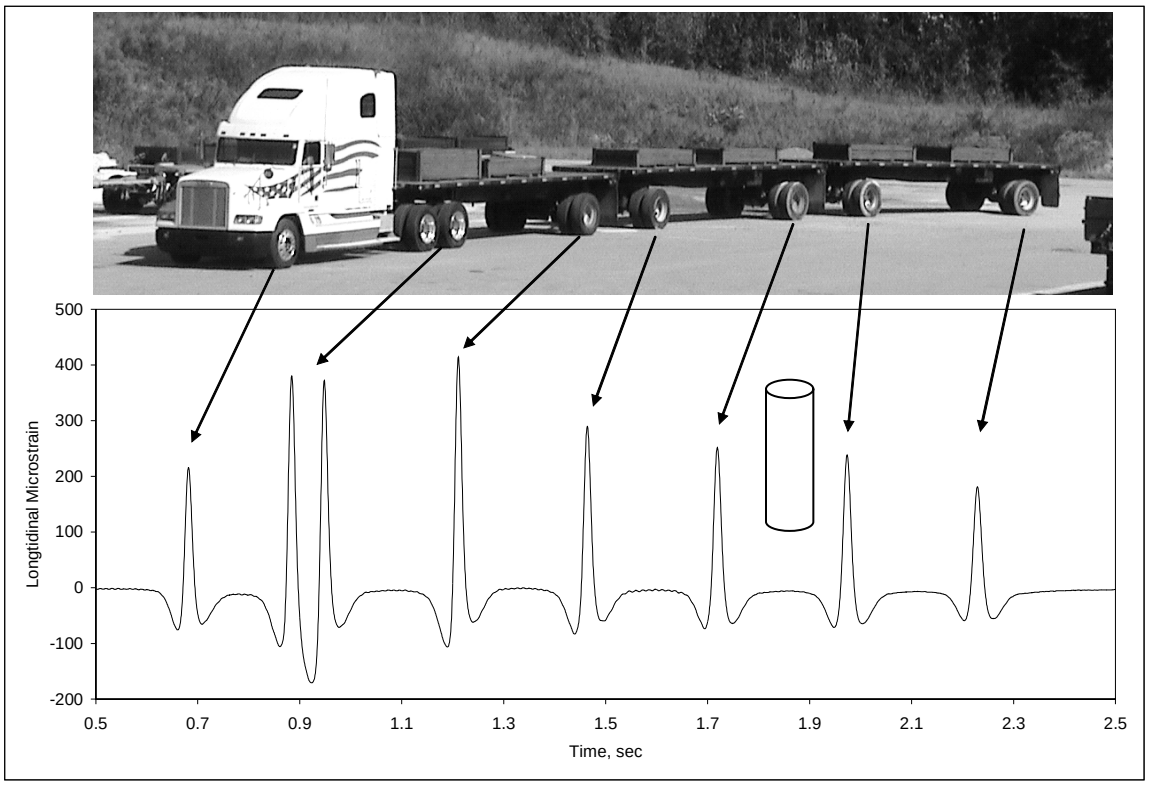

Figure 4.9 Asphalt Strain Trace Under Triple Trailer Vehicle.

Mechanistic Pavement Properties

The material properties pertaining to the component pavement layers in the Structural Study were characterized in both the laboratory and in situ. Full details regarding the characterization are documented elsewhere (Timm and Priest, 2005). The discussion presented herein focuses on the field characterization using a falling weight deflectometer (FWD).

FWD Apparatus and Testing Scheme

ALDOT provided both the FWD and technical personnel for field testing on a monthly basis. The FWD was a Dynatest 8000, pictured in Figure 4.10, with seven sensors spaced at 12 inches on center. The load plate had a radius of 5.91 in. and was a split configuration to ensure good seating on the pavement surface. Testing was conducted at three longitudinal random locations, in both the inside and outside wheelpaths, of each test section. For each location, two drops of a 9,000 lb. load were executed.

Figure 4.10 Dynatest 8000 Used at Test Track.

Supplemental FWD testing was conducted on April 27, 2004 directly on top of embedded instrumentation in each test section. This was done, in part, to aid in determining the optimal cross-section for backcalculation. Pavement responses gathered under the FWD load were used as additional degrees of freedom in the backcalculation process which will be described later. Within each test section, two drops of the 9,000 lb. load were conducted on each pressure plate and two strain gauges (longitudinal and transverse). It is important to note that while the FWD load was dropped on top of individual gauges, responses were measured for the entire gauge array. This enabled measurements with multiple offset distances from the center of the load.

Backcalculation Cross Section

Backcalculation was accomplished using EVERCALC 5.0. Several simulated cross sections were attempted to determine the best grouping of the pavement layers for backcalculation. While further details are provided elsewhere (Timm and Priest, 2005), the optimal cross section is shown in Figure 4.11. In this cross section, the aggregate base and fill material were combined into a single layer. Previous lab studies had also shown that these materials had very similar moduli (Timm and Priest, 2005).

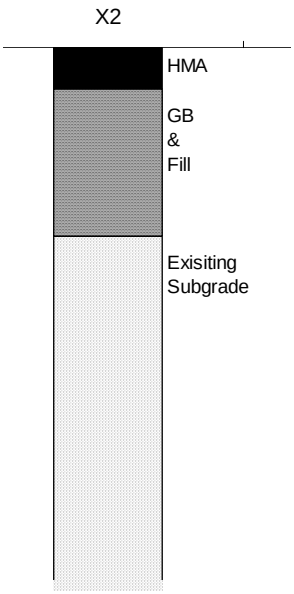

Figure 4.11 Backcalculation Cross Section.

Pavement Response Under FWD Load

Figure 4.12 illustrates an example of the strain response measurements made under the FWD load. The first peak of each trace indicates the primary FWD impact with residual peaks as the load settles onto the pavement. In this example, the load was dropped on the longitudinal gauge in the center of the wheelpath (BLC). The other two traces represent another longitudinal gauge (BLR) two feet to the right of the load center and a transverse gauge (BTC) two feet away from BLR, but also in the wheelpath. Strain readings were recorded from the baseline to the first peak of each trace.

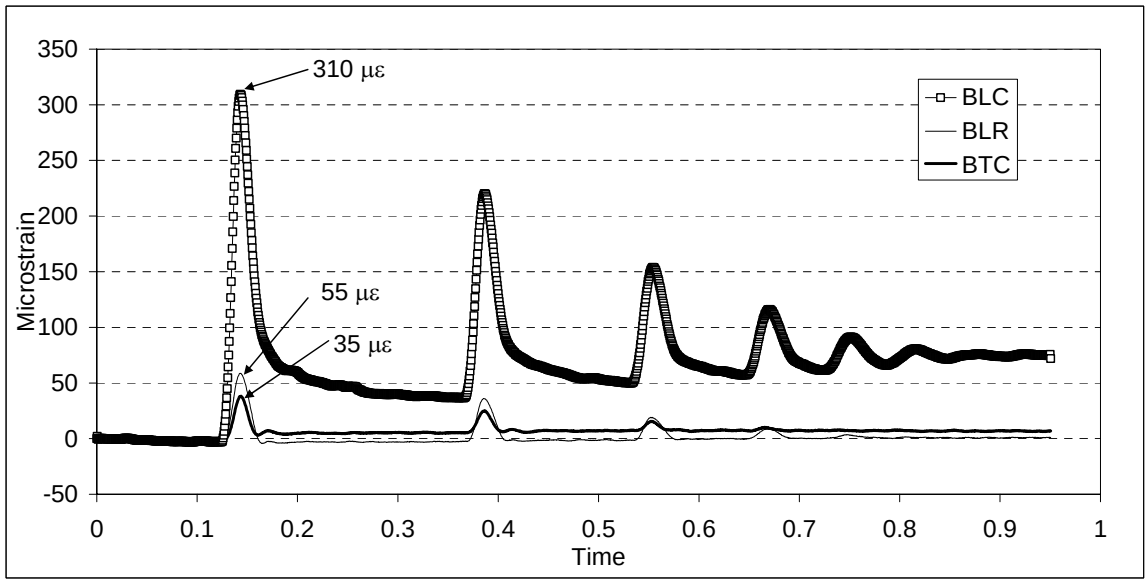

Figure 4.12 Example of Strain Response Under FWD Load.

For each drop of the FWD, backcalculated moduli were obtained which were then input with corresponding thicknesses to WESLEA for Windows 3.0, a forward calculation layered elastic mechanistic pavement model. The contact pressure and impact load recorded by the FWD were also input to WESLEA. Finally, the coordinates of each active gauge in the array, relative to the center of the load, were entered as evaluation locations so that comparisons could be made between measured pavement responses and those computed from WESLEA using the backcalculated moduli as a primary input.

Figure 4.13 and 4.14 summarize the strain and pressure response comparisons, respectively. The figures indicate a reasonably good match between theoretical and measured pavement responses. According to the regression equation in Figure 4.13, the theoretical strains were within about 20% of that measured under FWD loading. A larger deviation was noted in the vertical stresses which showed the theoretical stresses, on average, 30% lower than the measured pressures. It was also noted from Figure 4.14, that the match between measured and theoretical stresses deviated the most above 8 psi. This could be the result of some non-linear behavior of the material exhibited at higher stress levels. Further investigations are warranted to investigate this deviation. However, it must be noted that measured responses are not necessarily perfect either. Therefore, the theoretical and measured responses should just be checked relative to one another. Based on the results in Figures 4.13 and 4.14, the measured and theoretical responses were judged to be a reasonable validation of each other.

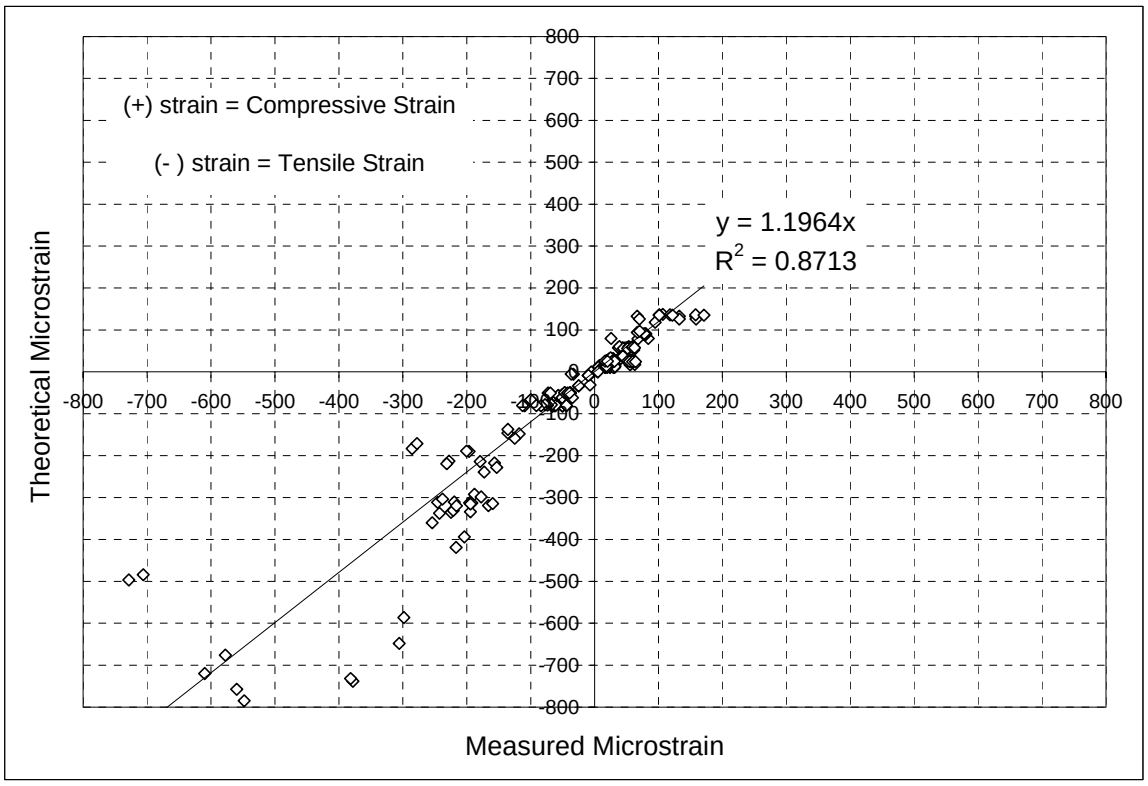

Figure 4.13 Theoretical versus Measured Strain (Timm and Priest, 2005).

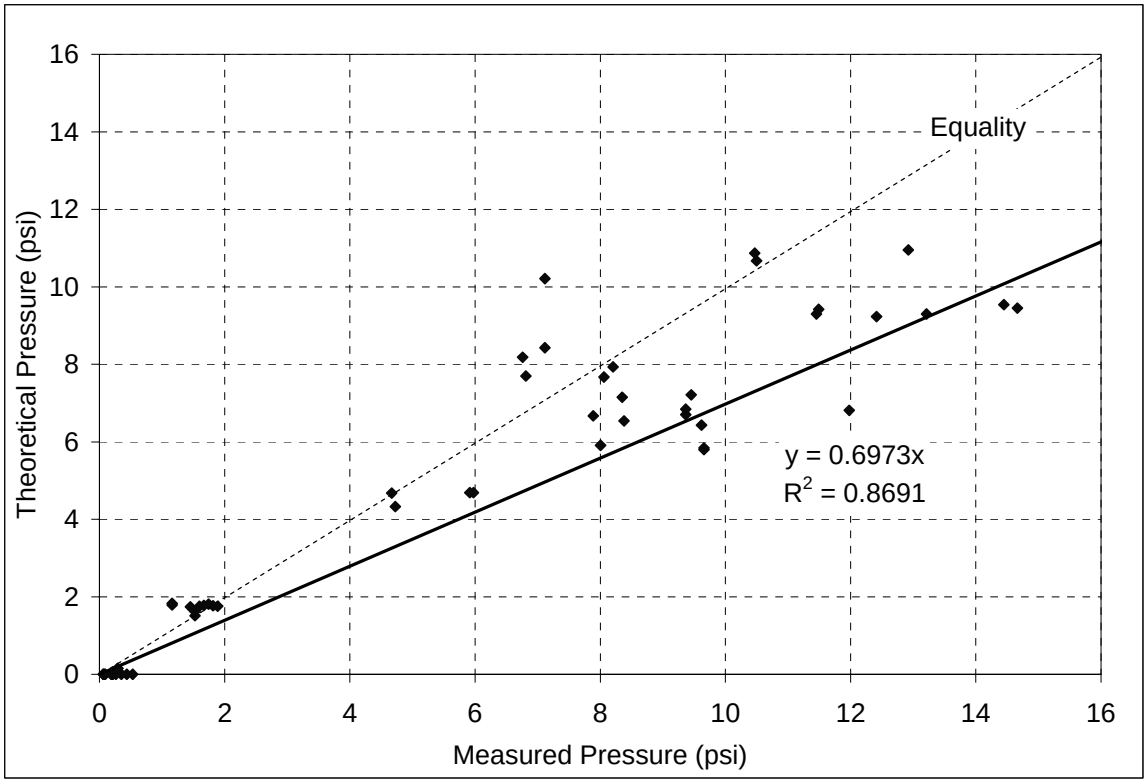

Figure 4.14 Theoretical versus Measured Vertical Stresses (Timm and Priest, 2005).

Seasonal Trends in Layer Moduli

Figures 4.15 through 4.17 show the seasonal trends, by test section, for the HMA, granular base/fill and subgrade layers, respectively. The HMA was most affected by seasonal changes, which was expected since it is well known that HMA stiffness has a strong dependence upon temperature. The underlying pavement layers were not as severely affected by changes in season. This was especially the case for the existing subgrade, which maintained a modulus near 30,000 psi throughout the two-year research cycle (Timm and Priest, 2005).

There were not clear distinctions between test sections, based upon moduli, for any of the three pavement layers. This was expected for the granular base/fill and subgrade layers, respectively, since they were made of the same materials and constructed according to the same specifications. This was also expected for the HMA, based upon the results of dynamic modulus testing in the laboratory (Timm and Priest, 2005), where it was shown that the different mixtures were not statistically different except in the highest temperature ranges.

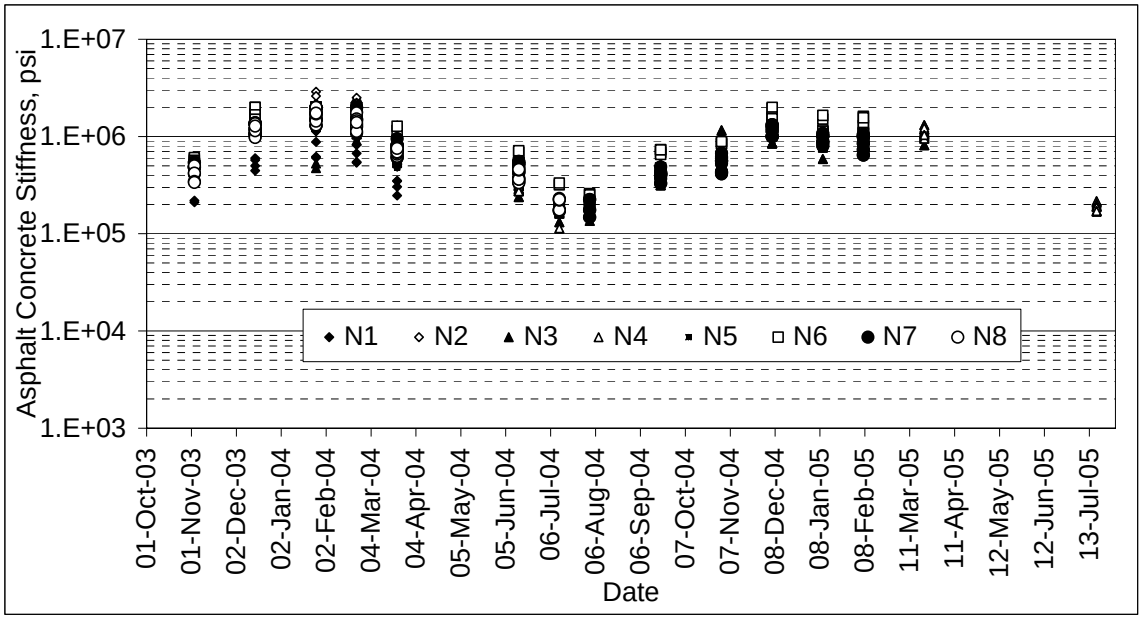

Figure 4.15 HMA Moduli versus Date (Timm and Priest, 2005).

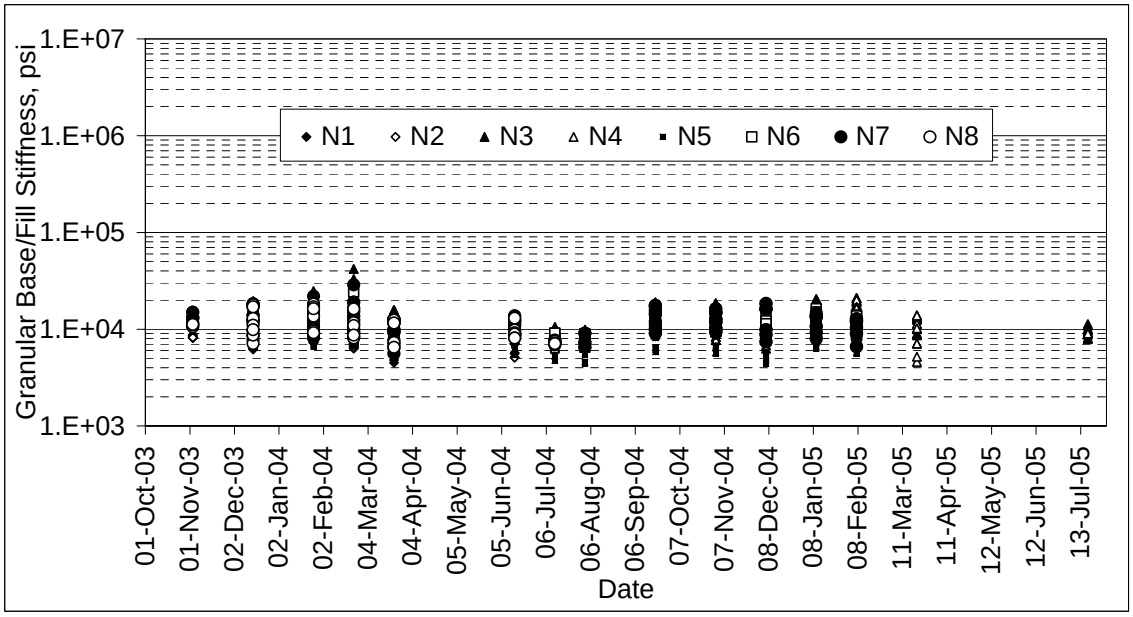

Figure 4.16 Granular Base/Fill Moduli versus Date (Timm and Priest, 2005).

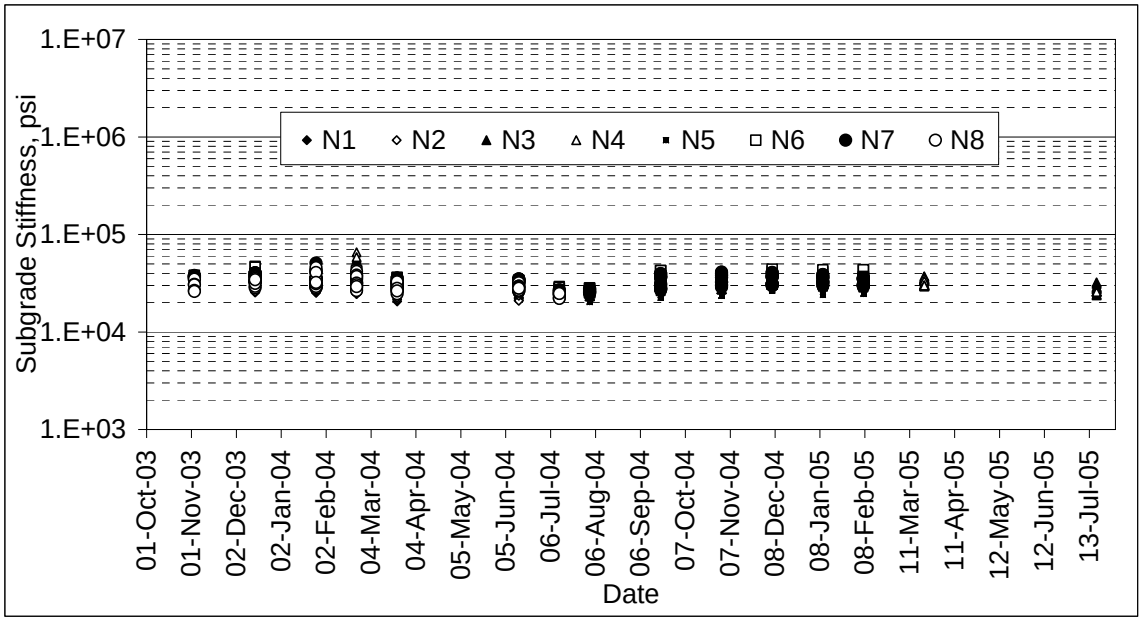

Figure 4.17 Existing Subgrade Moduli versus Date (Timm and Priest, 2005).

Granular Base/Fill Layer Characterization

An ANOVA was conducted, at a 95% confidence level, to examine differences among the test sections in terms of granular base/fill modulus. Figure 4.18 illustrates the statistical data used in the ANOVA. While the null hypothesis was rejected that all sections were equivalent (F-statistic = 39.75), there did not appear to be obvious trends in the data. For example, the sections could not be statistically grouped into thin (N1-N2), medium (N5-N8) or thick (N3-N4). The differences, then, were simply attributed to natural spatial variability, not necessarily dependent upon particular pavement parameters. However, it is recommended that section-specific moduli be used for M-E analysis (Timm and Priest, 2005).

Other investigations of the granular base/fill moduli considered seasonal differences and differences between wheelpaths. Examination of the seasonal granular base/fill moduli, as shown in Figure 4.16, seems to indicate a reduction in stiffness during the warmer parts of the year. ANOVA was again conducted and the differences between average moduli on each date were shown to be significant at the 95% confidence level (F-statistic = 10.57). However, the lower moduli can be explained as an artifact of the backcalculation process. Simply stated, it appears that EVERCALC attributed the increased deflection at warmer temperatures to slight reductions in granular base/fill modulus in addition to greater reductions in HMA modulus. A reasonable approach to mitigating these effects is to establish an average modulus for each test section, which amounts to what was presented in Figure 4.18.

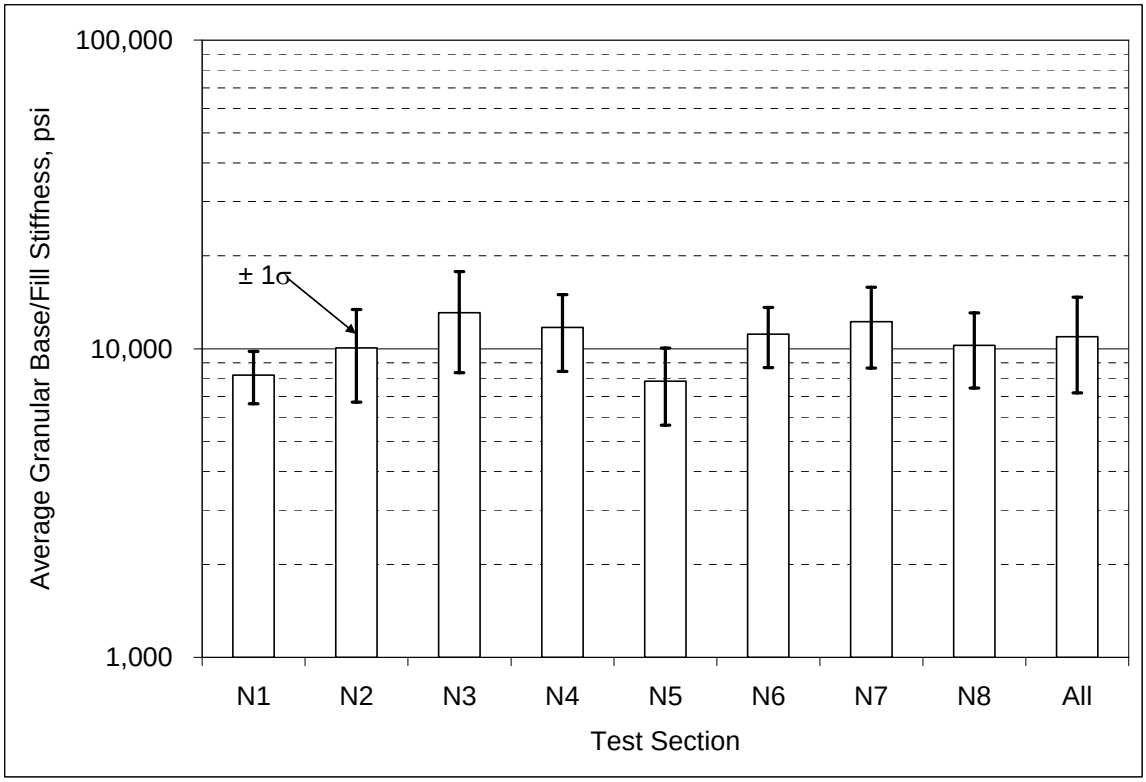

Figure 4.18 Granular Base/Fill Modulus – By Section (Timm and Priest, 2005).

The granular base/fill moduli, divided into respective wheelpaths for all the sections, are presented in Figure 4.19. An ANOVA demonstrated significant differences (95% confidence level; F-statistic = 159.03) between the two with the inside wheelpath significantly higher. The reason for higher stiffnesses in the inside wheelpath is not immediately clear, but it is consistent with the observation that distresses at the Test Track tend to be higher in the outside wheelpath than the inside. This is also the case for most open access facilities (i.e., distress tends to be greater in the outside wheelpath). It is recommended that the differences between the outside and inside wheelpaths be taken into consideration when considering the data with respect to the embedded instrumentation (Timm and Priest, 2005).

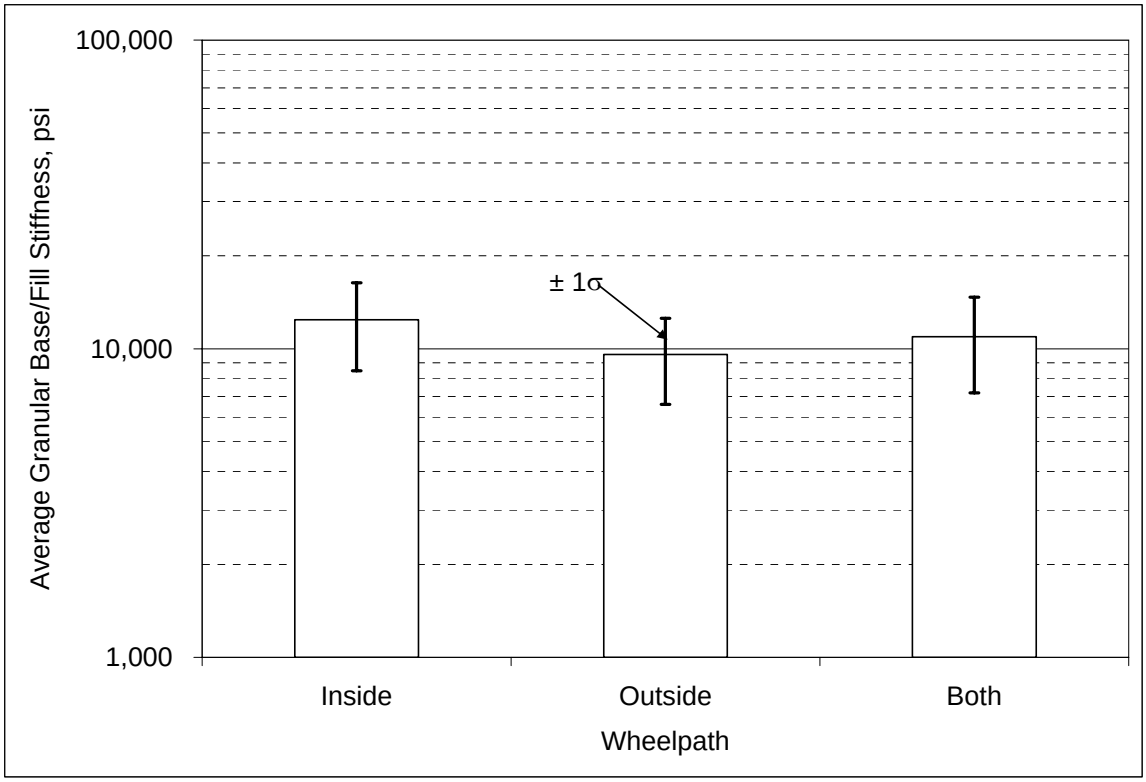

Figure 4.19 Granular Base/Fill Modulus – By Wheelpath (Timm and Priest, 2005).

Subgrade Characterization

Following the same approach devised for the granular base/fill, the subgrade moduli were analyzed in terms of differences by section, by date and by wheelpath. The average subgrade modulus and standard deviation, for each test section, are shown in Figure 4.20. It is notable that these moduli are significantly higher than the granular base/fill layer (Figure 4.18). Specifically, the average subgrade stiffness between all sections was 32,000 psi while the average granular base/fill stiffness was 11,000 psi. An ANOVA of the data in Figure 4.20 resulted in the sections having statistically different subgrade moduli (F-statistic = 32.39). However, as was found with the granular base/fill, there were no general trends that could be attributed to design characteristics of the test sections. Rather, the differences were attributed to spatial variability and it is recommended that section-specific subgrade moduli be used for further analysis.

Regarding seasonal changes, a similar observation was made regarding the subgrade modulus during the warmer times of the year as was made with the granular base/fill material. Namely, there appeared to be a reduction in stiffness with increased temperature. This can again be attributed to an artifact of the backcalculation program and best mitigated by simply taking an average over all the dates, per section.

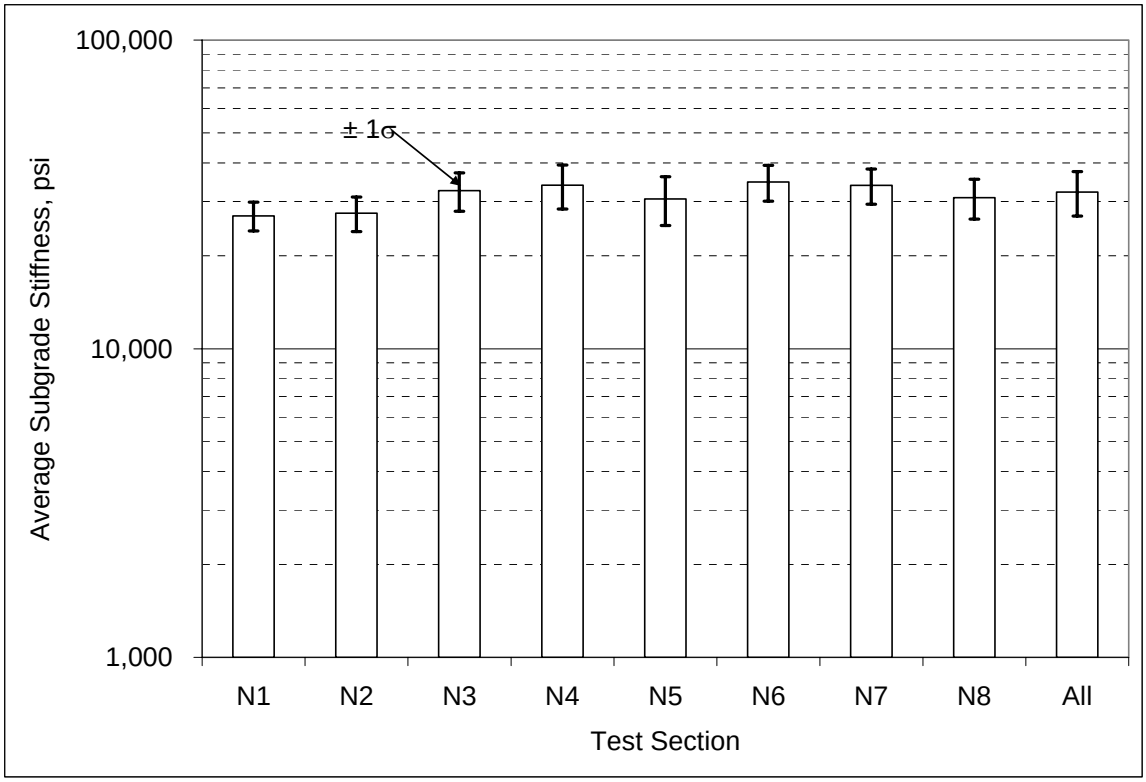

Figure 4.20 Subgrade Modulus – By Section (Timm and Priest, 2005).

The outside wheelpath moduli were lower than the inside wheelpath for the subgrade moduli. Figure 4.21 illustrates the statistical data and an ANOVA clearly demonstrated the statistical differences between the inside and outside wheelpath (F-statistic = 177.55). Therefore, it is again recommended to use wheelpath-specific moduli for analysis (Timm and Priest, 2005).

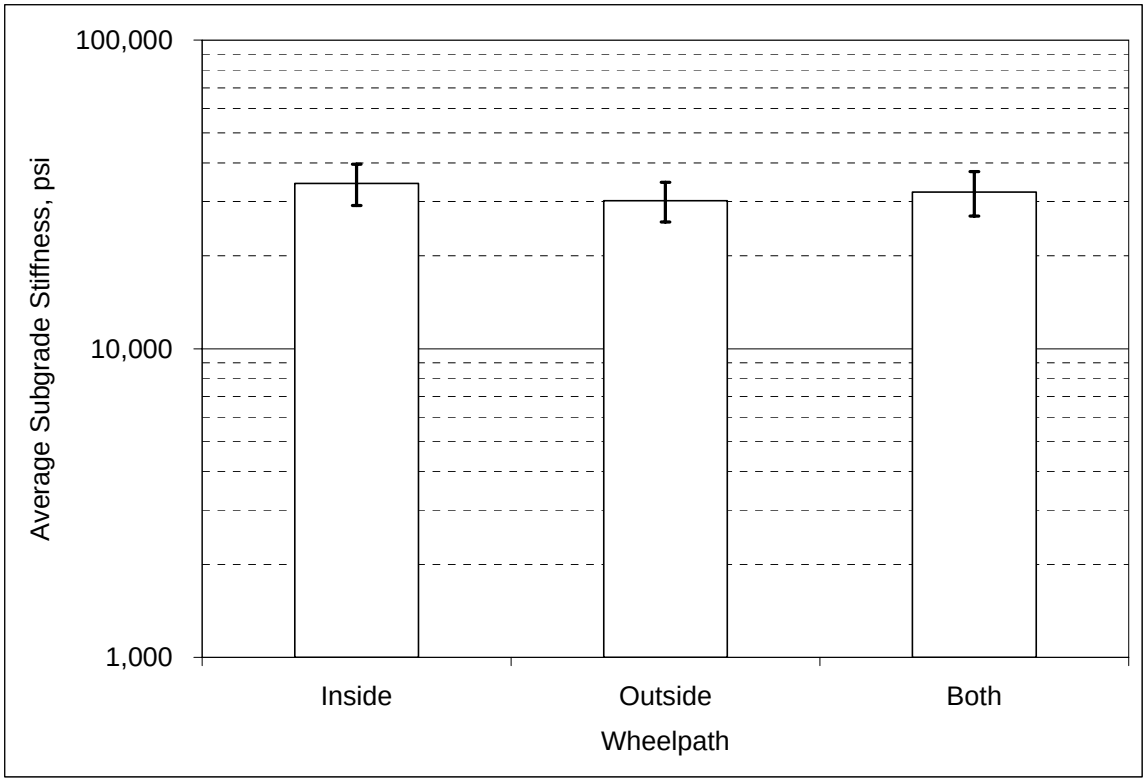

Figure 4.21 Subgrade Modulus – By Wheelpath.

HMA Characterization

Before closely examining the HMA stiffness – temperature relationship, it was decided to look for correlations between the various HMA as-built parameters, temperature and the backcalculated HMA stiffness. The as-built parameters were presented elsewhere (Timm and Priest, 2005), while the temperature presented in this discussion represents the interpolated mid-depth temperature during the hour of the corresponding FWD test. Table 4.4 shows the correlations between the various parameters from which the following observations were made:

- As expected, temperature was highly negatively correlated to HMA modulus.
- The asphalt binder performance grade and asphalt content had the lowest correlations to the HMA stiffness. This was not surprising given the laboratory study (Timm and Priest, 2005) which showed that these parameters were also not significant in determining the dynamic modulus.
- The asphalt binder performance grade and air voids are strongly positively correlated. This seems to indicate that the binder modification resulted in greater difficulty in compacting the mixture.

Based upon the above observations, it was decided to first establish temperature-stiffness relationships and then more closely examine the effects of the other mixture parameters. Each of these analyses is presented below.

Table 4.4 HMA Correlations.

	Percent Passing #4 Sieve	Performance Grade	Air Voids	Asphalt Content	Mid-Depth HMA Temperature	HMA Stiffness
Percent Passing #4 Sieve	1.000					
Performance Grade	0.369	1.000				
Air Voids	0.226	0.807	1.000			
Asphalt Content	0.176	-0.043	0.320	1.000		
Mid-Depth HMA Temperature	-0.080	-0.027	-0.026	0.027	1.000	
HMA Stiffness	0.129	-0.061	-0.153	0.002	-0.793	1.000

HMA Modulus – Temperature Characterization

The backcalculated HMA moduli were plotted versus mid-depth HMA temperature (T) to establish stiffness-temperature relationships. Figures 4.22 through 4.25 illustrate the raw data best-fit regression lines for all the sections, the unmodified sections, the modified sections and SMA sections, respectively. The regression equation had the form:

$$E_{HMA} = k_1 e^{k_2 T} \tag{4.3}$$

and the regression parameters, with corresponding R^2 values are listed in Table 4.5. In general, the equations were good predictors of stiffness. The one exception was section N1 ($R^2 = 0.35$) which can be seen to have high variability in Figure 4.24.

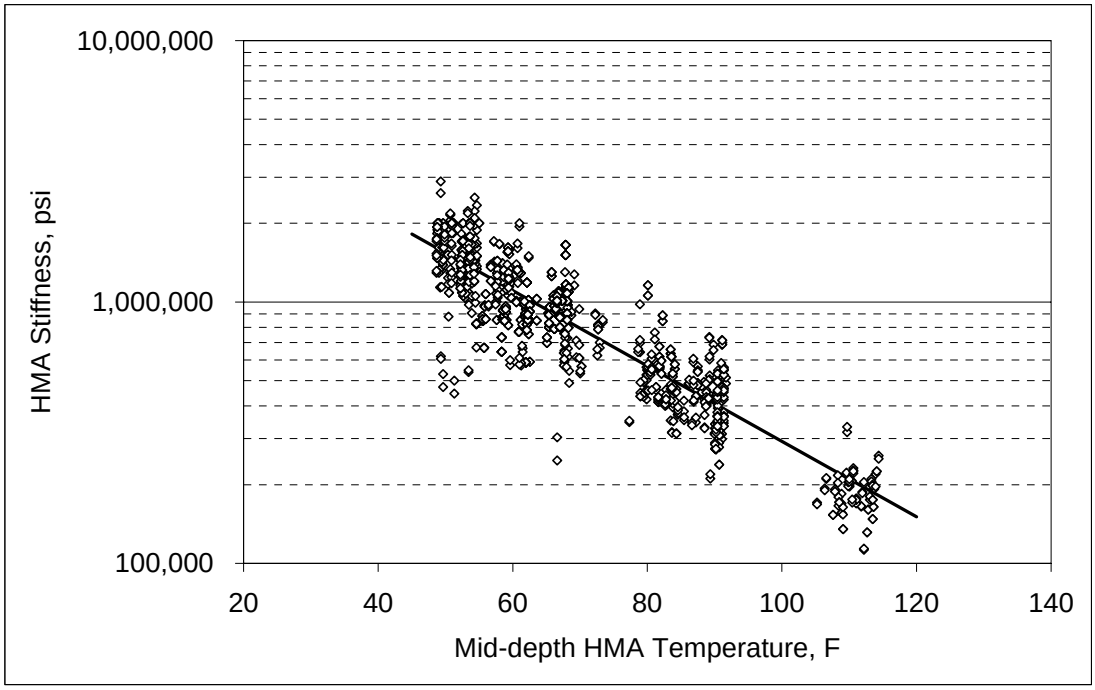

Figure 4.22 HMA Stiffness versus Temperature – All Sections.

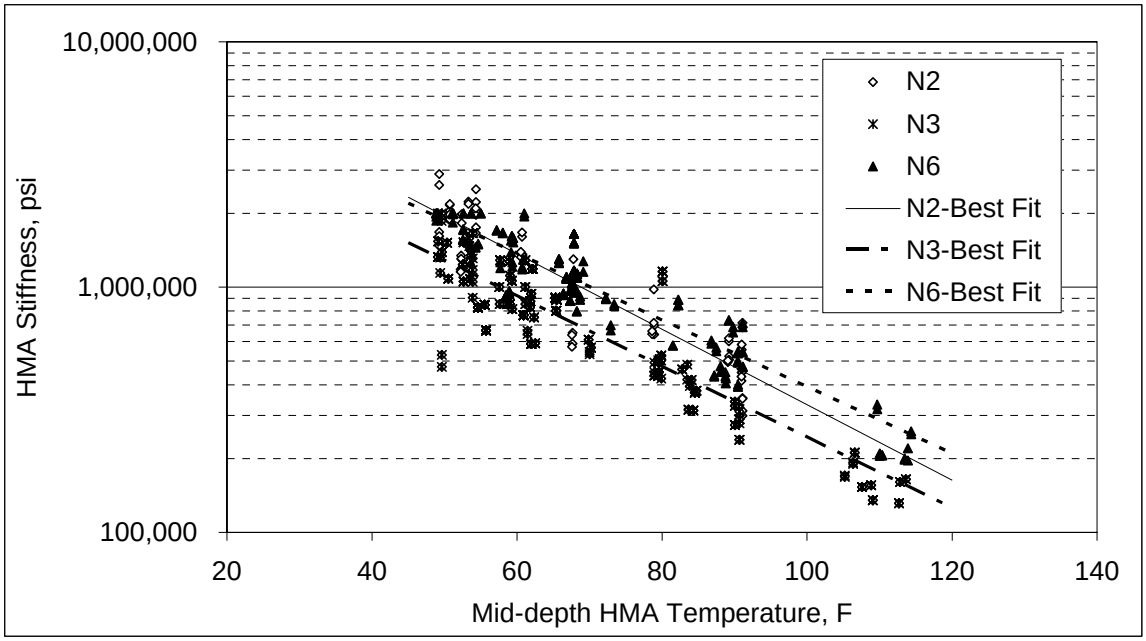

Figure 4.23 HMA Stiffness versus Temperature – Unmodified Sections.

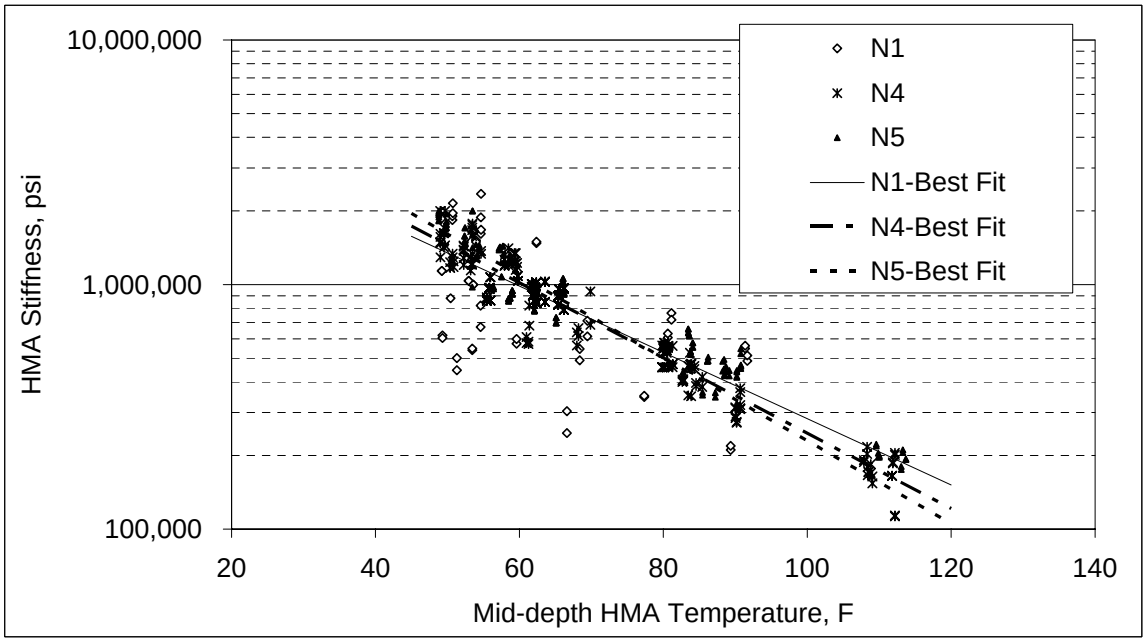

Figure 4.24 HMA Stiffness versus Temperature – Modified Sections.

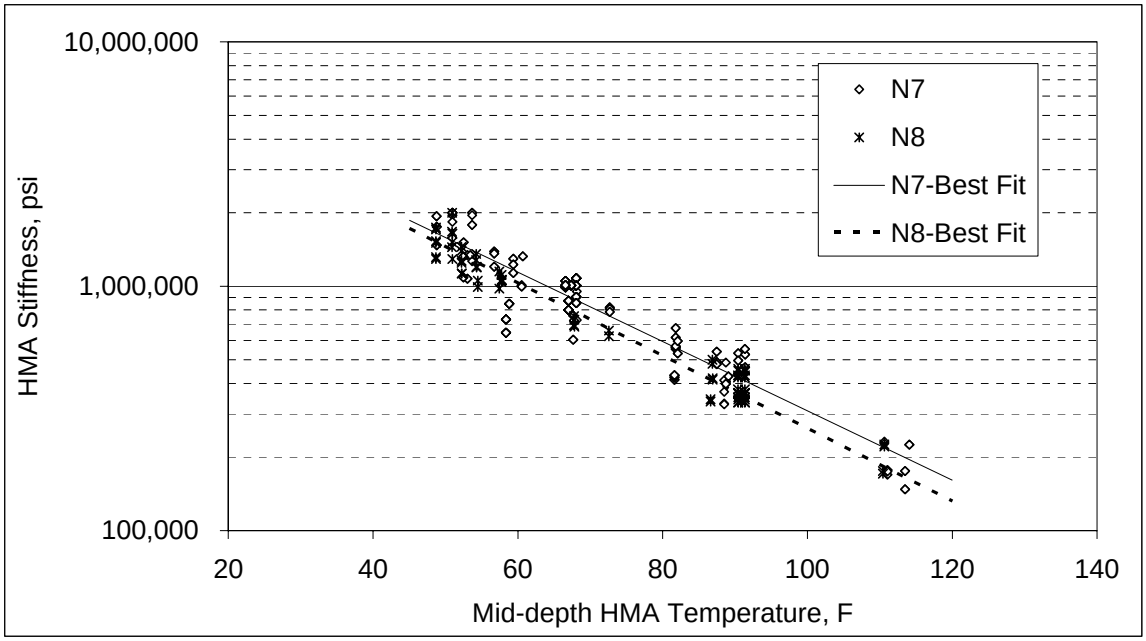

Figure 4.25 HMA Stiffness versus Temperature – SMA Sections.

Table 4.5 Stiffness – Temperature Regression Parameters.

Section	k_1	k_2	R^2
N1	6.427E+06	-0.0312	0.35
N2	1.145E+07	-0.0354	0.81
N3	6.776E+06	-0.0332	0.71
N4	8.561E+06	-0.0355	0.86
N5	1.126E+07	-0.0389	0.86
N6	8.987E+06	-0.0313	0.80
N7	8.088E+06	-0.0326	0.76
N8	8.046E+06	-0.0342	0.94
ALL	8.082E+06	-0.0332	0.68

To further examine the other parameters listed in Table 4.4, a temperature correction needed to be applied to adjust all the stiffness data to a single reference temperature. The reference temperature was set at 68^{o}F since it was near the middle of the temperature range presented in Figures 4.22 and also is used as the reference temperature in the current AASHTO Design Guide (1993). Further details regarding the temperature correction were presented by Timm and Priest (2005).

Figure 4.26 shows the effectiveness of the temperature correction scheme for all the test sections while Figure 4.27 shows the distribution of HMA modulus for all the test sections combined. The average was approximately 850,000 psi and the distribution appeared to be approximately log-normal with a 26% coefficient of variation. It must be noted that this level of variability is comparable to those found in other studies (Timm et al, 1999).

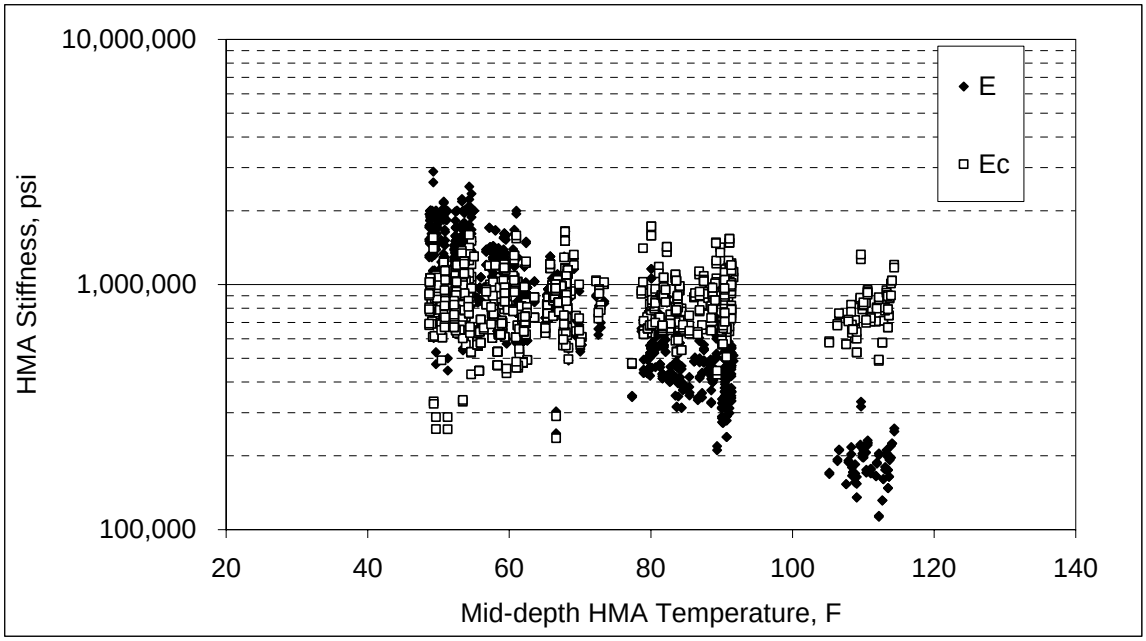

Figure 4.26 Effectiveness of Temperature Correction – All Sections.

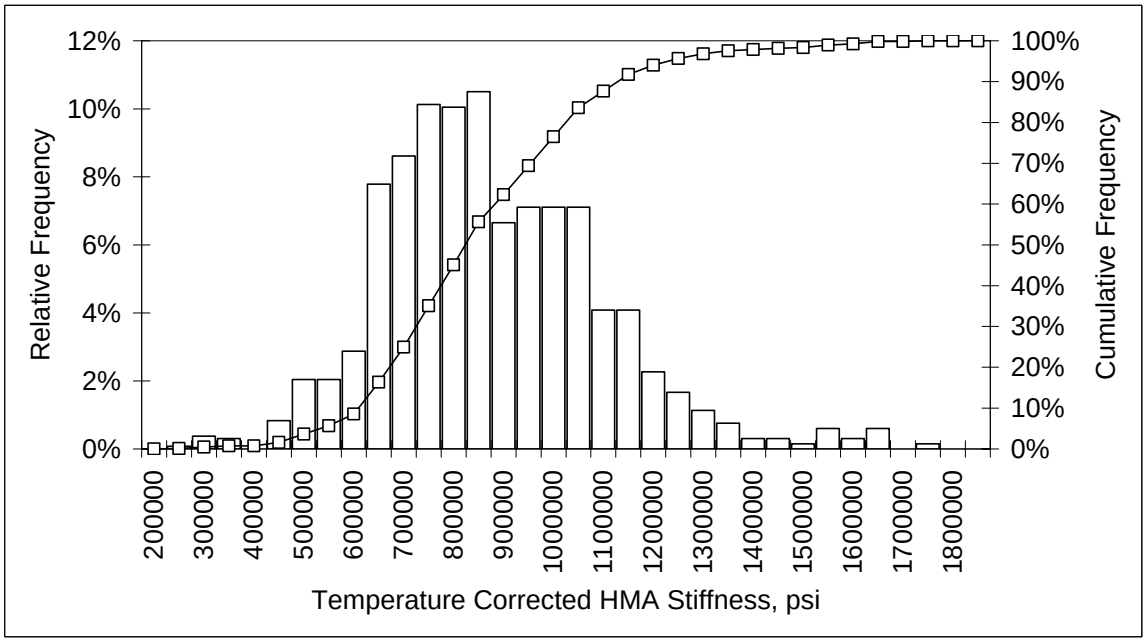

Figure 4.27 HMA Stiffness Variability – All Sections.

Figure 4.28 shows a sectional comparison of HMA moduli, while Table 4.6 lists the values and coefficients of variation. Note that section N1 was much more variable than the other test sections. An ANOVA was conducted on the test sections and the average stiffnesses were found to be statistically different at a 95% confidence level (F-statistic = 82.69). However, a Tukey comparison test, also conducted at the 95% confidence level, did not divide the sections into logical groups (i.e., modified, unmodified, SMA). For example, N1 (modified) was found to not be statistically different from N3 (unmodified), N4 (modified), N5 (modified) and N8 (SMA with rich bottom). Further regression analyses were conducted to look for significant effects that could be attributed to asphalt content, air voids, gradation. Figures 4.29 through 4.31 show the

influence of these factors, respectively, on HMA stiffness. Only air void content (Figure 4.30) showed a slight effect, but the corresponding low R^2 value does not support a meaningful relationship between the stiffness and air void content. These results are also consistent with the correlation coefficients listed in Table 4.4.

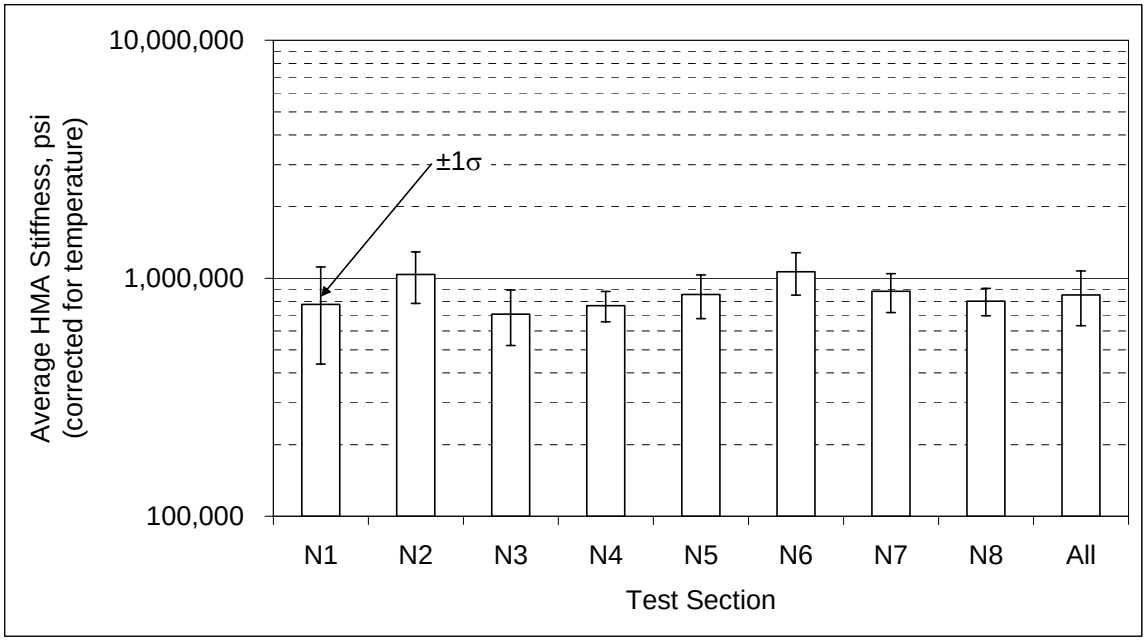

Figure 4.28 HMA Stiffness versus Section – Corrected for Temperature (Timm and Priest, 2005).

Table 4.6 HMA Stiffness versus Section – Corrected for Temperature (Timm and Priest, 2005).

Section	Average, psi	Standard Deviation, psi	Coefficient of Variation
N1	776,190	340,185	44%
N2	1,037,764	253,385	24%
N3	707,303	185,870	26%
N4	767,759	112,144	15%
N5	854,371	177,249	21%
N6	1,064,386	214,964	20%
N7	881,303	164,059	19%
N8	800,680	105,294	13%
All	852,033	220,571	26%

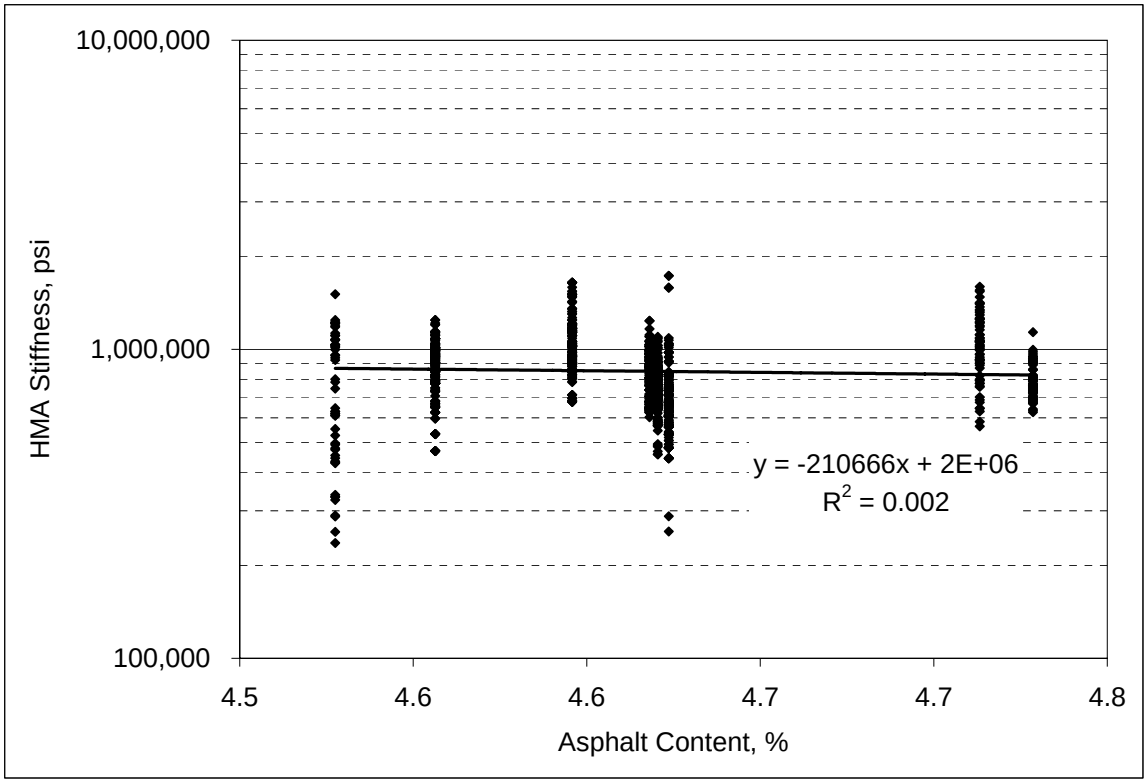

Figure 4.29 HMA Stiffness versus Asphalt Content – Corrected for Temperature.

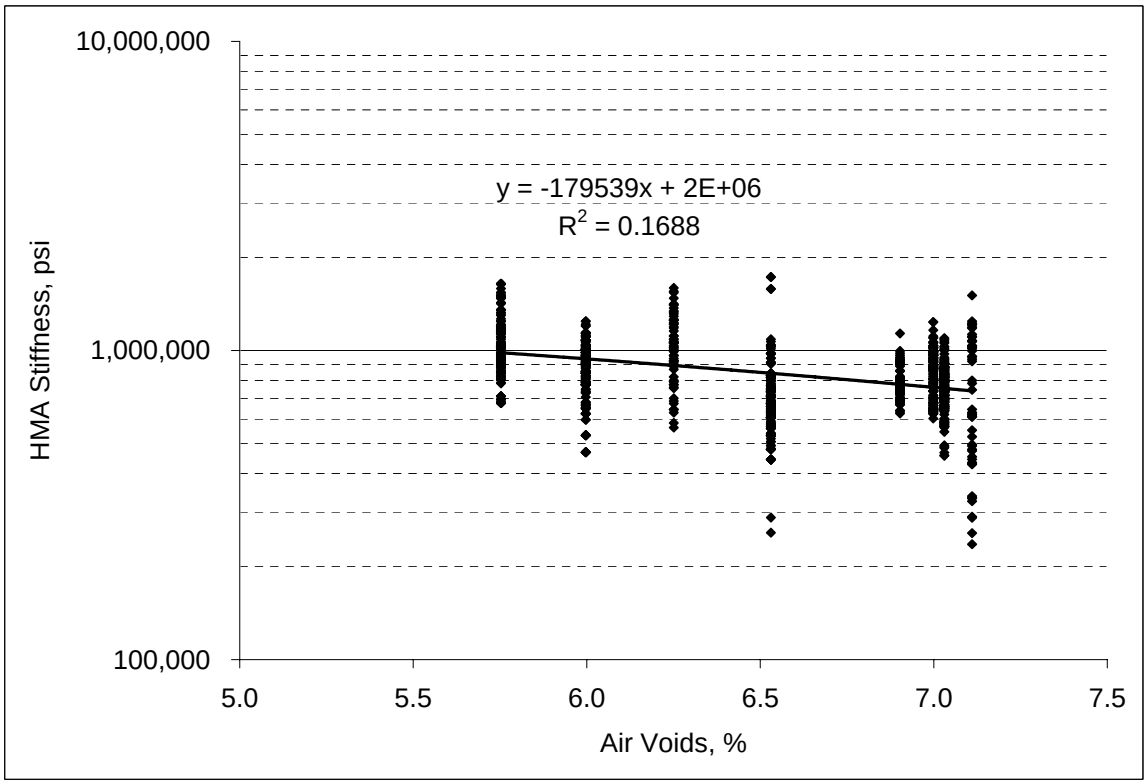

Figure 4.30 HMA Stiffness versus Air Voids – Corrected for Temperature.

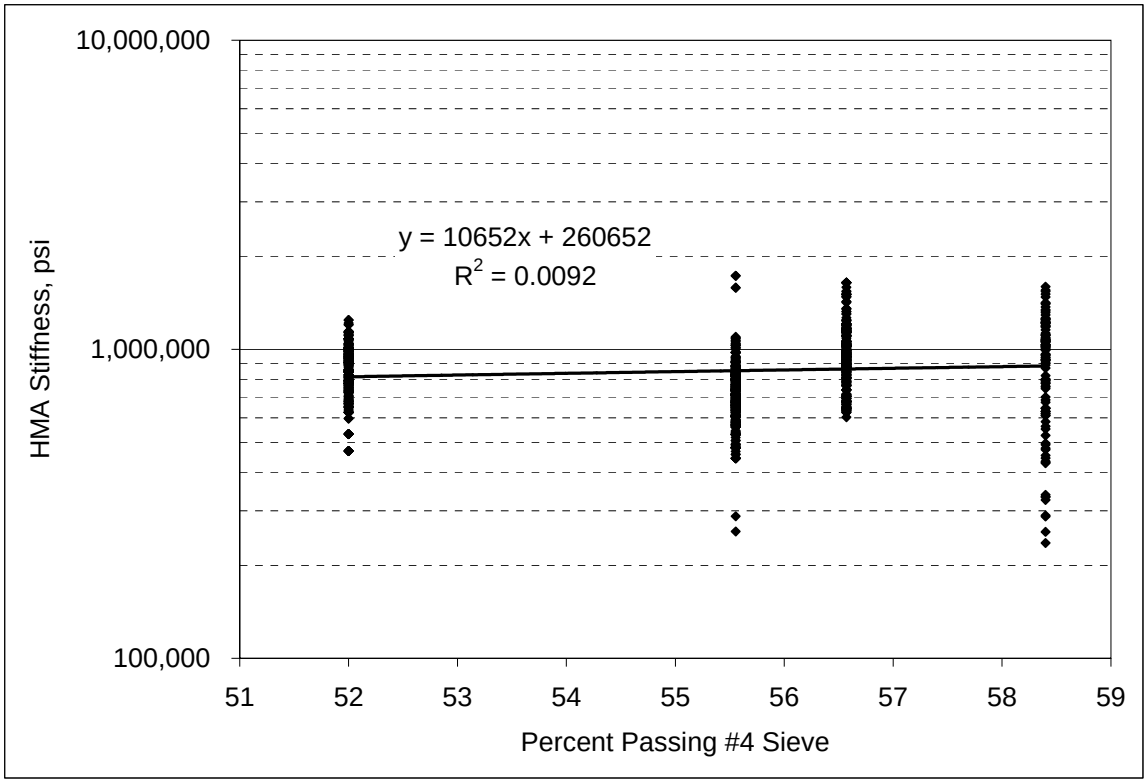

Figure 4.31 HMA Stiffness versus Gradation – Corrected for Temperature.

A final analysis of the HMA stiffness data examined the effect of wheelpath. Presented in Figure 4.32, the wheelpath was found to be significant through ANOVA at a 95% confidence level (F-statistic = 60.29). As with the granular base/fill and subgrade, the HMA stiffness was also higher in the inside wheelpath than the outside wheelpath.

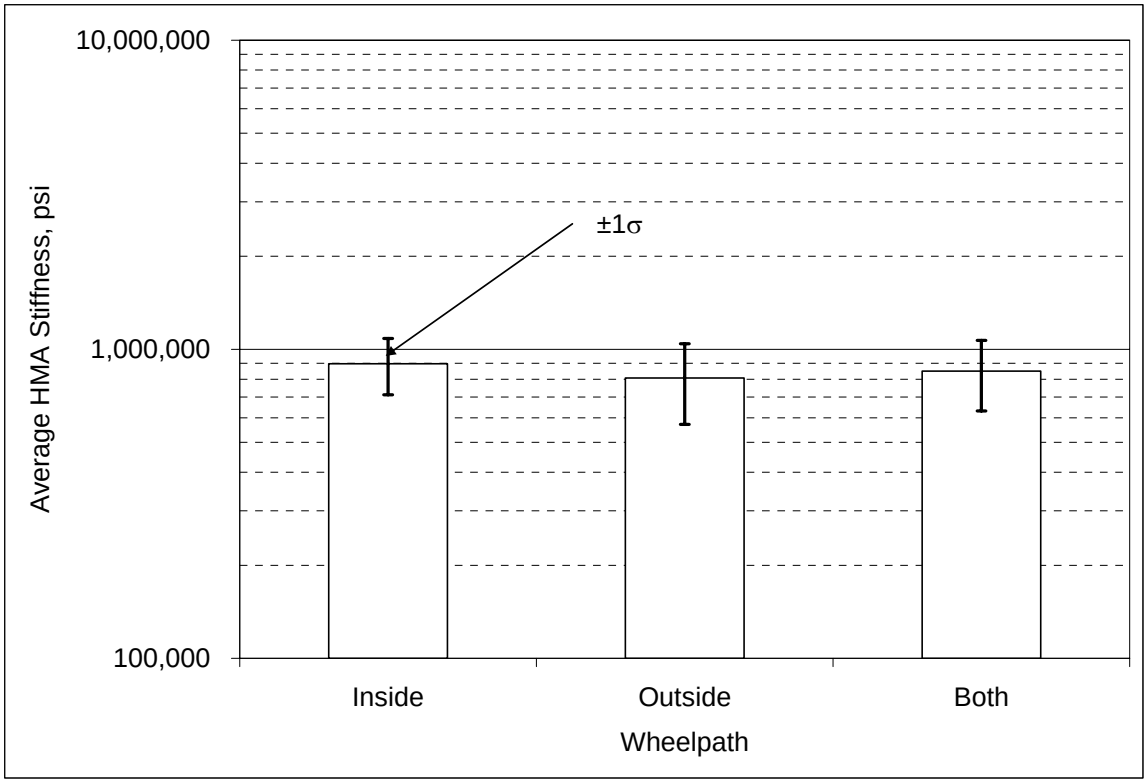

Figure 4.32 HMA Stiffness versus Wheelpath – Corrected for Temperature.

Based upon the results presented above, it is recommended that section and wheelpath specific moduli be used for mechanistic analysis. Also, the stiffness – temperature relationships presented in Table 4.5, can be used to characterize the seasonal changes in each test section. The other parameters were not found to have a meaningful or significant effect on HMA stiffness.

Fatigue Performance and Model Development

One of the main objectives of the Structural Study was to develop performance models for use in M-E design. The model development methodology as well as parameter characterization will be discussed here. Further, the dynamic strain data will also be discussed in context of the fatigue model development. More detail regarding model development in general, dynamic data collection, strain data processing and parameter characterization can be found elsewhere (Priest, 2005).

The fatigue transfer functions developed at the Test Track were derived strictly from field data without the use of laboratory testing or theoretical models. Therefore, the process was fairly unique and required a massive amount of data collection and synthesis. The inputs of M-E analysis (material properties, environment, traffic and the pavement structure) were measured and quantified, in situ, at the Test Track. The material properties were determined using FWD testing; the environmental data were collected continuously via temperature probes, TDRs and the weather station; the traffic was monitored by weight and mileage data; and the layer thicknesses were directly measured during construction. Further, the pavement response was measured from field instrumentation (strain gauges and pressure plates) rather than calculated using a theoretical model. And finally, the pavement performance was monitored and recorded in the field.

From the field data collection efforts, the fatigue transfer functions were developed or calibrated by working the M-E analysis procedure in both the forward and backward direction, as shown in Figure 4.33. Simply stated, the transfer functions were calibrated to most closely relate the pavement response to performance through a transfer function. The methodology section will further describe how the damage was calculated and accumulated, and the parameter characterization section will describe in more detail how all the components in Figure 4.33 were quantified.

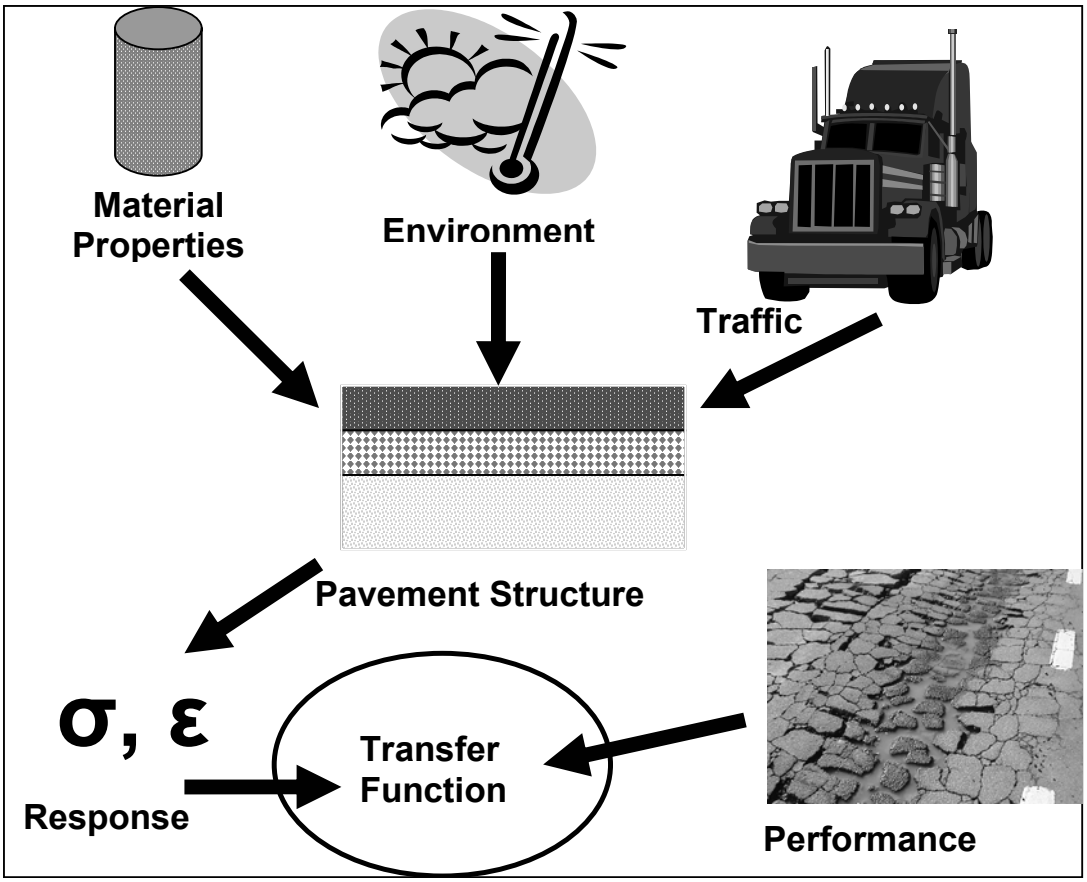

Figure 4.33 Illustration of Transfer Function Development.

Methodology

As a very general explanation, the fatigue transfer functions were developed by first summing or accumulating the damage, according to Miner's hypothesis, due to the applied truck loads and then calibrating the functions so that the damage equaled unity at the time of observed failure. For this study, failure was considered when fatigue cracking reached 20 percent of the total lane area, which approximately equaled 50 percent of the wheelpath. The damage was calculated hourly to account for changes in strain magnitude and HMA stiffness due to daily temperature fluctuations. The induced strain is dependant on temperature due to its effect on the stiffness of the HMA layer.

The two variables in the ratio of Miner's hypothesis are the allowable cycles until failure, N_f, and the applied loads, n. In order to successfully develop transfer functions, these two parameters had to be calculated over the testing time to accurately accumulate the damage. A record of the traffic data, or applied cycles, and temperature data was kept continuously over the test cycle, but the strain data and FWD data was collected only periodically. It was not practical nor necessary to collect continuous dynamic or stiffness data for every truck pass or every hour. As a result, relationships were developed to accurately estimate the stiffness and strain data at a given condition (temperature). The stiffness – temperature and strain – temperature relationships are presented later in this chapter.

In summary, the procedure employed to calibrate fatigue transfer functions in this study followed these steps:

1. Determine the number of truck passes for the given hour (triple-trailer trucks and box trailer).
2. Determine the mid-depth temperature of the HMA layer for the given hour from temperature probe data.
3. Use the strain – temperature relationship to estimate the induced strain due to the given truck at the given temperature.
4. Use the stiffness – temperature relationship to estimate the HMA stiffness at the given temperature.
5. Calculate the cycles to failure (N_f) for the given condition.
6. Calculate the incremental damage (D_i) for the given traffic cycles (n) and cycles to failure (N_f).
7. Repeat for each hour and accumulate the damage over the test cycle until the failure criteria is met.
8. Calculate the regression constants (calibrate the model) so that the total damage (D) equals 1 at time of failure.

The remaining topics of this section will discuss in more detail how the data were generated and how the relationships were quantified in the steps above.

Dynamic Strain Data

The instrumentation at the NCAT Test Track and the dynamic data generated from the instrumentation was a unique and central aspect of the Structural Study. The embedded strain gauges and pressure plates allowed for direct measurement of the pavement response; thus, there was no reliance on mechanical models. This situation was beneficial because all models are based on a set of assumptions that simplifies real world conditions to some degree. By measuring the responses directly, the assumptions and simplifications were not of concern. Further, the collected dynamic data could serve to evaluate mechanical models, if needed.

With the benefits of dynamic response data, came unique challenges. The raw dynamic strain traces, the focus of this discussion, were highly variable and often unpredictable. The variability was largely attributed to dynamic effects of the trucks and trailer alignment along with electrical noise and drift. Once the data were collected, the signals had to be cleaned, processed and stored in an efficient and streamlined manner. With the variety of traces, along with noise in the signal and signal drift, the task was not simple. A brief explanation of the strain data processing scheme is given here. As mentioned above, more information regarding how the strain data was handled can be found (Priest, 2005).

The strain gauges were very sensitive to the lateral placement of the load and were susceptible to noise and signal drift. Therefore, there were many challenges in determining how to best handle the data. A list of some of the important issues and concerns that were addressed with the developed processing procedure are given below:

- Clean the signal of electrical noise.
- Record the important data.
- Produce an accurate and relevant strain value.
- Robust enough to handle all varieties of strain traces (one scheme for all traces).
- Reproducible output (not overly dependant on processor judgment).

- Automated and efficient system.
- Easily sort and query data.

A graphical engineering software package, DADiSP, was used to develop the processing algorithms and procedures. The steps below are contained in one window worksheet within DADiSP that allowed for ease of processing and organization. Further, the method that was developed at the Test Track to handle and process the dynamic data was automated yet required some engineering judgment and interaction.

First, the signal was cleaned of electrical noise by taking a moving average of 20 points. The moving average smoothed the curve without losing the important peaks and valleys. Then the inflection points of the signal were established and marked. The processor could adjust certain parameters, including the spread of points that the program scans and the minimum strain difference between consecutive inflection points, to manipulate the program to mark the relevant points. This step involved human judgment and interaction. In most cases, the parameters did not have to be adjusted, but for some traces they did due to large inflection points or other issues. Once the signal was satisfactory, the processor "recorded" the truck pass.

After the processor was satisfied with the inflection points, an algorithm was conducted that computed an average strain amplitude of the entire truck pass. The amplitude took into account both the compressive and tensile responses into an overall amplitude. Also, the amplitude averaged the effect of different strain responses due to mechanical alignment. Figure 4.34 is an illustration of the strain amplitude that was computed for a longitudinal strain trace. Notice that the inflection points are marked, and the strain amplitude is between the top and bottom line. The figure does not show the scale in strain, but the value is not of importance in this discussion, merely how the inflection points were gathered and the strain magnitude was quantified. The information was then "recorded" and the gauge factor (which is unique to each strain gauge), truck, pass, maximum and minimum inflection point, and the amplitude in microstrain were stored.

At this point, the gauge identification, truck identification and the pass number were entered to keep the information organized. The recorded data included the gauge factor (which is unique to each strain gauge), truck, pass, maximum and minimum inflection point, and the amplitude in microstrain.

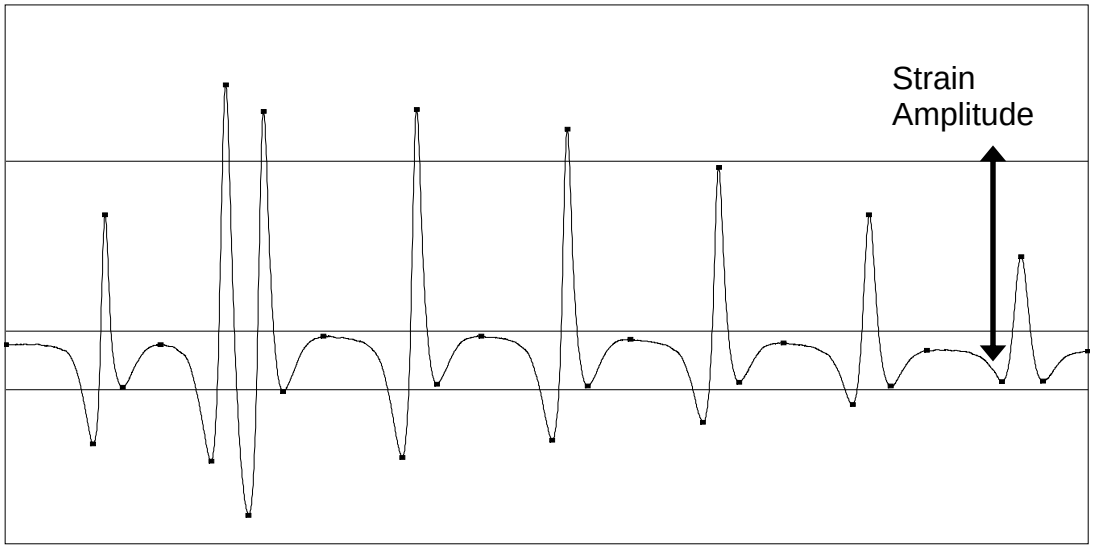

Figure 4.34 Strain Amplitude Illustration.

All of the truck passes for each strain gauge were collected, processed, and stored. But recall that there were twelve strain gauges per test section; therefore, one truck pass produced at most, six readings in both the longitudinal and transverse orientation. The maximum reading of each orientation (transverse and longitudinal) was considered the "best hit" of a tire over a gauge strain, and was therefore, the value for that truck and pass. The strain gauges were installed at three lateral orientations to help ensure that one of the three offsets would very closely register a direct hit of the tire over the gauge, thus producing the maximum strain value.

Strain Response Characterization

One of the main objectives of the NCAT Structural Study was to evaluate the two different binders, neat PG 67-22 and SBS modified PG 76-22, and quantify any difference in response and performance. One portion of the investigation included the strain response data. Figure 4.35 shows a summary of the strain data collected from the eight test sections. The data presented are pre-cracking longitudinal strain response under the triple-trailers, and the data were corrected to a reference temperature of 68^{o}F following the same correction procedure used for HMA stiffness discussed earlier.

Figure 4.35 shows the average temperature-corrected strain value along with the standard deviation. Notice from the figure that the three thicknesses are not extremely obvious in the strain data. On average, the thinnest sections (N1, N2) register the highest strains, while the thickest (N3, N4) show the lowest. Yet, if inspected closely, N2 and N6 along with N3 and N8 have fairly similar values. Section N8 strain values were more on the order of the 9 in. sections, yet it showed cracking first among the 7 in. sections. It is not immediately clear why the strain in section N8 is lower than the other 7 in. sections because the bottom layer should be more flexible, and thus deform more, than the other sections.

N2 shows lower strains than N1 because it is slightly more stiff than N1 (shown in Figure 3.28). Further, there may be some data in the N1 set that includes results after cracking had begun. The cracking in section N1 occurred first and it may have existed for some time before it was first

observed. On the other hand, the effect of HMA layer thickness is conclusive. An ANOVA analysis was conducted by pooling the test sections, considering only the three different HMA thicknesses, and it was determined that all three were statistically different (p-value < 0.000).

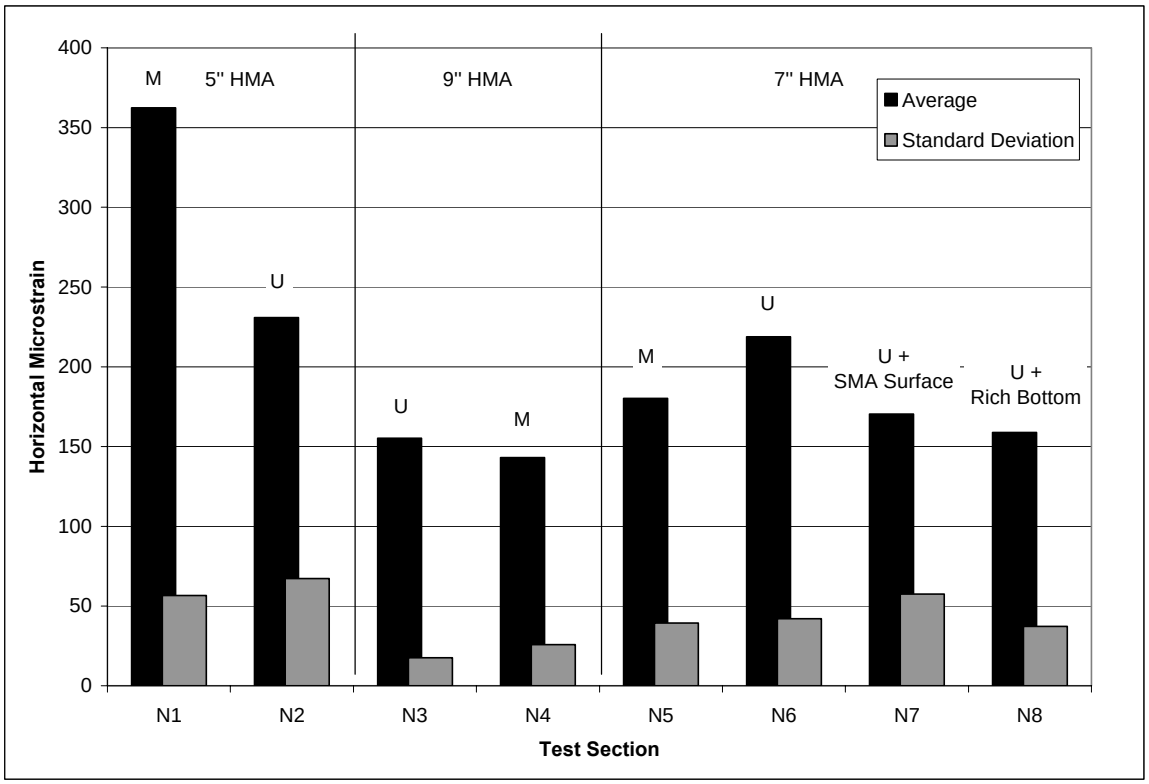

Figure 4.35 Temperature-corrected Strain Data by Test Section.

Like the thickness effect, it is not easy to make any sweeping conclusions on the effect of binder type on strain data by simple inspection of Figure 4.35. The modified section N1 seemed to have significantly higher strain than its counterpart, while there is less difference between the other paired sections.

To better quantify the effect of binder type, a statistical analysis was performed using the data presented in Figure 4.35. A two sample t-test was conducted to determine if sections N1 and N2 were statistically different considering the strain data. From the analysis, section N1 had statistically higher strain response than N2 at a 95 percent confidence level (two-sided p-value = 0.003). Further, the thick sections, N3 and N4, were also statistically different from each other (two-sided p-value = 0.002). The difference between N3 and N4 might be statistically different, but a difference of only 12 microstrain is not practically different.

To compare the four 7 in. sections, an analysis of variance, ANOVA, was conducted at the same confidence level. From the analysis, there was a difference amongst the four sections (p-value = 0.000). Further, from a Tukey comparison, it was determined that section N6 was statistically higher than the other 7 in. test sections.

From the analysis, no sweeping conclusions can be made in regards to the effect of binder grade and modification on strain response. The modified 5 in. section has higher strain values than the

unmodified section, the thickest sections are practically the same, and the modified 7 in. section has lower strain values than its unmodified partner. The above observations in strain data are probably due to construction and spatial variability rather than an effect of binder type.

The effect of temperature on strain is shown in Figures 4.36 and 4.37 for the triple-trailers and the box trailer, respectively. The regression followed a power relationship:

$$\varepsilon_t = \beta_1 T^{\beta_2} \quad (4.4)$$

where: ε_t = Horizontal tensile strain
β_1, β_2 = Regression constants

The regression constants and R^2 value are presented in Tables 4.7 and 4.8 for the triple-trailers and box trailer, respectively. It should be noted that there was not enough collected strain data to develop a relationship for the box trailer in section N1. This was because the box trailer was not used until further into the test cycle, and section N1 showed signs of cracking after six months of traffic. The generic equation (4.6) was used. From the R^2 values, the mid-depth HMA temperature was a reasonable predictor of the induced strain from each respective vehicle.

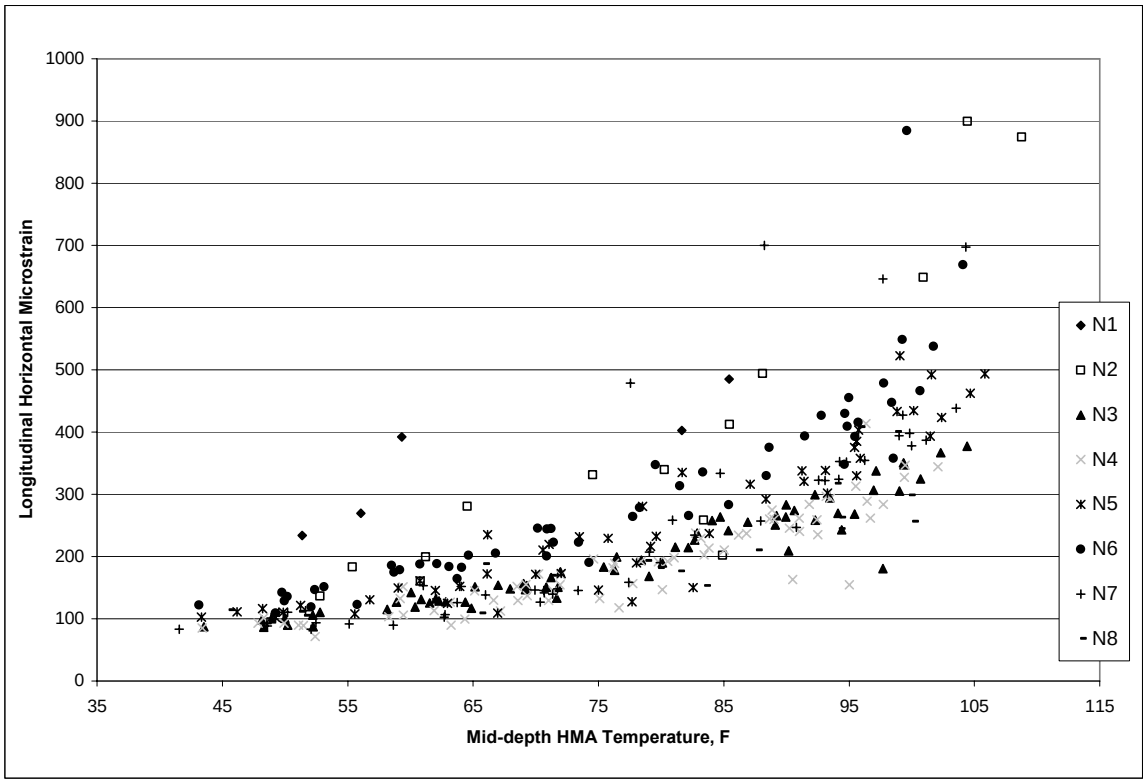

Figure 4.36 Triple-Trailer Strain – Temperature Relationship.

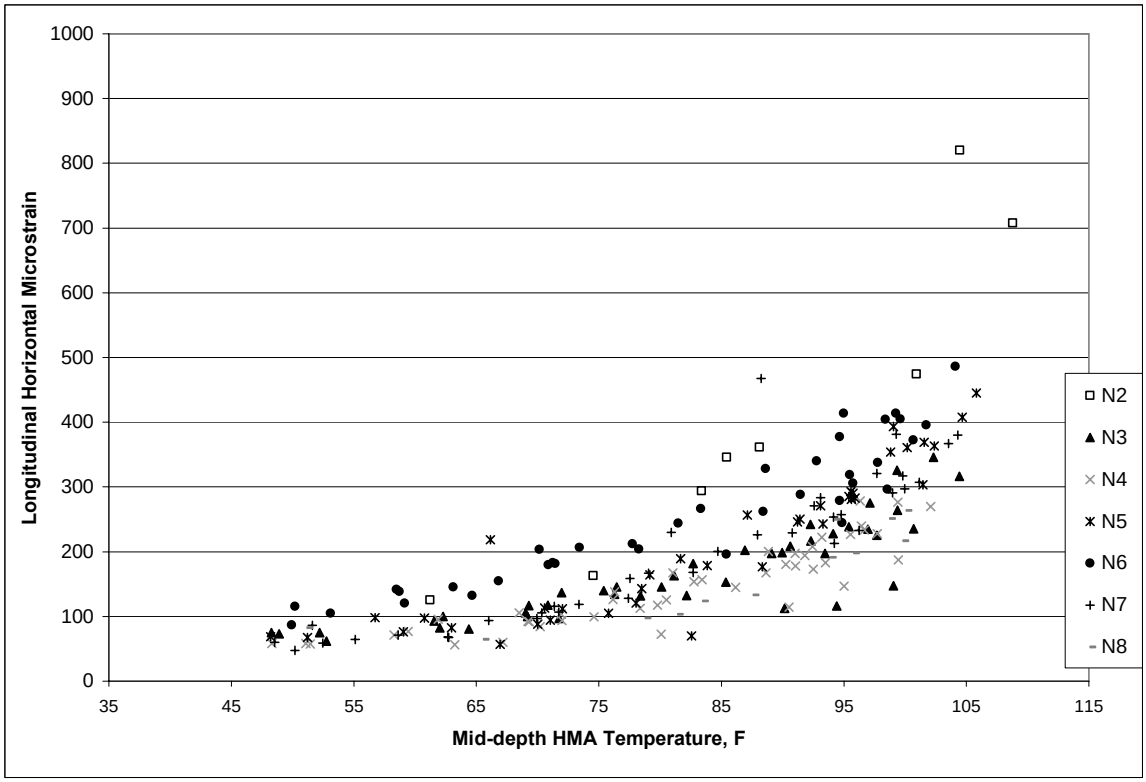

Figure 4.37 Box Trailer Strain – Temperature Relationship.

Table 4.7 Triple-Trailer Regression Analysis for Strain – Temperature Relationship.

Section	β_1	β_2	R^2
N1*	4.0439	1.066	0.763
N2	0.0005	3.081	0.877
N3	0.0508	1.899	0.909
N4	0.0211	2.086	0.822
N5	0.0109	2.291	0.881
N6	0.0132	2.293	0.810
N7	0.0022	2.652	0.705
N8	0.0532	1.887	0.730

* Limited data available

The generic relationships including thickness are given in Equations 4.5 and 4.6 below for the triple and box trailer, respectively.

$$\varepsilon_t = 5.557T^{1.0258} - 30.730t \qquad (R^2 = 0.70) \qquad (4.5)$$

$$\varepsilon_t = 2.1228T^{1.190} - 26.448t \qquad (R^2 = 0.71) \qquad (4.6)$$

where:
t = HMA thickness, in.

Table 4.8 Box Trailer Regression Analysis for Strain – Temperature Relationship.

Section	β1	β2	R^2
N1**			
N2	3.922E-05	3.579	0.871
N3	5.501E-03	2.332	0.773
N4	1.304E-03	2.632	0.773
N5	1.440E-04	3.185	0.887
N6	1.852E-02	2.155	0.881
N7	8.310E-04	2.796	0.821
N8	1.170E-04	3.157	0.850

****** Not enough data to perform regression

Fatigue Performance Characterization

Sections N1, N2 and N8 have shown significant fatigue failure cracking, and the distress of all three sections progressed in a similar fashion. First, small transverse cracks appeared in the wheelpath, as shown in Figure 4.38. Then the cracks progressed to the edge of the wheelpath and often curled in the direction of traffic (Figure 4.39). Later, the individual transverse cracks became interconnected into the classical alligator pattern fatigue cracking, also shown in Figure 4.39. umping of the fines from the unbound aggregate base through the cracks was also observed in the individual transverse cracks as well as the alligator cracked areas. The pumping proved that the cracks propagated all the way through the HMA layer. Cores were also taken in the cracking area to verify that the cracks were in fact bottom-up cracking. Once the first cracks appeared, the progression of failure was fairly rapid, especially once pumping began. The granular base was easily pumped as water infiltrated through the cracks and into the structure, and the base support was lost. This led to further deterioration and rutting.

Figure 4.38 Transverse Cracking in the Wheelpath - Section N8.

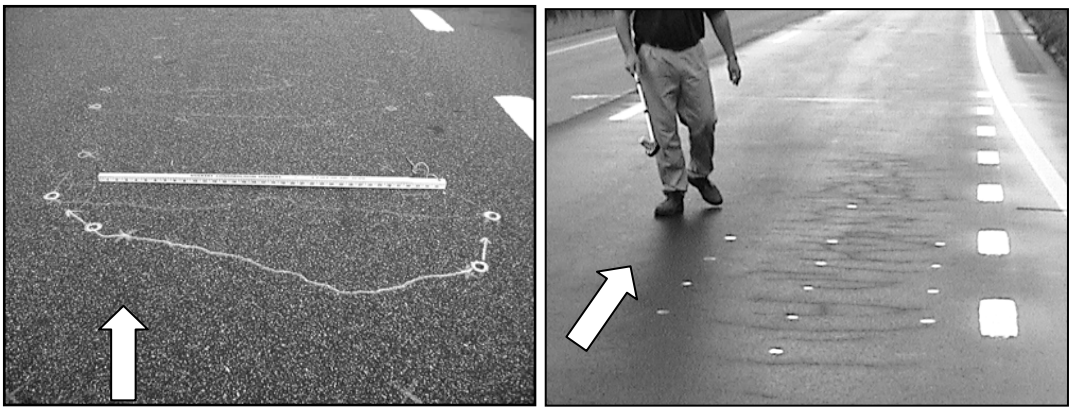

Figure 4.39 Progressed Fatigue Cracking.

Weekly, the test sections were examined, and the cracks were marked and recorded. From this, coordinates of individual cracks and cracked areas were stored to be displayed graphically in crack maps and to quantify the amount of cracking and crack progression. An example of the crack maps generated is shown in Figure 4.40. Further details regarding the cracking data and processing can be found elsewhere (Priest, 2005).

Figure 4.41 shows the progression of fatigue cracking by date for the four sections that experienced fatigue cracking. The dates of fatigue failure for sections N1, N2 and N8 were determined from Figure 4.41 and the failure criteria was selected as 20 percent of the lane area showing fatigue cracking. The failure dates are given in Table 4.9.

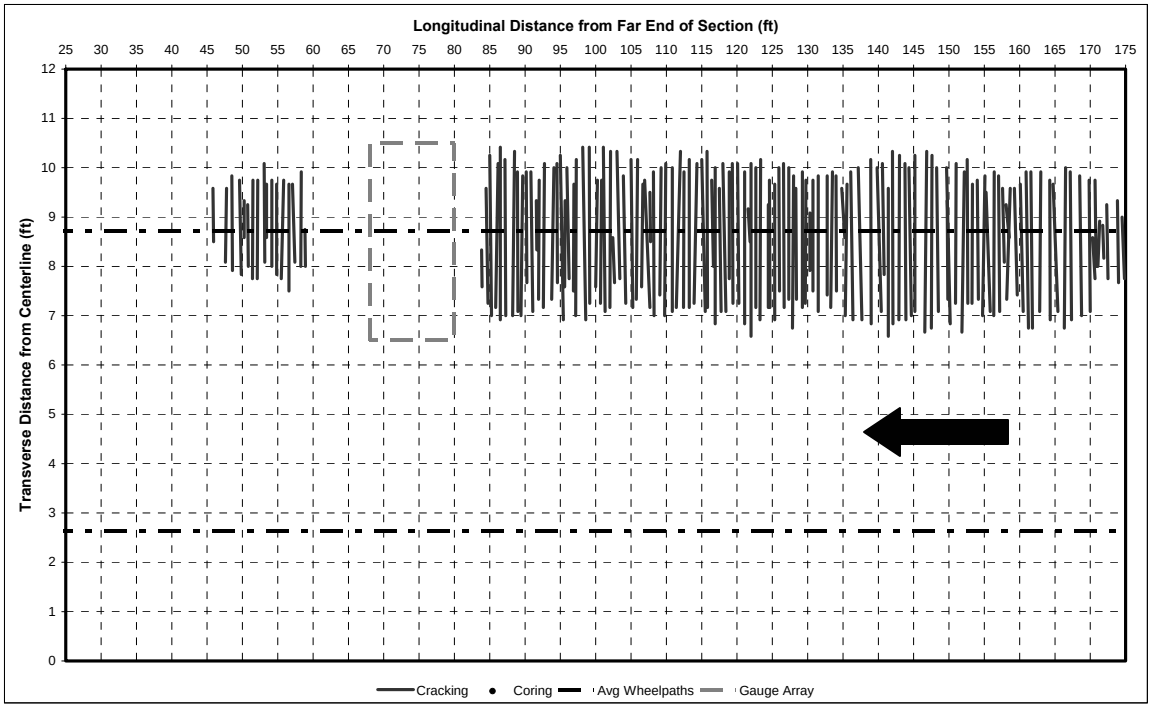

Figure 4.40 N2 Crack Map 6/28/2004.

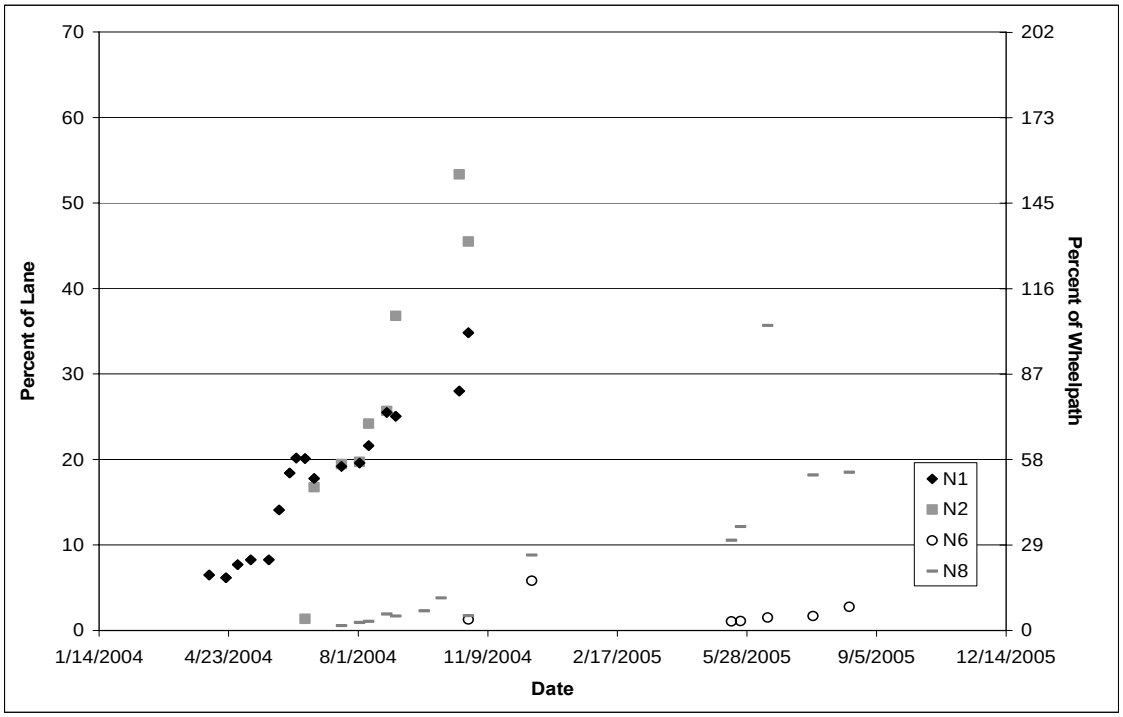

Figure 4.41 Percent Fatigue Cracking by Date.

Table 4.9 Section Failure Data.

Section	Failure Date	Cracking of Lane, %	Cracking of WP, %
N1	6/14/2004	20.2	58.3
N2	7/19/2004	19.5	56.2
N8	8/15/2005	18.5	53.5

Model Development

The number of truck laps was determined by vehicle type on a per hour basis. The hourly traffic volume was then queried with the hourly temperature data. The applied load cycles for each hour, n_i, was computed using these data. The number of load cycles equaled the number of truck laps times the number of strain cycles, or axles, for that vehicle. For example, the triple-trailer trucks had eight strain cycles, while the box trailer had five. The HMA stiffness and strain amplitude were then calculated from the hourly temperature data, given the test section and vehicle type. With the applied loads, stiffness and strain values, the cycles to failure, N_{fi}, was calculated given a fatigue transfer function. From this, the incremental damage, D_i, was computed each hour using Miner's hypothesis (Miner, 1959):

$$D_i = \frac{n_i}{N_{fi}} \tag{4.7}$$

where D_i = incremental damage for hour i
n_i = number of cycles for hour i
N_{fi} = number of cycles until failure under conditions of hour i

The total damage at any time was then the sum of the incremental damage.

Using the generated data described above, the fatigue models were then calibrated to fit the observed performance. The regression coefficients were determined such that the total damage, *D*, equaled unity at the determined date of failure. It is important to note that the effort of this research was to calibrate models previously developed using full-scale field response, material, and performance data. The exact models followed and the calibration results are discussed below.

The current state of practice for fatigue transfer functions, including AI MS-1, Shell Oil Design Guide and the 2002 Design Guide, is in the form of:

$$N_f = k_1\left(\frac{1}{\varepsilon_t}\right)^{k_2}\left(\frac{1}{E}\right)^{k_3} \quad (4.8)$$

where: N_f = Number of load cycles until fatigue failure
ε_t = Applied horizontal tensile strain
E = HMA mixture stiffness
k_1, k_2, k_3 = Regression constants

These functions are often developed in the laboratory and then shifted or calibrated to field performance with correction factors.

In a similar manner as the 2002 Design Guide, all three regression constants were calibrated to fit the data collected at the Test Track for the models presented here. Also following the 2002 Design Guide and accepted practice, the AI MS-1 equation was used as the base model and guide to the calibrated functions. The AI MS-1 fatigue transfer function is (AI, 1982):

$$N_f = 18.4 * C * (0.00432 * \varepsilon_t^{-3.29} * E^{*-.854}) \quad (4.9)$$

where: $C = 10^M$

$$M = 4.84 * \left(\frac{V_B}{V_B + V_V} - 0.69\right) \quad (4.10)$$

The volumetric term in the AI equation was not used for the models calibrated here. It was determined above that there was not enough variation in the volumetrics of each test section to make an impact. Therefore, the volumetric term was not considered, and the equation was simplified to:

$$N_f = 0.0795 * \left(\frac{1}{\varepsilon_t}\right)^{3.29} * \left(\frac{1}{E}\right)^{0.854} \quad (4.11)$$

The above equation served as the base model that was then calibrated using the field data to create final transfer functions.

The two 5 in. sections, N1 and N2, reached their terminal life within the span of the 2003 research cycle as well as one of the 7 in. sections, N8. Recall that section N8 included the rich bottom layer consisting of 2 in. of HMA with an additional 0.5 percent asphalt content. It was found that this section behaved differently in fatigue than did sections N1 and N2. Consequently, one fatigue function could not be developed that explained the performance of both the 5 in. sections and section N8. Upon further investigation, it was determined that section N8 performed differently than the other test sections, also. Therefore, three transfer functions are presented here. One function for the 5 in. test sections was developed, termed the thin model. This model is separate because the data set is complete. Further, it is widely accepted (El-Basyouny and Witczak "Calibration", 2005; Monismith et al, 1985; Tangella et al, 1990) that thin asphalt pavements are subjected to a different loading mechanism than are thicker pavements. Although sources do not agree with what is considered "thin", the range is typically less than 2 in. to 5 in. The second transfer function developed was for section N8 and termed the rich bottom model. And finally, the third model presented, termed the thick model, was a first attempt at a calibrated model for the remaining test sections, N3-N7 based on data up to August 2, 2005. The three models are presented and discussed below.

Thin Model

The response, material property and performance data from both sections N1 and N2 were considered to develop the fatigue transfer function given below in units of strain (in./in.) and psi:

$$N_f = 0.4875 * \left(\frac{1}{\varepsilon_t}\right)^{3.0312} * \left(\frac{1}{E}\right)^{0.6529} \quad (4.12)$$

Both test sections failed in a very similar manner and within two months of each other. Section N1 failed prior to section N2, which was expected because the strain values were statistically higher at section N1 than N2.

Rich Bottom Model

Equation 4.11 was also calibrated according to the performance data of section N8, giving the following transfer function:

$$N_f = 0.4658 * \left(\frac{1}{\varepsilon_t}\right)^{3.087} * \left(\frac{1}{E}\right)^{0.5702} \quad (4.13)$$

The response and performance of section N8 warrants further discussion. Recall from Figure 4.28, the stiffness of section N8 was approximately the same as the other sections. However the strain values were relatively low until they began to increase around November 2005, when cracking was observed in the section. In fact, the strain values measured in section N8 prior to cracking were closer to the values of the 9 in. sections than the other 7 in. sections. Yet, even with the lower measured strain values, the section performed poorly compared to the other medium-thickness sections. The rich bottom concept hypothesizes that the added asphalt will create a more fatigue resistant bottom layer without compromising the overall strength and stability of the structure in regards to rutting. From this experiment, the rich bottom concept did not provide better fatigue life considering the performance of N8 and the control section, N7,

which had only small signs of cracking at the time of this report. As a result, further investigation into the rich bottom concept should be pursued at NCAT and elsewhere before it is widely used in pavement design.

Thick Model

In order to calibrate a fatigue equation using the data from sections N3-N7, a current damage ratio was assumed for each section based on its performance as of the beginning of August 2005. Section N6 had the highest amounts of cracking and was the only section with areas of interconnected cracks; therefore, it was assigned a damage of 0.7. Section N5 had some cracking in both wheelpaths, and there were some transverse cracks in section N7; consequently section N5 and N7 were assigned damage ratio values of 0.4 and 0.5, respectively. The two 9 in. sections (N3 and N4) had no observed cracking at the time and were assigned a value of 0.2. Using the data from the five sections and the damage assumptions, the general model developed is given below:

$$N_f = 0.4801 * \left(\frac{1}{\varepsilon_t}\right)^{3.143} * \left(\frac{1}{E}\right)^{0.4834} \quad (4.14)$$

The fatigue transfer functions presented here were developed to aid state DOTs in adopting M-E design procedures. The models are applicable to public highway analysis and design for similar conditions to the Test Track. Two separate models were presented for thick and thin HMA pavements, avoiding any necessary shift factors. The rich bottom model was developed using only one test section, so further investigation may be warranted, especially considering the section did not perform as expected.

Subgrade Pressure And Rutting Performance

Introduction

Mechanical responses of pavements are very important to develop accurate pavement performance models. Recent advancements in the pavement engineering field have made it easier to measure pavement responses accurately. In this regard, accelerated pavement testing, such as that performed at the Test Track, helps to simulate the traffic conditions and the embedded instrumentation such as strain gauges and pressure plates help to measure pavement response accurately for varying loads and climatic conditions. The recent AASHTO pavement design guide relies heavily on the mechanistic empirical design approach.

One of the main objectives of the NCAT structural study was to develop pavement performance models that can be used in mechanistic empirical design. In this section, the measured pressures, pressure and strain prediction models, and the trend of rutting are explained in detail.

Data Collection

The earth pressure cells available in all eight structural sections measure the dynamic vertical pressures generated under moving wheel loads. In all sections, these pressure cells were placed at the top of the granular base course and at the top of the subgrade layer. The arrangement and other details of earth pressure cells were documented in the earlier part of this report. The pressure and strain data were collected once per week, for three passes of live traffic loads (triple

trailer and box truck) and under different environmental conditions. By collecting three passes and using the maximum pressure response for analysis, the effect of natural wheel wandering is minimized. The traffic and temperature data were recorded continuously during the entire period of the test cycle. Data collection and processing of the vertical pressure pavement response measurements followed the same approach detailed above for the strain gauges.

The sections that were 5 in. thick (thin Sections) Sections, N1 and N2, had failed in fatigue cracking within a few months and the pressure responses quickly over ranged the embedded instrumentation. So they were not included in the detailed analysis because of very few data. FWD tests were conducted periodically to measure material properties (stiffness) and relationships were developed to predict their properties at any time of the day. Similarly, the pressure and strain prediction models were also developed from the measured responses to predict pressure and strain at any time in the pavement structure.

Trends in Base and Subgrade Pressures

Seasonal temperature variations have a profound effect on measured pressures. In winter periods, lower temperatures increase HMA stiffness, which in turn reduces the pressure in the base and subgrade layers. Conversely, summertime pressures tended to be the highest due to reductions in HMA stiffness. After the sections were cracked, the measured pressure was not very accurate, and somewhat erratic. So only the intact pavement pressure responses were taken for analysis. The cutoff date for pressure data is given in Table 4.10.

Table 4.10 Pressure Cutoff Date Details

Sections	Pressure Cutoff Date
N1	22-March-04
N2	14-Jaunuary-04
N3	02-August-05
N4	02-August-05
N5	07-February-05
N6	07-February-05
N7	07-February-05
N8	12-July-04

The seasonal trend in pressure is clearly visible in Figure 4.42. Each pressure value indicated in the figure is the maximum pressure value of three passes of four triple trailer vehicles in Section N6. The same trend was also seen for the box trailer. All the structural sections showed similar trends in pressure response with season changes. Figure 4.43 summarizes the data from Figure 4.42 and shows that the pressure measurements are repeatable between different passes (pass 1, 2 and 3).

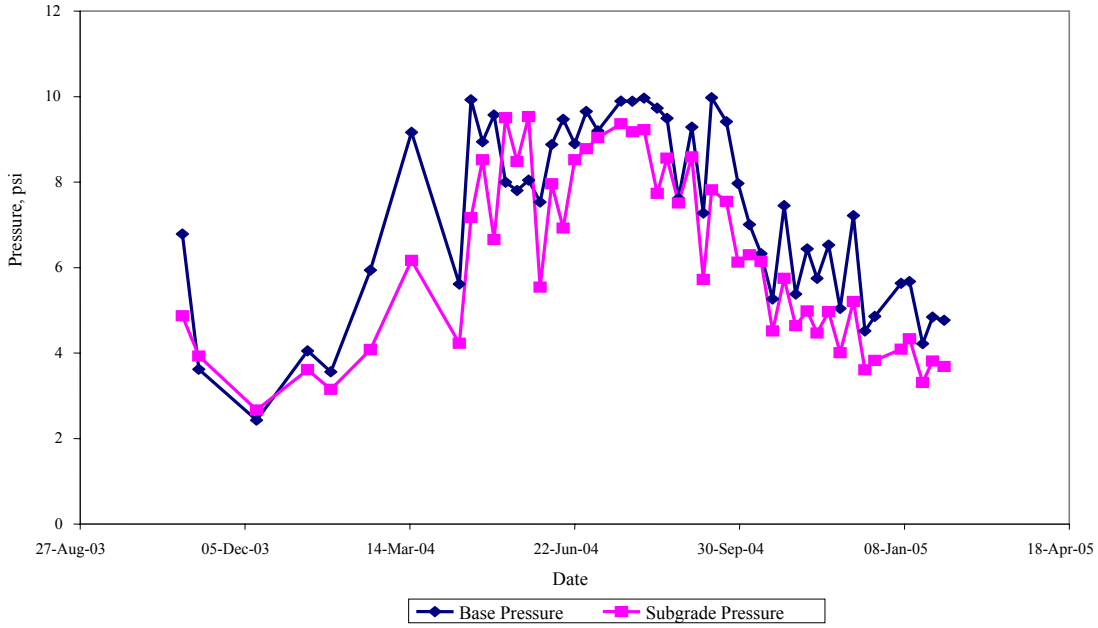

Figure 4.42 Trend of Base and Subgrade Pressures in Section N6.

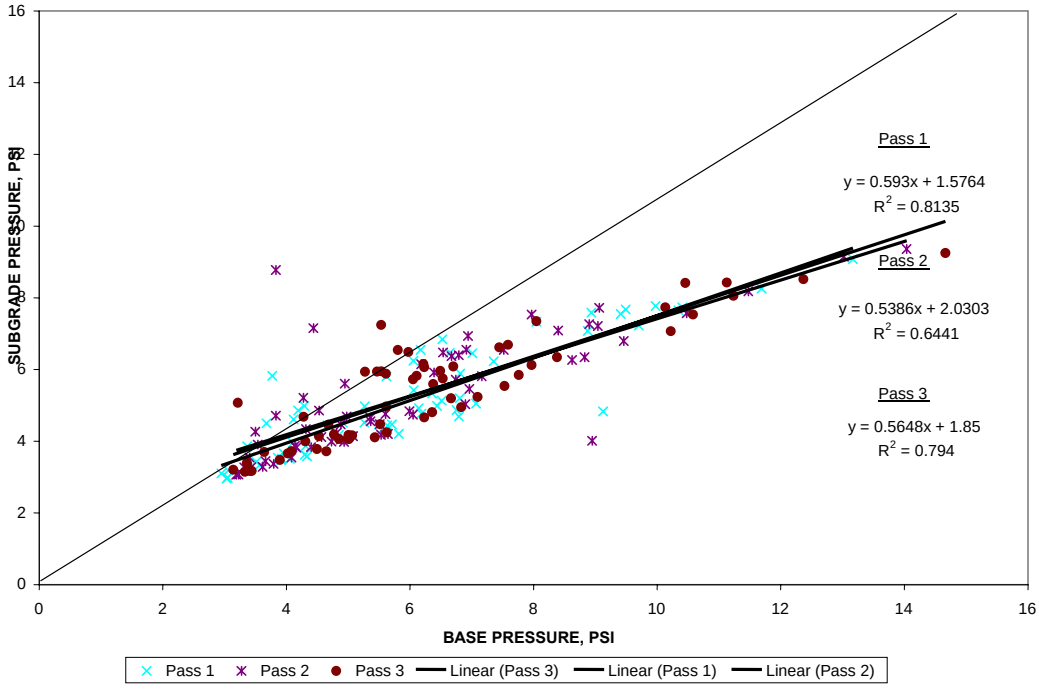

Figure 4.43 Base and Subgrade Pressures for Three Passes of Triple Trailers in N6.

Pressure Prediction

Most experiments with APT facilities include studies of stress and strain behavior of pavement layers. The measured responses were compared with theoretical responses based on back calculation of moduli from the use of FWD data. It is common to find claims of reasonable agreement between theoretical and measured values, but usually after some adjustment of estimates for local conditions (Metcalf, 1996).

When base and subgrade pressures were plotted against pavement temperature at 2 inches from the surface, a good correlation was found. Similarly, theoretical analysis was done using a layer elastic analysis computer package (WESLEA) for various pavement thicknesses and the results indicated good correlation between HMA thickness and base and subgrade pressures. By using the collected pressure data from the Test Track, a pressure prediction model was built using pressure as a function of temperature and thickness. For pressure prediction purpose, the sections were grouped as Modified (N1, N4 & N5), Unmodified (N2, N3 and N6) and SMA sections (N7, N8). The pressure prediction coefficients for triple and box trailers were different since both trucks have different loads, and their values are tabulated in Table 4.11 and Table 4.12. These models predict base and subgrade pressures with 85-95% accuracy. The basic form of the pressure prediction model is:

$$\text{Pressure} = C_0+C_1*\text{Temp}^2+C_2*\text{Temp}+C_3*\text{Thickness}^2+C_4*\text{Thick} \quad (4.15)$$

Where:

C_0, C_1, C_2, C_3, C_4 = Regression constants
Temp = HMA temperature at 2 inch depth, ^oF
Thickness = HMA thickness, in.

Table 4.11 Pressure Prediction Model Coefficients for Triple Trailer Truck.

Coefficients	Base Pressure, psi			Subgrade Pressure, psi		
	Unmodified	Modified	SMA	Unmodified	Modified	SMA
C_0	31.2088	50.6896	9.8642	13.2399	32.6746	4.7975
C_1	-0.0003	0.0012	0.0011	0.0008	0.0011	0.0010
C_2	0.1540	-0.0705	-0.0598	-0.0270	-0.0819	-0.0347
C_3	0.5038	0.7616	0.3912	0.1032	0.3807	-0.4742
C_4	-8.3668	-12.0968	-3.6308	-2.2165	-6.6296	3.0303
R^2	0.88	0.88	0.71	0.93	0.94	0.95

Table 4.12 Pressure Prediction Model Coefficients for Box Trailer Truck.

Coefficients	Base Pressure, psi			Subgrade Pressure, psi		
	Unmodified	Modified	SMA	Unmodified	Modified	SMA
C_0	29.6941	50.8963	9.9379	13.2288	34.4752	4.4874
C_1	0.0006	0.0016	0.0011	0.0004	0.0007	0.0013
C_2	-0.0117	-0.1605	-0.0624	-0.0112	-0.0621	-0.1129
C_3	0.4072	0.7129	0.3561	0.1308	0.4333	-0.2557
C_4	-6.7424	-11.3306	-3.3831	-2.4843	-7.3735	1.9554
R^2	0.60	0.89	0.73	0.74	0.90	0.88

Theoretical Pressure Calculation

To check the measured pressures from the Test Track, they were compared with theoretical pressures. For the theoretical pressure calculation, a layered elastic analysis software package called WESLEA for Windows was used. Temperature-stiffness relationships which were documented earlier in this report were used to calculate HMA stiffness for different temperatures. As mentioned in the earlier part of this chapter, section-specific average modulus values were used for base stiffness and average modulus was used for subgrade materials. Poisson ratios of 0.35, 0.40 and 0.45 were used for HMA, base and subgrade materials, respectively.

After running the WESLEA simulations for different axle loads (steer, tandem and single) and pavement configurations, the pressure values were plotted against the measured pressures from the track. From Figures 4.44 and 4.45, it is shown that both theoretical and measured base pressures are reasonably close to each other (theoretical pressure is 6% more than the measured base pressure). Measured subgrade pressure for a triple trailer is 16% less than the theoretical pressure. Since these values are reasonably close to each other, it can be claimed that the layered elastic software WESLEA can be used to accurately predict pavement responses.

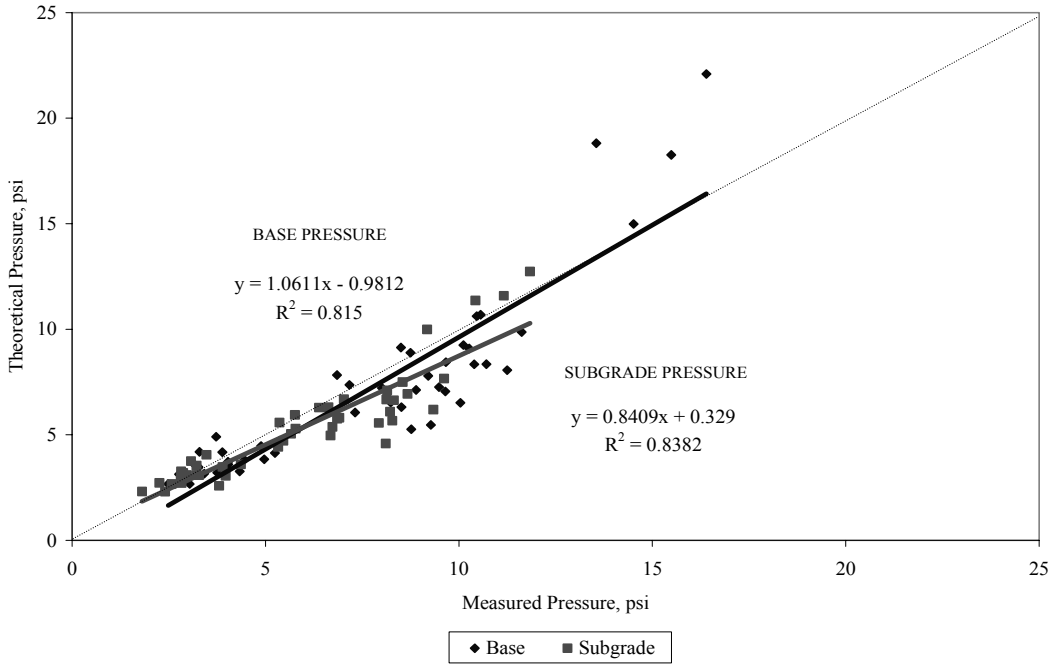

Figure 4.44 Measured and Theoretical Pressure Comparison for Triple Trailer (N6).

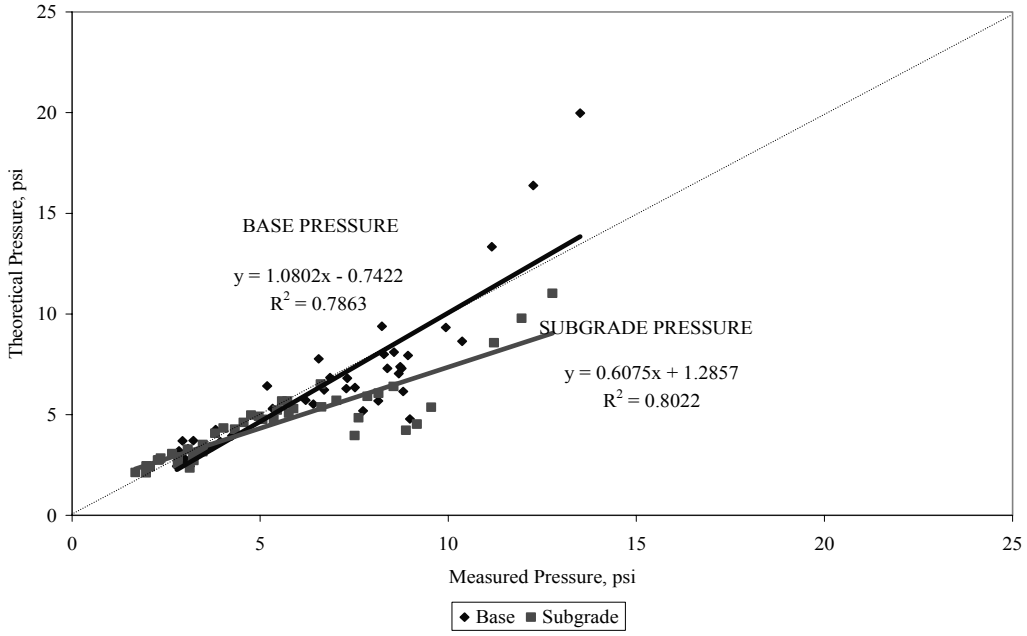

Figure 4.45 Measured and Theoretical Pressure Comparisons for Box Trailer (N6).

Base and Subgrade Strain Calculations

Historically, flexible pavement rutting performance models have been built by incorporating pavement strains, rather than pressure, as one of the mechanistic responses. So, there is a need to calculate the vertical base and subgrade strain in all pavement sections. However in the Test Track there was no instrumentation to measure vertical strains at the base and subgrade. Since the measured pressure from the pressure plate conforms with the layered elastic analysis derived pressures, it was reasonable to use the same layered elastic analysis program to calculate vertical strains at the top of the base and subgrade layers.

Strain Prediction Models

Using the same material properties and load configuration which was used earlier for the theoretical pressure calculations, the vertical strain at the top of base and subgrade was calculated from WESLEA. For various HMA temperatures the strains were calculated and the strain model was built, having vertical strain as a function of temperature. With the help of environmental data from the track, the base and subgrade vertical strains can be calculated whenever the truck load is applied to the pavement. As mentioned earlier, sections N1 and N2 did not produce enough data and their fatigue cracking failure kept these sections out of rutting analysis.

Tables 4.13 and 4.14 summarize the strain prediction models for the triple-trailer and box-trailer vehicles, respectively. As shown in the tables, the prediction model had the form:

$$\varepsilon_v = \beta_0 e^{(\beta_1 * Temp)} \quad (4.16)$$

Where:
ε_v = Vertical Strain
Temp = HMA Temperature at 2 inch depth, ^oF
β_0, β_1 = Regression Constants

From the model results given in Tables 4.13 and 4.14, vertical strain at the top of base and sub grade layers can be predicted from the pavement temperature at 2 inches from the surface for different pavement configurations (thin, medium, and thick sections).

Table 4.13 Strain Prediction Model for Triple Trailer.

Section	Triple Trailer	
	Base Strain	Subgrade Strain
N1	-	-
N2	-	-
N3	$69.57*e^{(0.0208*Temp)}$	$74.70*e^{(0.0173*Temp)}$
N4	$68.95*e^{(0.0191*Temp)}$	$72.03*e^{(0.0160*Temp)}$
N5	$116.19*e^{(0.0221*Temp)}$	$138.41*e^{(0.0179*Temp)}$
N6	$105.76*e^{(0.0164*Temp)}$	$112.07*e^{(0.0136*Temp)}$
N7	$124.47*e^{(0.0181*Temp)}$	$135.21*e^{(0.0146*Temp)}$
N8	$123.07*e^{(0.0186*Temp)}$	$135.14*e^{(0.0151*Temp)}$

Table 4.14 Strain Prediction Model for Box Trailer.

Section	Box Truck	
	Base Strain	Subgrade Strain
N1	-	-
N2	-	-
N3	$69.55*e^{(0.0207*Temp)}$	$66.59*e^{(0.0168*Temp)}$
N4	$61.43*e^{(0.0189*Temp)}$	$64.64*e^{(0.0154*Temp)}$
N5	$118.59*e^{(0.0200*Temp)}$	$136.13*e^{(0.0159*Temp)}$
N6	$93.67*e^{(0.0164*Temp)}$	$99.03*e^{(0.0132*Temp)}$
N7	$108.20*e^{(0.0183*Temp)}$	$116.75*e^{(0.0144*Temp)}$
N8	$107.67*e^{(0.0187*Temp)}$	$117.88*e^{(0.0148*Temp)}$

The pavement temperature was substituted in the above model, and the response strain values were noted. As expected, the base strain value was higher than the subgrade strain in all the sections. For the same temperature, the base and subgrade strain in thick sections are less than thin and medium HMA sections which matches the theory. There was not much difference in the strain level between sections N7 and N8.

Rutting Progression

Figure 4.46 shows the progression of rutting in structural sections. After a certain period of loading, the rutting did not show any appreciable increase. For the same number of load repetitions and thickness, the modified and unmodified binder sections performed differently in terms of rutting. Modified binder sections have less rutting when compared to unmodified binder sections. It is interesting to note that the 7-inch and 9-inch sections exhibit similar rutting performance.

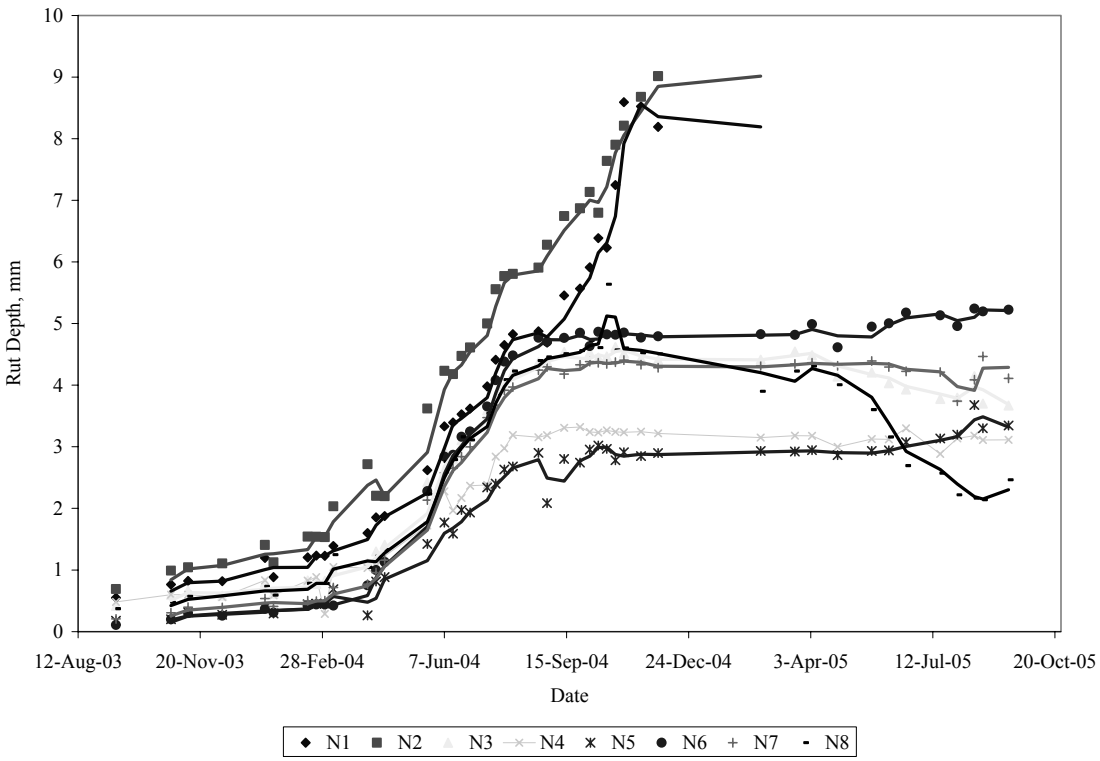

Figure 4.46 Rutting Progression in Structural Sections.

After the fatigue failure of sections N1 and N2, the trucks were veered around those sections, which in turn affected the rut measurements in section N3. The amount of rutting began to decrease since the trucks were transversing on the ridges of the ruts. Section N8 started showing fatigue failure in July 2004, which affected the rut measurements at that section. As a result, rutting in section N8 showed a downward trend.

Axle Passes and Pavement Strain

The trucking data was linked with the environmental database and thereby at any given time, the strain produced by a certain number of axle passes was calculated. The number of laps per hour was multiplied with the number of axles in a truck to get the total number of axle passes per hour for both types of trucks. The base and subgrade strain corresponding to that hour was calculated using the strain model given in Tables 4.13 and 4.14. The rut depth data were interpolated using a straight line interpolation so that a measured rut depth was available for each date.

The observed rutting was modeled as a function of pavement strain and number of axle passes. Preliminary analysis showed that both base or subgrade strain can be used in the rutting model and the developed model closely traces the observed rutting in the field.

$$RD = f(\varepsilon, N) \quad (4.17)$$

Where:

RD = Rut depth
ε = vertical strain
N = number of axle passes

Even after the application of approximately 10 million ESALs, none of the structural sections showed rutting failure and the measured rutting in all sections was very small (less than 5 mm). So the remaining sections will be monitored continuously in the next trafficking cycle for another 10 million ESALs and their rutting performance will be monitored and modeled. The AASHTO M-E design rutting model will be calibrated with the field data collected from the test track.

CHAPTER 5: ITEMS IMPLEMENTED BY DOTs

Introduction

The NCAT Test Track was built to develop and evaluate better ways to design and construct hot mix asphalt (HMA) pavements. For the test track to be beneficial items must be implemented as a result of work at the track. Some items that had been implemented, at the time this report was published, are discussed below. Some of these items have supporting data while other items were adopted based on visual observations or selected limited data on performance of individual sections. Much of the supporting information can be found in the report on Phase I at the track (Brown et al, 2002).

Grinding to Improve Smoothness

Eleven of the transverse joints built during the original construction and several additional joints built during the 2003 reconstruction were ground to remove the bump at the joint. The grinding process performed on these joints resulted in a very smooth surface at the joint. Although eleven joints were leveled with the grinding equipment during the first cycle of tests, none had any performance issues during the initial two years of traffic. Some of these leveled areas have now been in place for up to 5 years with no performance problems. No sealing was provided to these treated surfaces.

Fine and Coarse Graded Mixtures

Based on observations at the test track, at least 3 state DOTs have begun to use more fine-graded mixes. The track showed that these mixes would provide good resistance to rutting and experience has shown that these fine-graded mixtures have less permeability than the coarse-graded mixtures.

Grade Bumping

Superpave guidelines recommend that the high temperature PG grade be bumped for higher traffic volume roadways to minimize rutting. The results from the first cycle of testing indicated that on the average, there was more than a 50 percent reduction in permanent deformation when the high temperature grade was bumped from PG 64 to PG 76. As a result of findings at the test track, some states have increased the number of projects requiring grade bumping.

Use of SMA

SMA mixtures have been used in the US for almost 15 years with very good results. Since SMA was adopted in the US, one of the requirements has been to use only crushed stone. Evaluations were conducted at the track using crushed gravel in an SMA mixture and it was determined that the SMA mixture performed well. As a result of this finding, two state DOTs have now begun producing SMAs with their localized gravel aggregates thus making the use of SMA a viable option.

Another state has begun to specify the use of SMA on projects. The test track work, as well as SMA performance in other states, has bolstered confidence in the SMA mixture.

Open-Graded Friction Course

As a result of the performance of open graded friction courses at the track, two states that had not been using OGFCs have begun to use these mix types to minimize hydroplaning.

Predicting Rutting Potential
There is interest in the pavement engineering field to identify a reliable test that can predict rutting performance. NCAT conducted several performance tests on the mixtures placed at the track including dynamic modulus, repeated load tests, and wheel tracking tests. As a result of the testing at the track, one state DOT has gained confidence in their newly-implemented APA specification. That confidence would have taken 10 to 15 years to develop without some type of accelerated testing.

Increasing Asphalt Contents
At least two state DOTs have taken action to increase the amount of asphalt in their designed mixes. The track showed that additional asphalt can be added to Superpave designed mixes, especially when the asphalt is modified, without experiencing rutting problems. Generally the amount of asphalt is increased by lowering the number of gyrations specified for mix design.

Comparisons with Other Accelerated Loading Facilities
Two sponsors of the track also utilize their own accelerated loading facilities. It is important that the performance measured using these accelerated loading devices be similar to that expected on the roadway. The work at the track has served to validate their facilities.

Aggregate Quality
Four state DOTs have evaluated local aggregates and made decisions about the utilization of those aggregates based on results from the test track.

Smaller Top Size Mixtures
Two states have evaluated performance of a 4.75 mm mix and have begun using these fine mixes based on performance at the track.

Other Research Issues
While the primary purpose of the track is to conduct the specific studies funded by the track sponsors, the track has supported additional research to solve national and local problems. Some of this work has involved effects of various mixtures on noise, friction, permeability, compactability, and performance testing. For example, the primary data for NCHRP 9-27, which developed recommendations for the minimum thickness of HMA layers, was developed during reconstruction of the test track. Work at the track is developing data that can be used in the design of perpetual pavements, warm asphalt, and noise reduction. Studies have also investigated tires and synthetic fuel.

Several states have made mix adjustments or adopted other mix types such as SMA or OGFC based on performance of some of the mixes at the track. Even though each sponsor has built test sections to answer their specific questions, each sponsor also has access to the data generated by all of the other states. This has significantly improved the confidence of these sponsors to make needed modifications to their mixtures without having to build test sections on their own highways where cost, safety, and time required would be concerns.

CHAPTER 6: OBSERVATIONS

- Most of the rutting and alligator cracking occurred in the outside wheel path.
- After Phase I testing, 23 sections were left in place for Phase II. The maximum rutting in any of these sections that were left in place and subjected to 20 million total ESALs was 7mm.
- In 2003, 22 new sections were constructed. Three of these sections, located within the structural study, failed due to alligator cracking. The most rutting in the sections that did not fail was approximately 9mm.
- Cracking occurred in only four sections outside of the structural sections. Most of the cracking was top-down and occurred in sections with modified asphalts. The cracking was minor at the time this report was prepared.
- Over 80 percent of the temperature gauges installed in 2000 were still operational at the end of 2005.
- SMA sections had more rutting than the Superpave sections but neither had significant rutting. It appears that initial rutting in the SMA was due to densification and/or aggregate reorientation. After this initial rutting little additional rutting occurred.
- No cracking had occurred in any of the SMA sections.
- SMA mixtures placed in 2003 were designed with 50 and 75 gyrations with the Superpave Gyratory Compactor. These mixes have performed well which indicates that this lower compactive effort can be used to increase the optimum asphalt content and produce improved durability.
- Laboratory air voids had a significant effect on dense graded mixes designed using an unmodified asphalt binder. However, the air voids had little effect on performance of those mixes using modified asphalts.
- The factor that most affected rutting of HMA pavements was the AC grade. The modified asphalt reduced the rutting by over 50% when compared to unmodified asphalt.
- The asphalt pavement analyzer (APA) showed a good trend with rutting performance. Additional work is needed with the APA along with other performance tests to clearly develop the best relationships.
- Coarse-graded and fine-graded mixes were compared. When fine-graded mixes were compared to coarse-graded mixes, they were equally resistant to rutting, less likely to be permeable, quieter, similar in friction, possibly easier to compact, and higher in optimum asphalt content.
- The total number of loads to failure for the structural sections at the track was very similar to that predicted by the 1993 AASHTO design guide.
- Instrumentation to measure pavement temperatures, strain in HMA, and stresses on top of base and subgrade worked very successfully. There was not a high rate of gauge failures and the accuracy appeared to be acceptable.
- There was a good comparison between theoretical and measured strain responses in the HMA and between theoretical and measured stresses on top of the subgrade and base courses.
- The amount of truck wander at the Test Track was determined to be similar to the measured wander on typical highways.
- Care had to be taken in selecting the measured strain under loads since the truck wander caused variations in measured strains due to each truck axle not passing directly over the strain gauges.

- The measured stiffness of the mixes with modified asphalt was approximately equal to that with unmodified asphalt. The modified asphalts did not seem to improve fatigue performance but did significantly improve mixture rutting resistance.
- The rich bottom concept did not provide improved performance. In fact, the performance was decreased. The reason for this poor performance is being investigated.
- Fatigue failure progression indicated that a transverse crack occurs first. Then other small transverse cracks occur. The crack progresses to the edge of the wheel path. At this point some pumping of fines can occur. Finally the cracks become interconnected resulting in alligator cracking.
- Based on results of the structural study, fatigue models were calibrated to better predict the observed performance.

REFERENCES

American Association of State Highway and Transportation Officials. *AASHTO Guide for Design of Pavement Structures*. Washington, D.C., 1993.

Baker, H.B., Buth, M.R. and Van Deusen, D.A., "Minnesota Road Research Project Load Response Instrumentation Installation and Testing Procedures," Report No. MN/PR-94/01, Minnesota Department of Transportation, St. Paul, MN, 1994.

Brown, E.R. et al, "NCAT Test Track Design, Construction and Performance", NCAT 02-12, National Center for Asphalt Technology, Auburn University, 2002.

Devore, Jay L., "Probability and Statistics for Engineering and the Sciences." Fifth Edition, 2000.

Distress Identification Manual for the Long-Term Pavement Performance Program (Fourth Revised Edition), FHWA-RD-03-031, 2003.

El-Basyouny, Mohammed and Matthew Witczak. "Calibration of the Alligator Fatigue Cracking Model for the 2002 Design Guide." *Transportation Research Board 84th Annual Meeting Compendium of Papers*. CD-ROM. Washington, D.C., 2005.

Epps, Amy, Lubinda F. Walubita, Pavement Response and Rutting for Full Scale and Scaled APT, Journal of Transportation Engineering, Vol. 129, No. 4, July/August 2003.

Faheem, A., and Bahia H. "Using the Gyratory Compactor to Measure Mechanical Stability of Asphalt Mixtures." Wisconsin Highway Research Program 0092-01-02. October 2004.

Freeman, Reed B., H. Tommy Carr, Tom McEwen, and R. Buzz Powell, "Instrumentation at the National Center for Asphalt Technology Test Track." U.S. Army Corps of Engineers, Engineer Research and Development Center, Report No. ERDC TR-01-9. Washington, D.C. August 2001.

Huang, Y.H., Pavement Design and Analysis, First Edition, Pearson Prentice Hall, 1993.

Hugo, F., Amy Epps, Significant Findings from Full-scale/Accelerated Pavement Testing, NCHRP Synthesis 325, Transportation Research Board, Washington DC, 2004.

Metcalf, J. B., NCHRP Synthesis of Highway Practice 235: Application of Full-Scale Accelerated Pavement Testing. Transportation Research Board, Washington, D.C., 1996.

Miner, Milton A. "Estimation of Fatigue Life with Particular Emphasis on Cumulative Damage." *Metal Fatigue*, edited by Sines and Waisman, McGraw Hill (1959): 278-89.

Minitab Reference Manual, Release 10 for Windows, Minitab Inc., State College, PA, 1994.

Monismith, C.L., J.A. Epps and F.N. Finn. "Improved Asphalt Mix Design," Proceedings, Association of Asphalt Paving Technologists Technical Sessions, San

Antonio, Texas (1985): 347-406.

Pine, Bill, "The Bailey Method. Achieving Volumetrics and HMA Compactability." Heritage Research Group. November 2004.

Priest, A.L., "Calibration of Fatigue Transfer Functions for Mechanistic-Empirical Flexible Pavement Design," M.S. Thesis, Auburn University, 2005.

Smart Road Pavement Research Team, http://www.cee.vt.edu/program_areas/tise/smart/, accessed December 1, 2003.

Tangella, R., J. Craus, J. A. Deacon, and C. L. Monismith. *Summary Report on Fatigue Response of Asphalt Mixtures*. TM-UCB-A-003A-89-3, SHRP Project A-003-A. University of California, Berkeley: Institute of Transportation Studies, 1990.

Thickness Design, Asphalt Pavements for Highways and Streets. Report MS-1, The Asphalt Institute, 1982.

Timm, D.H., Birgisson, B. and Newcomb, D.E., "WESLEA for Windows 3.0", 1999, available for download at: www.eng.auburn/edu/users/timmdav/WFW.msi.

Timm, D.H., David E. Newcomb and Theodore V. Galambos, "Incorporation of Reliability into the Minnesota Mechanistic-Empirical Pavement Design Method," Final Report, MN/RC-1999-35, Minnesota Department of Transportation, St. Paul, MN, 1999.

Timm, D.H. and Newcomb, D.E., "Calibration of Flexible Pavement Performance Equations," Transportation Research Record 1853, Transportation Research Board, 2003, pp. 134-142.

Timm, D.H. and A.L. Priest, "Dynamic Pavement Response Data Collection and Processing at the NCAT Test Track," Report No. 04-03, National Center for Asphalt Technology, Auburn University, 2004.

Timm, D.H., Priest, A.L. and McEwen, T.V., "Design and Instrumentation of the Structural Pavement Experiment at the NCAT Test Track," NCAT 04-01, National Center for Asphalt Technology, 2004.

Timm, D.H. and A.L. Priest, "Material Properties of the 2003 Test Track Structural Study," Draft NCAT Report, 2005.

Van Cauwelaert, F.J., Alexander, D.R., White, T.D., and Barker, W.R., "Multilayer Elastic Program for Backcalculating Layer Moduli in Pavement Evaluation," Nondestructive Testing of Pavements and Backcalculation of Moduli, ASTM STP 1026, A.J. Bush III and G.Y. Baladi, Eds., American Society for Testing and Materials, Philadelphia, 1989, pp. 171-188.

Vavrik, W.R., W.J.Pine, G.Huber, S.H.Carpenter and R.Bailey, "Bailey Method for Gradation Selection in HMA mixture design." Transportation Research Circular No. E-C044. Transportation Research Board. October 2002.

Zhou, F., Scullion, T., Discussion: Three Stages of Permanent Deformation Curve and Rutting Model, International Journal of Pavement Engineering, Volume 3, Number 4, 2002, pp. 251-260.

APPENDIX

SUMMARY OF TEST SECTION
QC RESULTS AND PERFORMANCE DATA

Section	**N1**	**N2**	**N3**	**N4**	**N5**	**N6**	**N7**	**N8**	**N9**	**N10**	**N11**	**N12**	**N13**
Cycle	2	2	2	2	2	2	2	2	2	2	1+2	1+2	2
Gradation Type	Fine	Fine	Fine	Fine	Fine	Fine	SMA	SMA	SMA	SMA	Intermediate	SMA	SMA
Aggregate Type[1]	Grn/Lms/Snd	Grn/Lms/Snd	Grn/Lms/Snd	Grn/Lms/Snd	Grn/Lms/Snd	Grn/Lms/Snd	Grn/Lms/Snd	Grn/Lms/Snd	Limestone	Lms/Chert	Granite	Granite	Granite
Compactive Effort[2]	G80	G80	G80	G80	G80	G80	M50	M50	G75	G75	G100	M50	G50
3/4"	100	100	100	100	100	100	100	100	100	100	100	100	100
1/2"	100	100	100	100	100	100	100	100	97	95	97	96	95
3/8"	100	100	100	100	100	100	100	100	83	87	80	73	71
No. 4	81	80	80	81	81	81	49	49	37	30	52	32	32
No. 8	63	63	63	61	61	62	24	24	17	21	37	23	21
No. 16	51	51	51	49	49	50	20	20	13	17	30	21	18
No. 30	38	38	38	37	37	37	17	17	12	15	24	19	16
No. 50	20	21	21	21	21	21	14	14	11	14	18	17	15
No. 100	12	12	12	12	12	12	12	12	10	13	11	14	14
No. 200	7	6.6	6.6	6.7	6.7	6.8	9.2	9.2	8.6	11.5	7.2	11.8	12.1
Asphalt Content	6.2%	6.1%	6.1%	6.1%	6.1%	6.2%	6.2%	6.2%	6.6%	6.2%	4.3%	6.2%	5.9%
Avg. V_a	4.4%	5.8%	5.7%	5.5%	5.5%	5.0%	7.3%	6.9%	5.0%	4.3%	3.4%	2.7%	2.9%
In-Place Air Voids	7.2%	7.1%	7.2%	6.6%	6.7%	6.3%	6.9%	6.9%	4.9%	4.4%	6.9%	5.4%	5.4%
PG Grade	76-22	67-22	67-22	76-22	76-22	67-22	76-22	76-22	70-22	70-22	76-22	76-22	76-22
Modifier Type	SBS	NA	NA	SBS	SBS	NA	SBS	SBS	SBS	SBS	SBS	SBS	SBS
Rutting[3] **(mm)**	Failed in Fatigue	Failed in Fatigue	4.3	3.5	4.8	6.3	4.7	1.7	5.1	6.6	0.9	2.1	3.0
Initial IRI	51.6	58.4	35.3	53.2	54.8	53.1	43.1	42.1	89.6	46.6	48.6	65.9	59.5
Final IRI[4]	219.5	296.9	37.6	59.9	68.3	55.2	52.6	153.5	64.5	47.8	46.2	56.3	72.0
Mean Texture Depth (mm)	0.76	0.85	0.40	0.48	0.51	0.46	0.68	0.67	0.54	0.58	0.90	1.07	0.77

Section	S1	S2	S3	S4	S5	S6	S7	S8	S9	S10	S11	S12	S13
Cycle	2	1+2	1+2	2	2	1+2	1+2	1+2	1+2	1+2	1+2	1+2	1+2
Gradation Type	SMA	Coarse	Coarse	OGFC	Intermediate	Fine	Coarse	Coarse	Coarse	Fine	Coarse	Intermediate	Fine
Aggregate Type[1]	Granite	Gravel	Lms/gravel	Limestone	Grv/Lms/Snd	Lms/RAP	Lms/RAP	Marble Schist	Granite	Granite	Marble Schist	Limestone	Granite
Compactive Effort[2]	G50	G100	G100	G50	G75	G100	G100	G100	G100	G100	G100	NA	G100
3/4"	99	100	100	100	100	100	100	100	100	100	100	100	100
1/2"	92	100	100	95	96	95	96	100	93	95	100	97	93
3/8"	74	96	100	78	87	87	88	93	82	88	92	82	80
No. 4	33	67	70	19	66	74	71	58	53	69	62	63	68
No. 8	25	41	43	5	43	53	34	38	36	52	47	46	50
No. 16	24	29	29	3	30	41	25	25	27	38	30	32	37
No. 30	22	22	21	3	21	33	20	19	20	27	22	23	27
No. 50	19	15	15	2	10	24	16	15	14	19	17	16	19
No. 100	16	10	11	2	7	12	10	12	9	11	13	10	11
No. 200	13	8.4	8.9	1.6	5.5	5.9	6.2	7.8	5.7	6.6	7.5	7	6.6
Asphalt Content	5.1%	6.0%	5.6%	5.8%	5.6%	6.2%	6.6%	4.2%	4.7%	5.2%	3.9%	4.5%	5.3%
Average QC Lab Air Voids	2.0%	4.7%	3.5%	NA	2.9%	4.5%	3.3%	2.7%	3.6%	3.2%	3.1%	3.8%	4.8%
In-Place Air Voids	4.4%	6.2%	7.3%	NA	6.9%	7.1%	6.8%	8.2%	6.6%	6.3%	6.8%	6.1%	6.6%
PG Grade	76-22	76-22	76-22	76-22	76-22	67-22	67-22	76-22	67-22	67-22	76-22	70-28	70-28
Modifier Type	SBS	SBS	SBS	SBS	SBS	NA	NA	SBS	NA	NA	SBS	SB	SB
Rutting[3]	5.6	1.4	1.1	4.1	3.8	2.9	5.8	3.3	3.1	5.1	2.0	3.3	2.3
Initial IRI	83.6	50.0	46.5	53.5	49.9	70.2	53.8	64.0	52.0	48.1	67.3	69.1	114.5
Final IRI[4]	80.7	47.7	41.8	49.8	63.9	61.7	44.5	63.2	33.0	43.4	75.9	75.2	123.6
Mean Texture Depth (mm)[4]	0.61	0.61	0.64	1.39	0.40	0.34	0.34	0.84	0.81	0.60	0.79	0.56	0.56

[1] Aggregate Type abbreviations: Grn = granite, Lms = limestone, Snd = sandstone.
[2] G indicates the gyratory compactor followed by the number of gyrations, M indicates Marshall hammer followed by the number of blows per face.
[3] Based on Dipstick profiles at 10/03/2005. For "1+2" sections the total accumulated traffic is 19 million ESALs, for "2" sections 9 million ESALs.
[4] Based on measurements at 10/03/2005. For 1+2 sections 19 million ESALs, for 2 sections 9 million ESALs.

Section	E1	E2	E3	E4	E5	E6	E7	E8	E9
Cycle	2	2	2	1+2	1+2	1+2	1+2	1+2	1+2
Gradation Type	SMA	Fine	Fine	Coarse	Intermediate	Intermediate	Intermediate	Fine	Fine
Aggregate Type[1]	Limestone	Limestone	Limestone	Granite	Granite	Granite	Granite	Granite	Granite
Compactive Effort[2]	G50	G100	G100	G100	G100	G100	G100	G100	G100
3/4"	100	100	100	100	100	100	100	100	100
1/2"	91	96	96	95	98	96	97	98	97
3/8"	69	93	92	75	83	81	83	86	85
No. 4	35	73	73	42	54	52	53	66	64
No. 8	23	55	54	29	40	37	38	51	49
No. 16	17	44	43	23	30	28	29	38	36
No. 30	14	37	36	18	24	22	22	28	27
No. 50	12	24	24	13	16	15	16	18	18
No. 100	11	10	10	8	9	8	9	10	10
No. 200	10	5.1	5.3	4.6	5.1	4.3	5.2	5.2	5.2
Asphalt Content	6.3%	7.8%	8.2%	4.7%	5.1%	5.0%	4.8%	5.6%	5.4%
Average QC Lab Air Voids	4.6%	3.0%	3.6%	3.8%	3.7%	3.9%	3.6%	4.2%	4.4%
In-Place Air Voids	3.6%	5.2%	6.1%	6.2%	7.3%	7.1%	6.8%	7.3%	7.1%
PG Grade	76-22	67-22	67-22	76-22	76-22	67-22	76-22	67-22	76-22
Modifier Type	SBS	NA	NA	SBS	SBS	NA	SBR	NA	SBS
Rutting[3] **(mm)**	6.3	8.3	5.7	4.6	5.1	6.8	4.3	5.8	2.7
Initial IRI	75.0	60.9	57.1	46.8	54.9	50.9	53.6	40.5	64.2
Final IRI[4]	67.1	62.8	62.7	51.9	62.1	43.6	47.1	39.7	72.7
Mean Texture Depth[4]	0.7	0.8	0.9	0.8	0.7	0.7	0.9	0.6	0.6

[1] Aggregate Type abbreviations: Grn = granite, Lms = limestone, Snd = sandstone.
[2] G indicates the gyratory compactor followed by the number of gyrations, M indicates Marshall hammer followed by the number of blows per face.
[3] Based on Dipstick profiles on 10/03/2005. For "1+2" sections the total accumulated traffic is 19 million ESALs, for "2" sections 9 million ESALs.
[4] Based on measurements on 10/03/2005. For 1+2 sections 19 million ESALs, for 2 sections 9 million ESALs.

Section	W1	W2	W3	W4	W5	W6	W7	W8	W9	W10
Cycle	1+2	2	2	1+2	1+2	2	1+2	2	2	1+2
Gradation Type	SMA	SMA	Fine	OGFC	OGFC	Fine	OGFC	OGFC	Fine	Coarse
Aggregate Type[1]	Granite	Porph/Lms	Limestone	Granite	Granite	Lms/Grv/Snd	Granite	Granite	Granite	Qtz gravel
Compactive Effort[2]	M50	G75	G50	NA	NA	G50	NA	G50	G100	G100
1"	100	100	100	100	100	100	100	100	100	100
3/4"	100	100	100	100	100	100	100	100	100	100
1/2"	95	88	100	95	95	100	95	100	100	96
3/8"	68	54	100	66	67	100	74	96	98	81
No. 4	28	22	79	23	22	98	32	40	83	51
No. 8	20	17	51	14	15	75	23	25	61	33
No. 16	18	14	39	13	12	50	18	19	43	22
No. 30	16	13	29	12	11	35	15	15	32	16
No. 50	14	12	21	11	11	22	12	13	23	12
No. 100	12	11	14	10	10	15	9	10	15	9
No. 200	9.7	9.7	8.7	8.6	8.5	11.3	5.9	7.5	7.5	6.5
Asphalt Content	6.1%	6.1%	6.2%	6.1%	6.2%	6.1%	4.8%	4.7%	5.8%	5.0%
Average QC Lab Air Voids	3.5%	5.0%	2.7%	NA	NA	4.0%	NA	NA	3.9%	4.0%
In-Place Air Voids	5.0%	3.2%	7.9%	NA	NA	7.8%	NA	NA	6.6%	6.7%
PG Grade	76-22	70-22	67-22	76-22	76-22	76-22	76-22	70-28	67-22	76-22
Modifier Type	SBR	SBS	NA	SBR	SBS	SBS	SB	SB	NA	SBR
Rutting[2] **(mm)**	5.7	7.2	6.6	7.3	5.7	8.1	1.9	4.5		3.8
Cracking										
Initial IRI	50.3	70.0	56.4	53.1	50.1	67.4	65.3	194.7	44.2	172.7
Final IRI[4]	47.2	62.8	57.9	52.3	49.0	62.0	79.6	188.6	77.3	
Mean Texture Depth[4]	1.0	0.8	0.5	1.5	1.5	0.3	1.1	0.8	0.3	

[1] Aggregate Type abbreviations: Porph = porphyry, Grv = gravel, Lms = limestone, Snd = sandstone, Qtz=quartz.
[2] G indicates the gyratory compactor followed by the number of gyrations, M indicates Marshall hammer followed by the number of blows per face.
[3] Based on Dipstick profiles at 10/03/2005. For "1+2" sections the total accumulated traffic is 19 million ESALs, for "2" sections 9 million ESALs.
[4] Based on measurements at 10/03/2005. For 1+2 sections 19 million ESALs, for 2 sections 9 million ESALs.